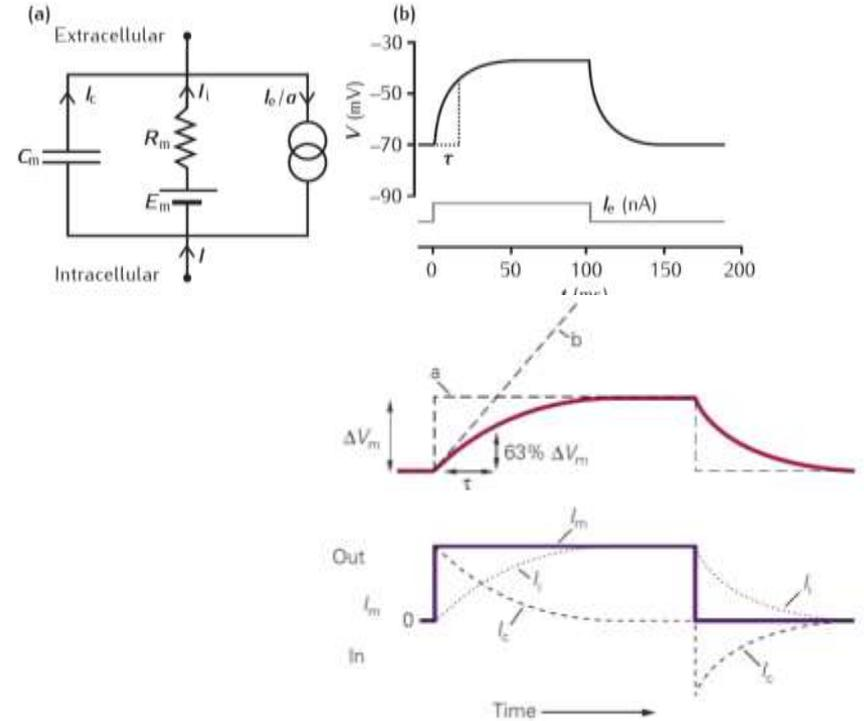
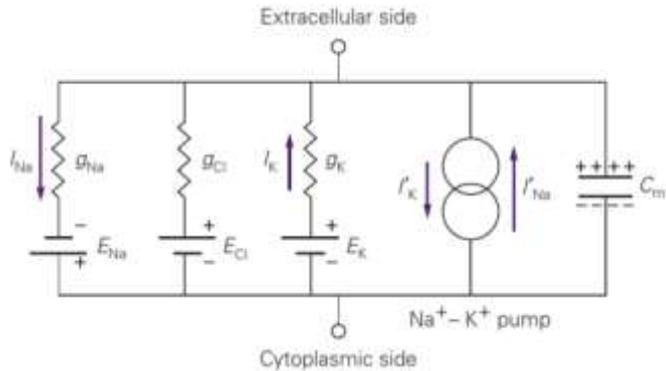
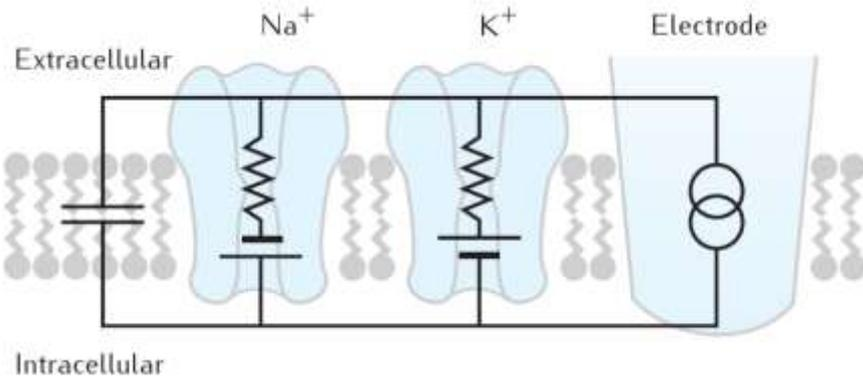


Биофизика возбудимости

А. Р. Браже



Пассивные электрические свойства мембран



Измерение электрических свойств мембраны

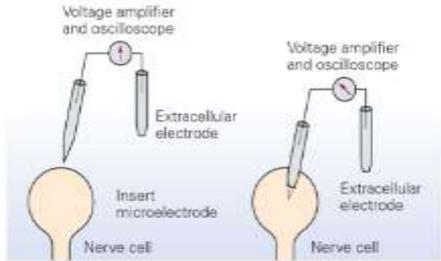


Figure 6-2A The recording setup.

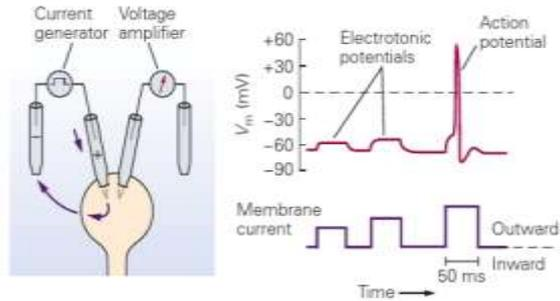


Figure 6-2C Depolarization.

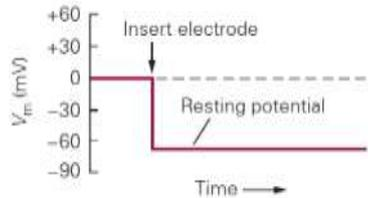


Figure 6-2B Oscilloscope display.

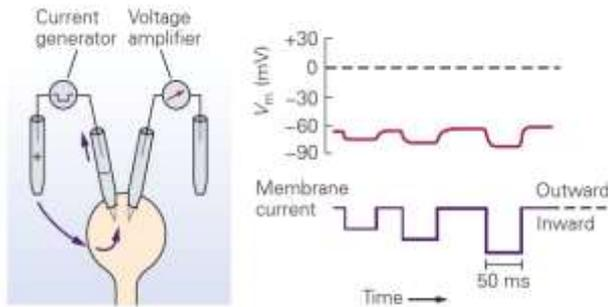
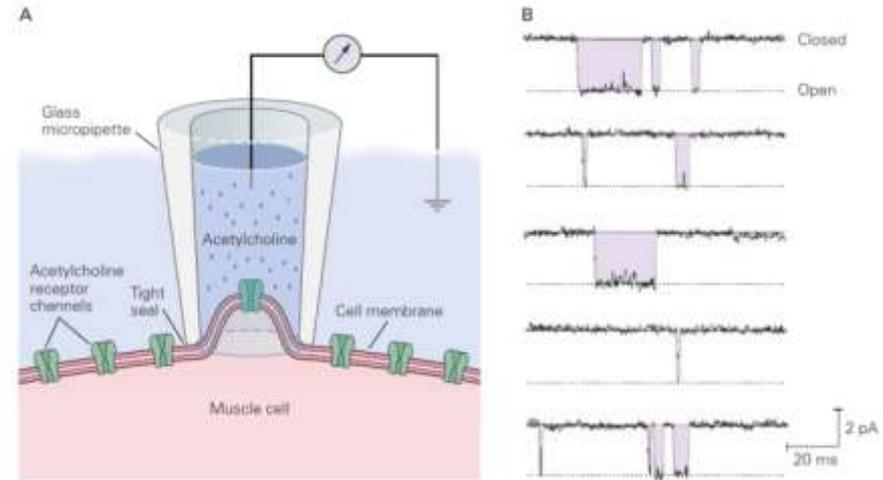
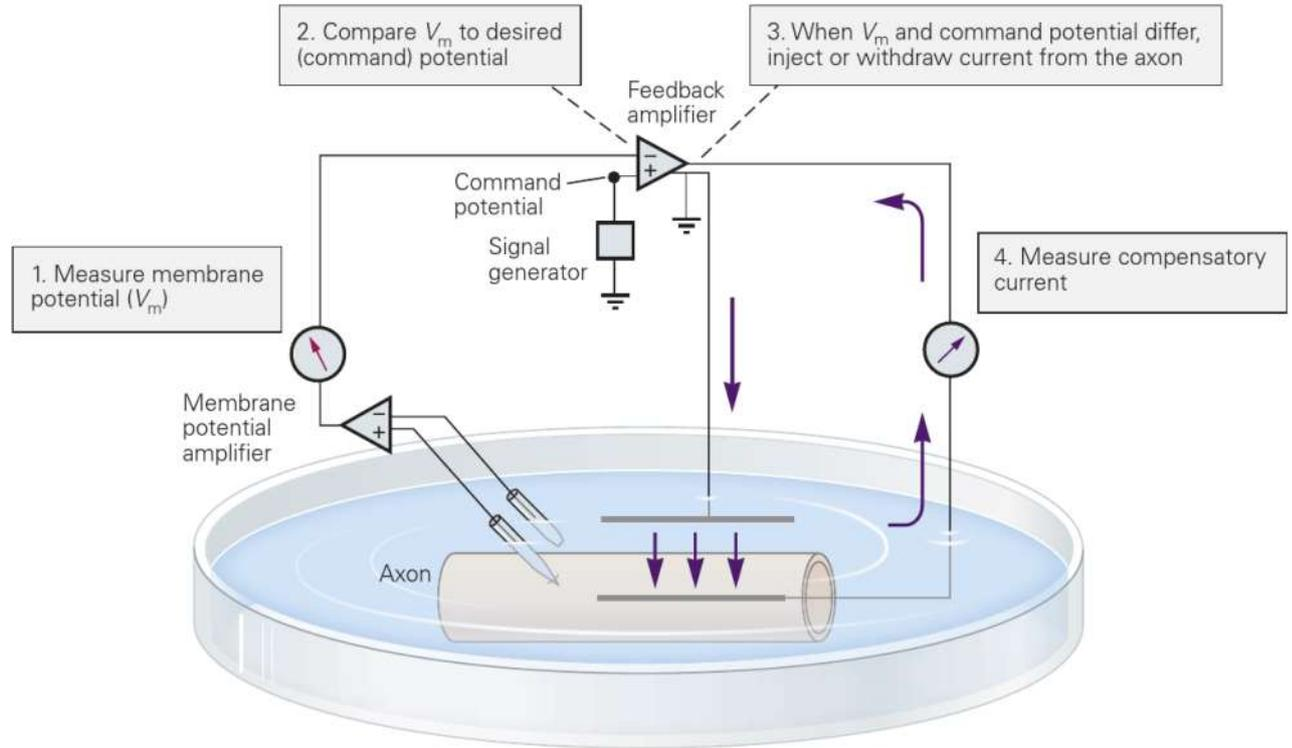
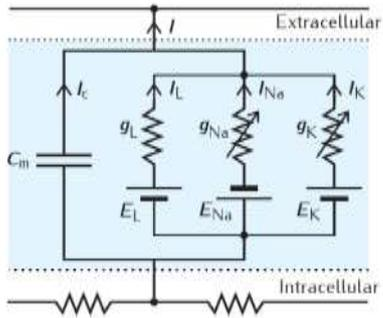
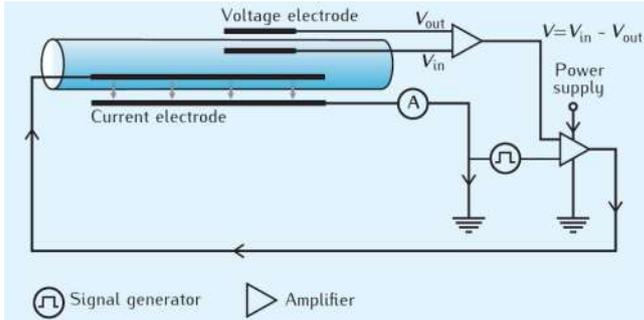


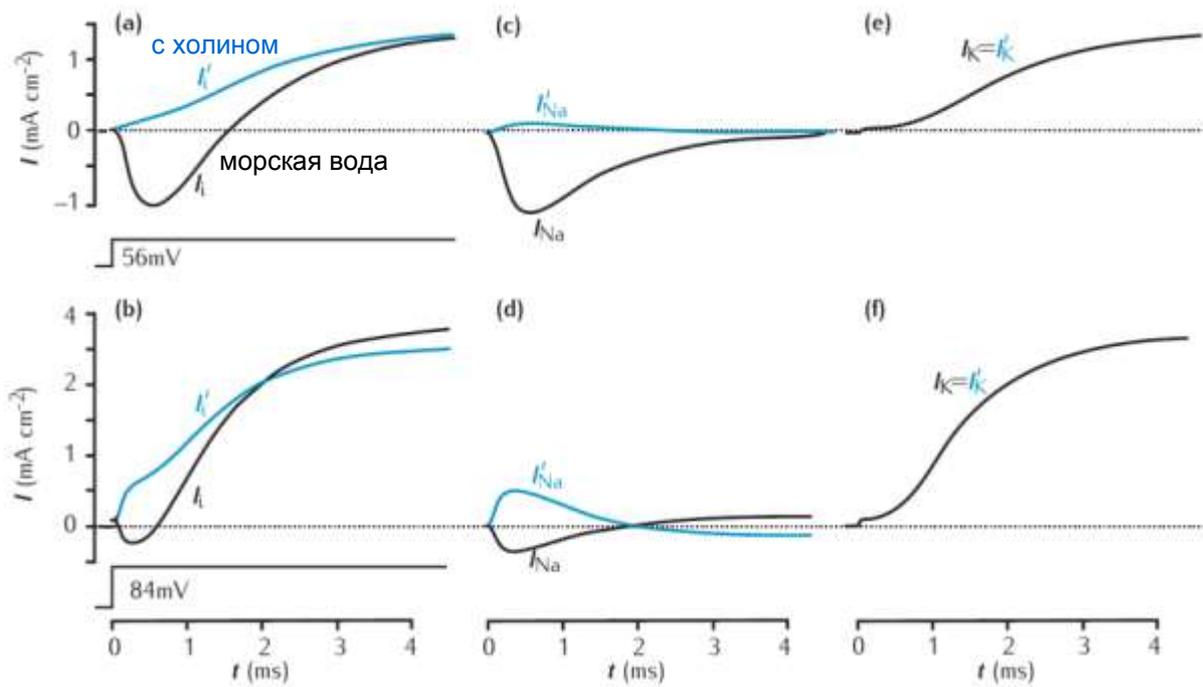
Figure 6-2D Hyperpolarization.



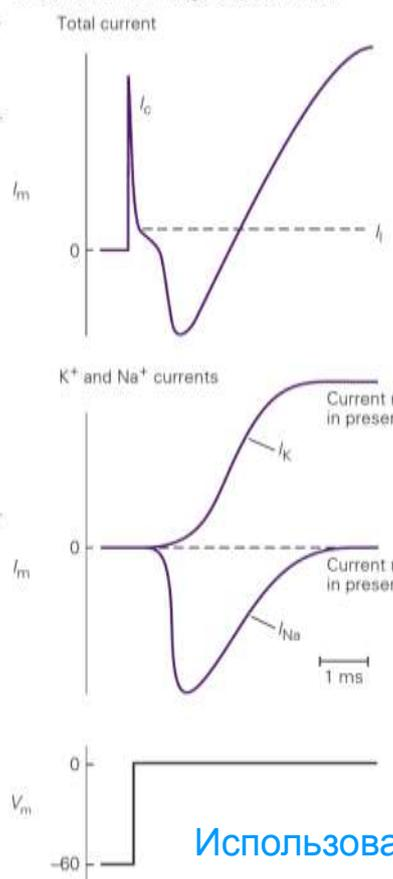
Исследования ионных токов в аксоне кальмара



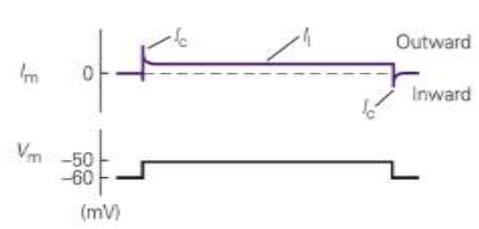
Ходжкин-Хаксли: разделение токов на I_{Na} и I_K



B Currents from large depolarization



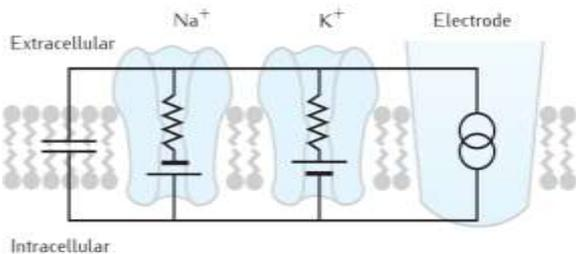
A Currents from small depolarization



Замена ионного состава среды

Использование блокаторов

Формализм описания ионных токов в модели Ходжкина-Хаксли



Уравнение для мембранного потенциала:

$$C_m \frac{dV}{dt} = I_{electrode} - \bar{g}_L (V - E_L) - \bar{g}_{Na} m^3 h (V - E_{Na}) - \bar{g}_K n^4 (V - E_K)$$

Общие положения:

- 1) $I_i = g_i (V - E_{iNernst})$ Мгновенные вольт-амперные характеристики линейны
- 2) $g_i = \bar{g}_i w^y v^\delta$ Мгновенная проводимость — макс. проводимость, умноженная на весовые коэфф. в определ. степени
- 3) $\frac{dw}{dt} = \frac{1}{\tau_w} (w_\infty - w) \equiv \alpha_w (1 - w) - \beta_w w$ кинетика весовых коэффициентов
- 4) $\alpha_w = f_1(V), \beta_w = f_2(V)$ Параметры кинетики — сложные функции от потенциала

$$I_k = \bar{g}_K n^4 (V - E_K)$$

К-ток (через К-каналы)

$$I_{Na} = \bar{g}_{Na} m^3 h (V - E_{Na})$$

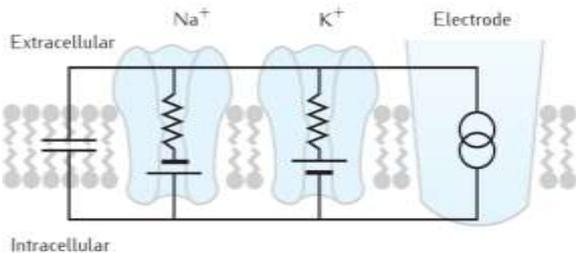
Na-ток (через Na-каналы)

$$I_L = \bar{g}_L (V - E_L)$$

непотенциалзависимая утечка

$$\frac{dn}{dt} = \alpha_n (1 - n) - \beta_n n$$

Формализм описания ионных токов в модели Ходжкина-Хаксли



Уравнение для мембранного потенциала:

$$C_m \frac{dV}{dt} = I_{electrode} - \bar{g}_L (V - E_L) - \bar{g}_{Na} m^3 h (V - E_{Na}) - \bar{g}_K n^4 (V - E_K)$$

Общие положения:

- 1) $I_i = g_i (V - E_{iNernst})$ Мгновенные вольт-амперные характеристики линейны
- 2) $g_i = \bar{g}_i w^\gamma v^\delta$ Мгновенная проводимость — макс. проводимость, умноженная на весовые коэфф. в определ. степени
- 3) $\frac{dw}{dt} = \frac{1}{\tau_w} (w_\infty - w) \equiv \alpha_w (1 - w) - \beta_w w$ кинетика весовых коэффициентов
- 4) $\alpha_w = f_1(V), \beta_w = f_2(V)$ Параметры кинетики — сложные функции от потенциала

$$I_k = \bar{g}_K n^4 (V - E_K)$$

К-ток (через K-каналы)

$$I_{Na} = \bar{g}_{Na} m^3 h (V - E_{Na})$$

Na-ток (через Na-каналы)

$$I_L = \bar{g}_L (V - E_L)$$

непотенциалзависимая утечка

$$\frac{dn}{dt} = \alpha_n (1 - n) - \beta_n n$$

$$\frac{dm}{dt} = \alpha_m (1 - m) - \beta_m m$$

$$\frac{dh}{dt} = \alpha_h (1 - h) - \beta_h h$$

динамика “воротных частиц”

$$\alpha_n = 0.01 \frac{V+55}{1 - \exp[-\frac{V+55}{10}]}$$

$$\alpha_m = 0.1 \frac{V+40}{1 - \exp[-\frac{V+40}{10}]}$$

$$\alpha_h = 0.07 \exp[-\frac{V+65}{20}]$$

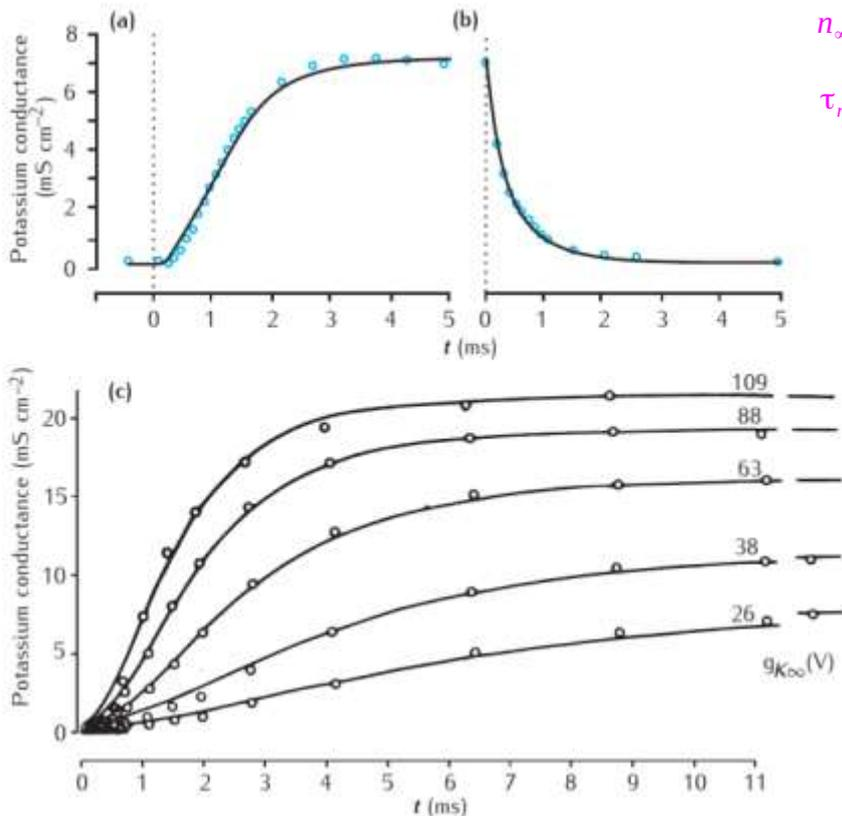
$$\beta_n = 0.125 \exp[-\frac{V+65}{80}]$$

$$\beta_m = 4 \exp[-\frac{V+65}{18}]$$

$$\beta_h = \frac{1}{\exp[-\frac{V+35}{10}] + 1}$$

Формализм (модель) Ходжкина-Хаксли

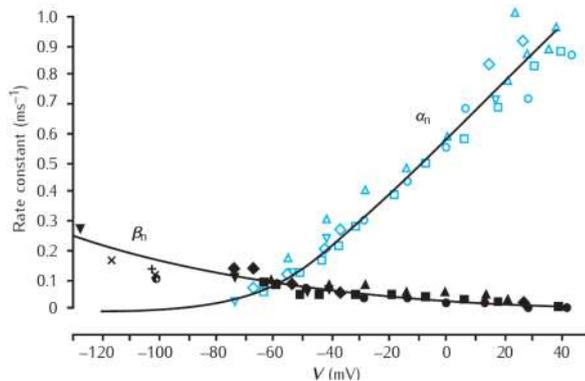
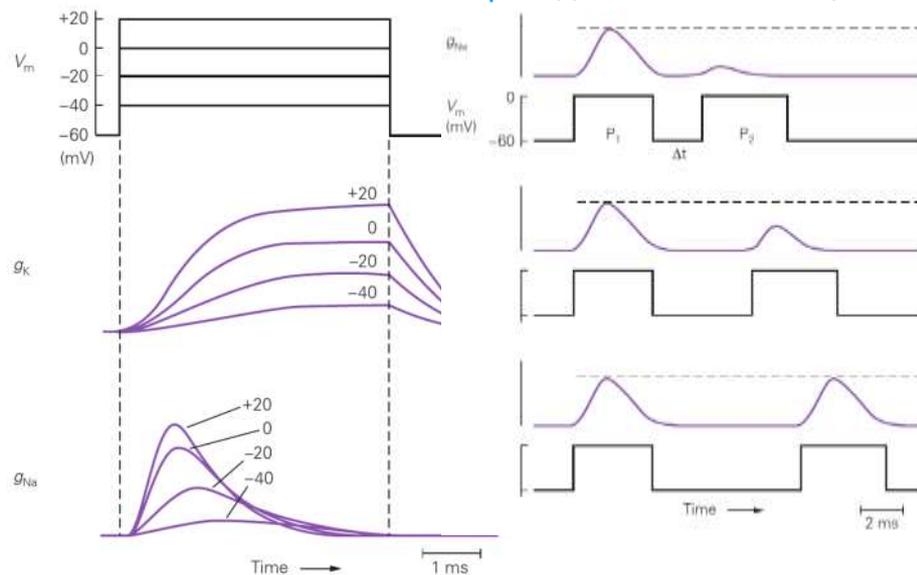
Зависимость K проводимости от потенциала



$$n_{\infty} = \frac{\alpha_n}{\alpha_n + \beta_n}$$

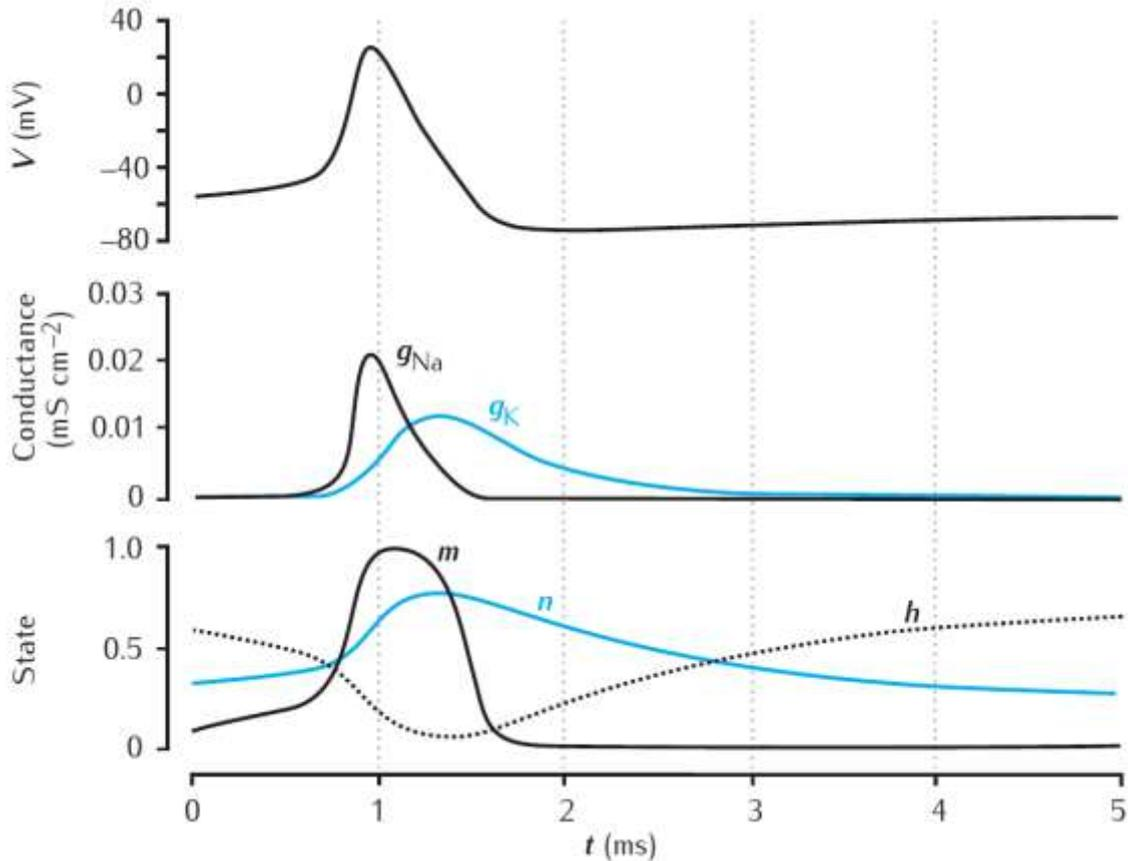
$$\tau_n = \frac{1}{\alpha_n + \beta_n}$$

Зависимость Na⁺ проводимости от потенциала

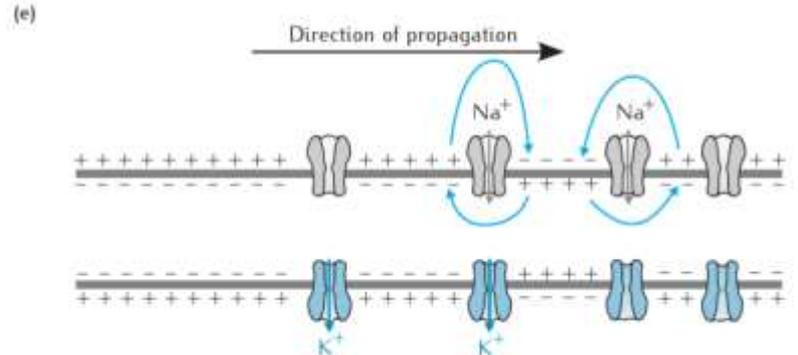
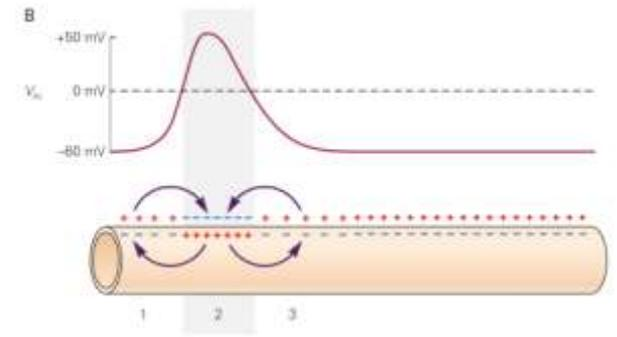
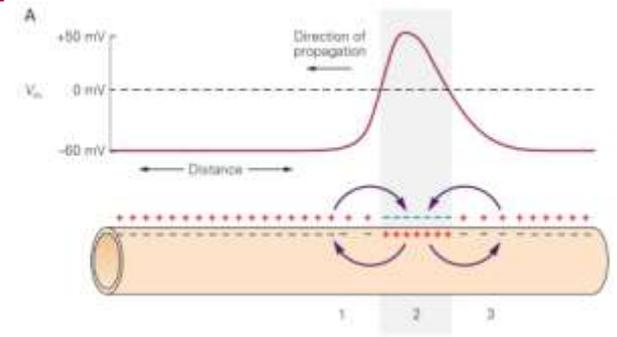


определение параметров α и β по экспериментальным данным

Генерация и проведение ПД в нервном волокне кальмара



$$C_m \frac{dV}{dt} = I_{electrode} - \bar{g}_L(V - E_L) - \bar{g}_{Na} m^3 h (V - E_{Na}) - \bar{g}_K n^4 (V - E_K)$$



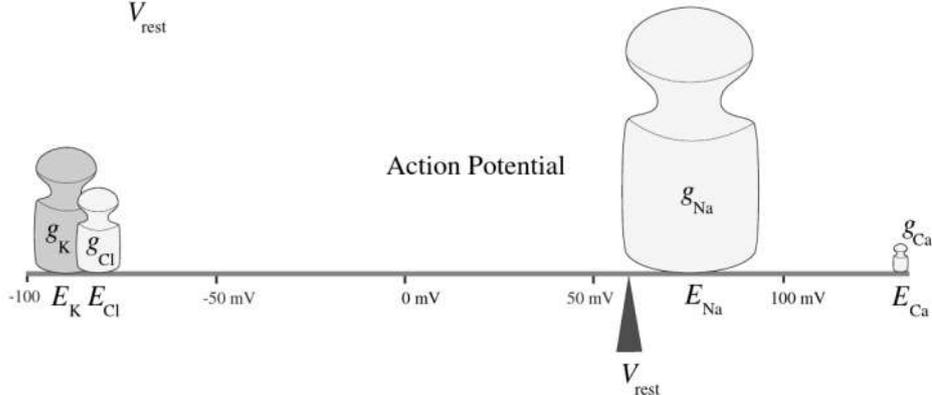
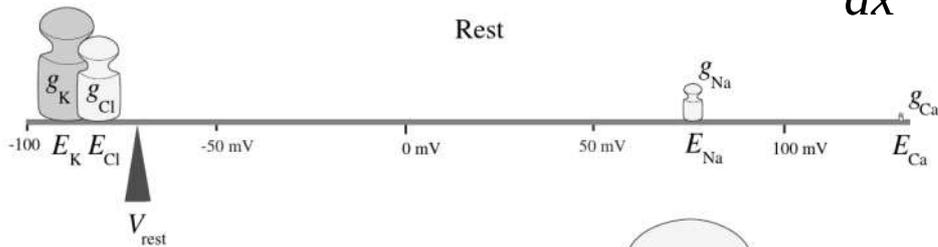
Электрохимический потенциал и электродиффузия

Электрохимический потенциал: $\bar{\mu} = \mu_0 + RT \ln a + zF \varphi$

a : активность
 z : заряд иона
 F : число Фарадея
 R : газовая постоянная
 φ : потенциал

Поток $J = a \left(-\frac{d\mu}{dx} \right) u = -au \left(RT \frac{1}{a} \frac{da}{dx} + zF \frac{d\varphi}{dx} \right)$

активность Движ. сила подвижность



$$J = -uRT \frac{da}{dx} - uazF \frac{d\varphi}{dx}$$

$\left[\frac{\text{МОЛЬ}}{\text{СМ}^2 \text{ С}} \right]$

Уравнение Нернста-Планка

Уравнения постоянного поля (ГХК)

$$J = C \left(-\frac{d\mu}{dx} \right) u = -u \left(RT \frac{dC}{dx} + CzF \frac{d\varphi}{dx} \right);$$

Приближение
постоянного поля $\frac{d\varphi}{dx} = \text{const} = \frac{\Delta\varphi}{h}$

$$\frac{dC}{dx} + C \frac{zF \Delta\varphi}{hRT} = \frac{-J}{uRT}$$

$$\frac{dC}{dx} = a + bC \rightarrow \int_{C'}^{C''} \frac{dC}{a + bC} = \int_0^h dx \rightarrow \frac{1}{b} \ln \frac{a + bC''}{a + bC'} = h$$

C', C'' — концентрации ионов внутри
мембраны на границах

$$J = \frac{zF}{h} \frac{C' - C'' e^{-zF \Delta\varphi / RT}}{1 - e^{-zF \Delta\varphi / RT}}$$

$C_i = \gamma C'$ коэффициент
распределения

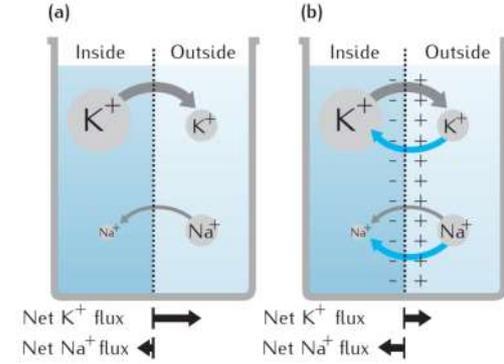
$C_o = \gamma C''$

$P = uRT \frac{\gamma}{h}$ проницаемость

$$\left[\frac{\text{моль}}{\text{см}^2 \text{с}} \right] J = P \frac{zF}{RT} \frac{C_i - C_o e^{-zF \Delta\varphi / RT}}{1 - e^{-zF \Delta\varphi / RT}},$$

$$I = zFJ$$

Уравнение Гольдмана-Ходжкина-Катца
для потока (тока) ионов через мембрану

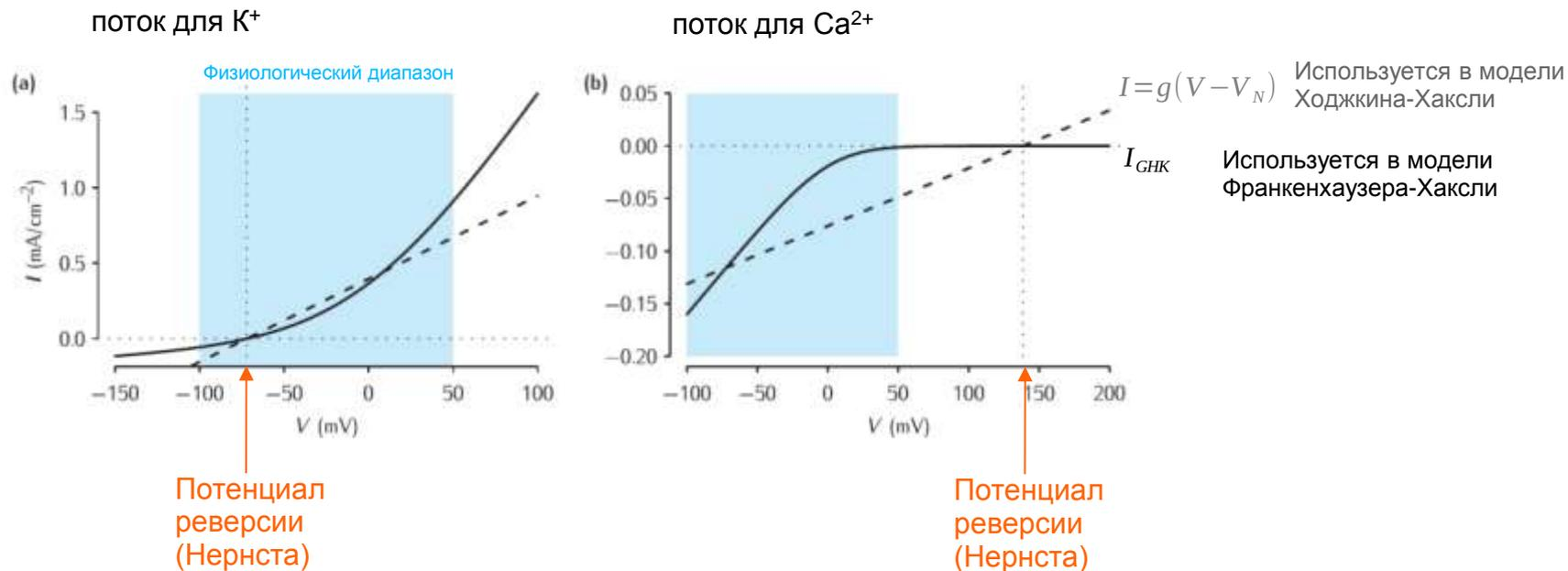


Равновесие суммарному
току, но не по потокам
каждого иона

Уравнение Гольдмана для
равновесного потенциала:

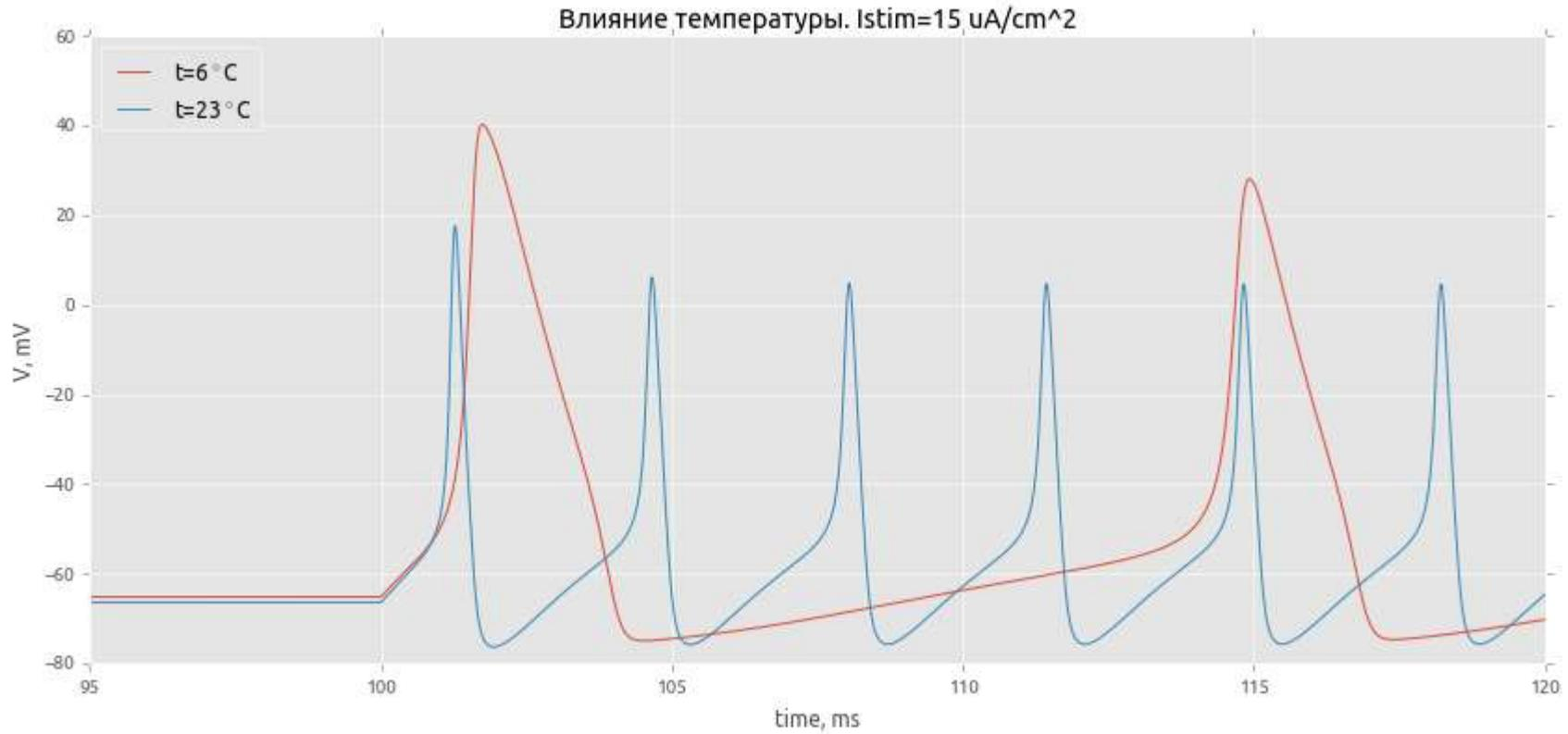
$$\sum_k I_k = 0 \rightarrow \Delta\varphi = \frac{RT}{F} \ln \frac{\sum_k P_k [Cat]_{k,out} + \sum_k P_k [Ani]_{k,in}}{\sum_k P_k [Cat]_{k,in} + \sum_k P_k [Ani]_{k,out}}$$

Вольт-амперные характеристики в приближении ГХК

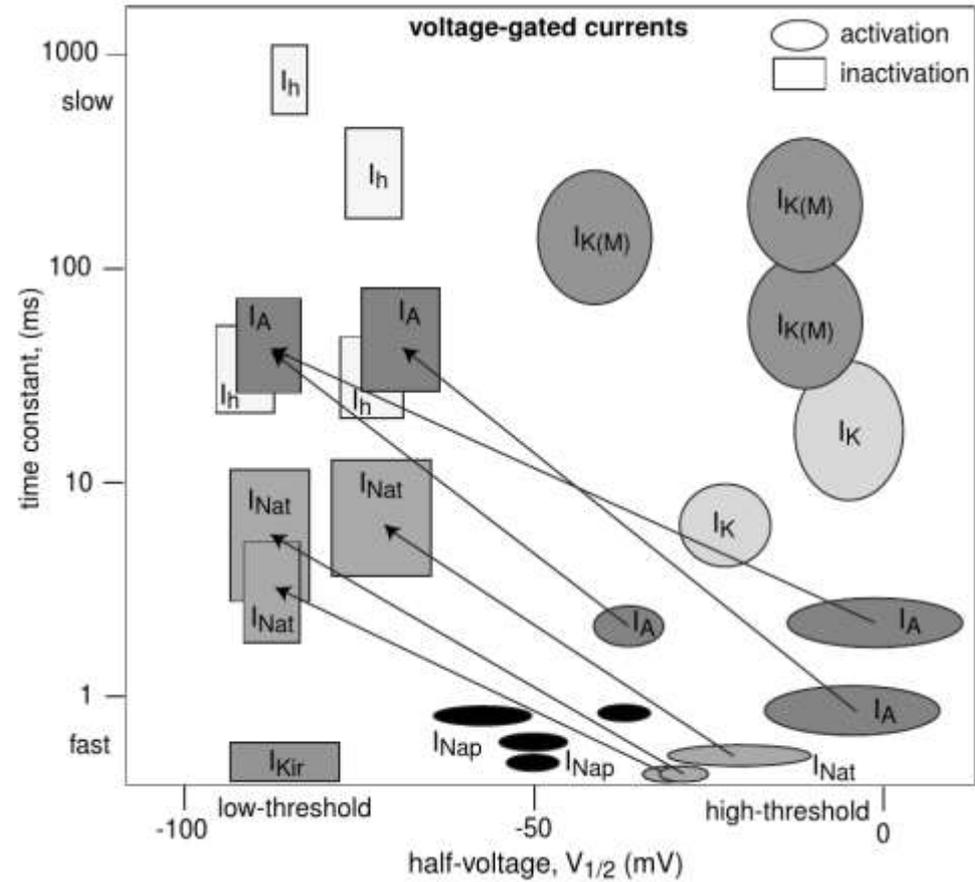


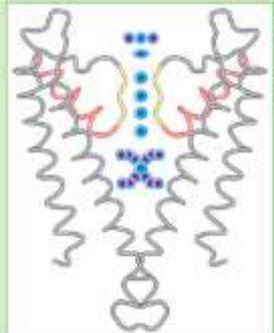
- “выпрямление” тока — проводимость в одну сторону выше, чем в другую
- чем больше разность концентраций иона, тем сильнее нелинейность

$$\alpha(T) = \alpha(T_0) Q_{10}^{\frac{T-T_0}{10}}$$



Зоопарк ионных токов





Ионные каналы

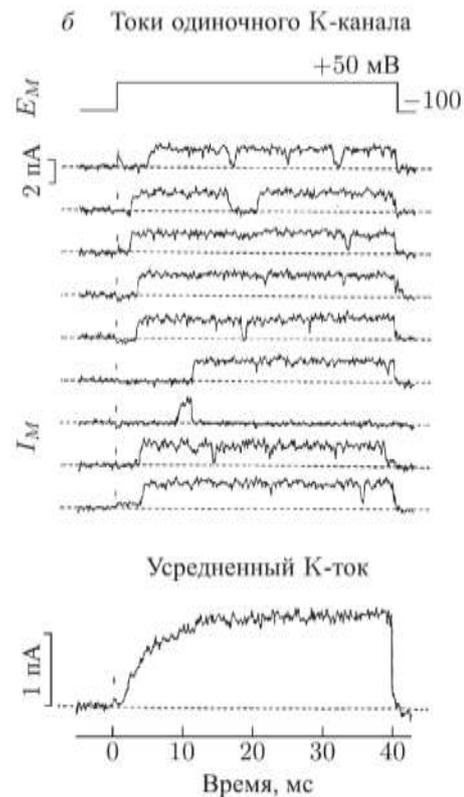
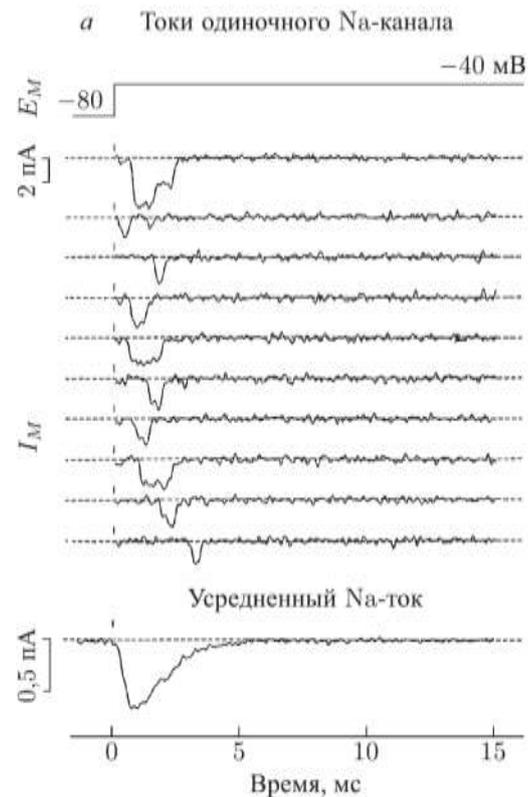
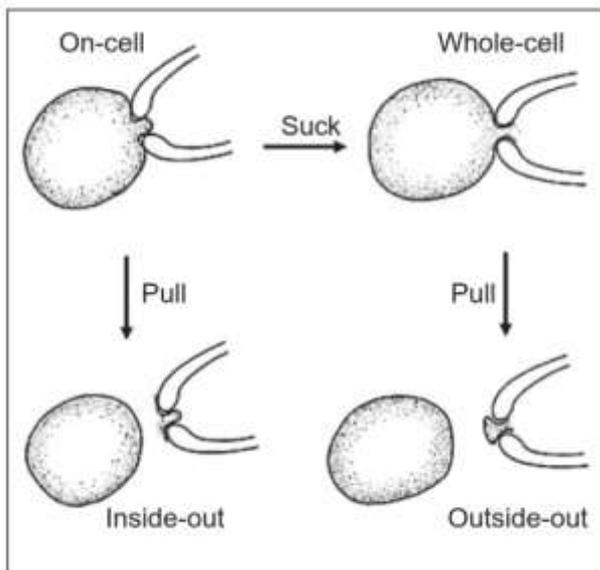
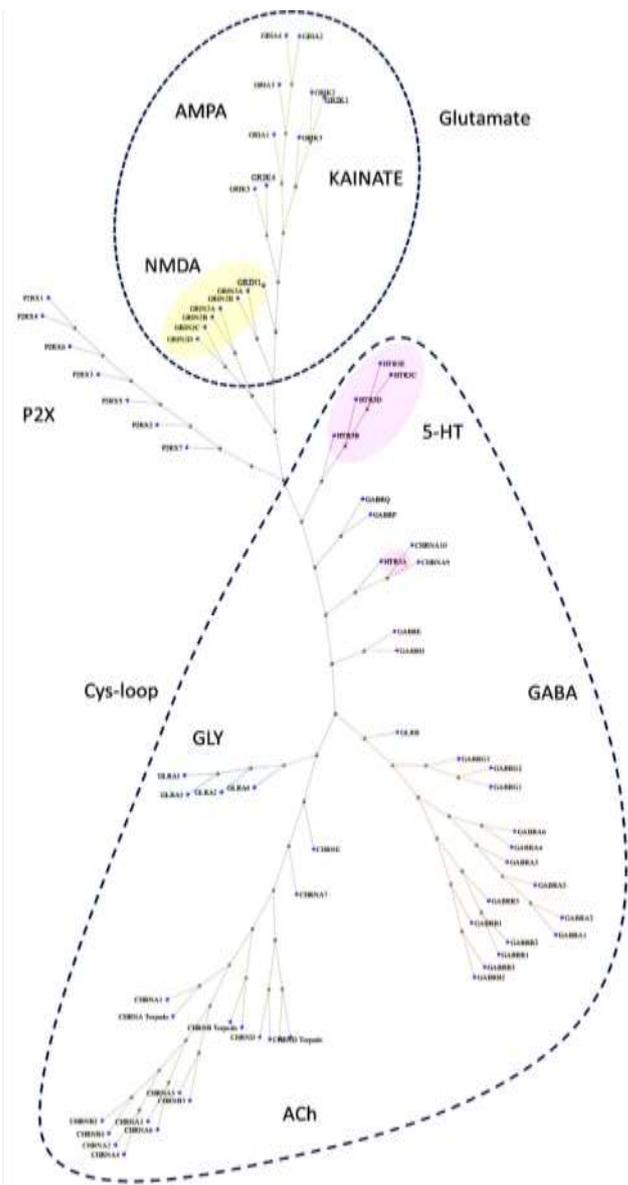
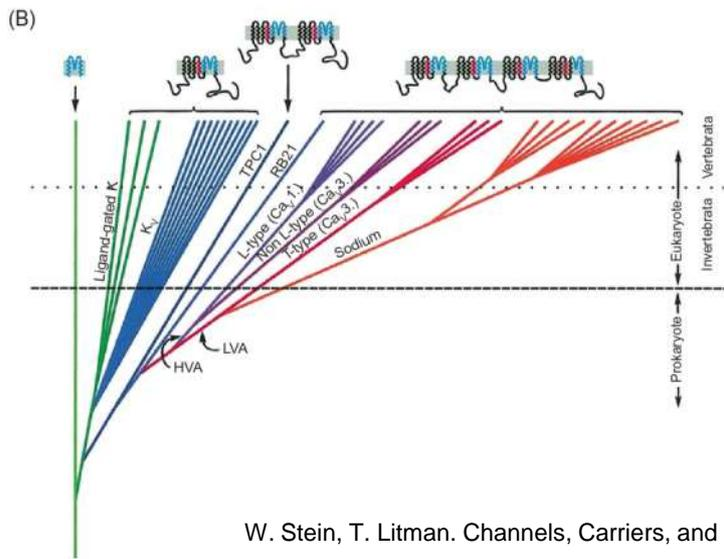
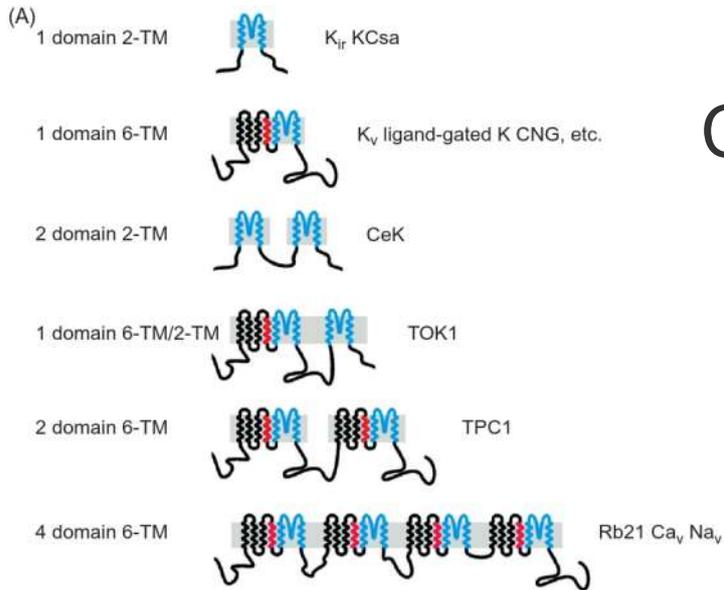


Рис. 18.10. Токи одиночных каналов и интегральный ионный ток (по Hille В., 1992)

Семейства каналов



Семейство потенциал-зависимых каналов

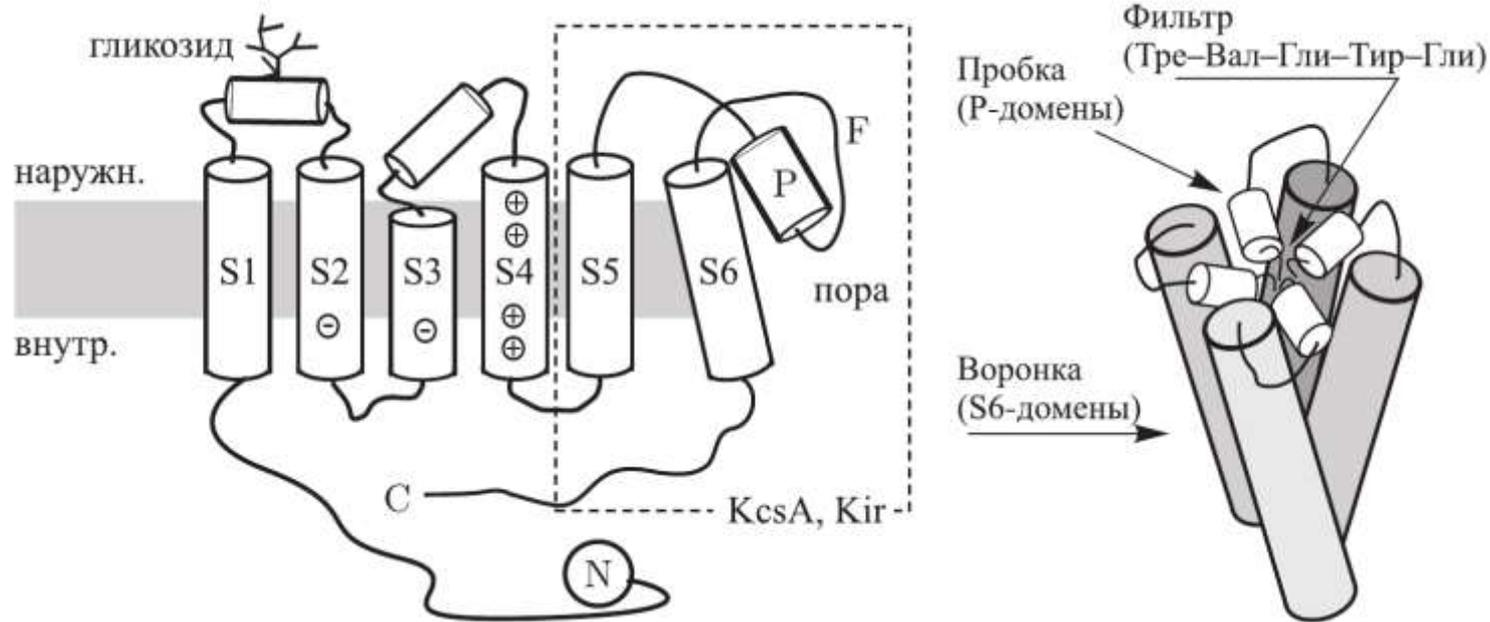


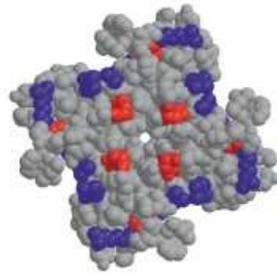
Рис. 18.12. Схема структуры α -субъединицы K-каналов (I) и организации поры доменами S6 и P при тетрамеризации (II)

I — Пунктиром выделены наиболее консервативные домены S5, S6, P — базовые трансмембранные домены всех K-каналов. Домен S4 несет заряженные аминокислоты, определяющие потенциалчувствительность. II — Показано, как четыре домена S6 образуют воронку с пробкой из доменов P и селективного фильтра. Изгиб граней воронки приводит к открытию ее нижней (воротной) части.

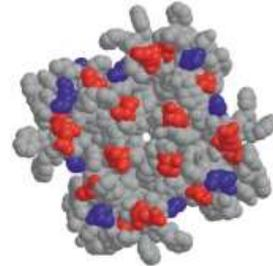
Семейство Kv-каналов

Human Molecular Genetics, 2002, Vol. 11, No. 20 2427

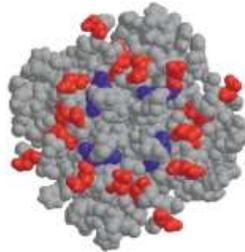
кислотные остатки
основные остатки



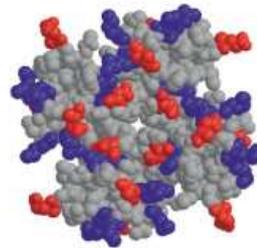
KcsA



Shak



Kir62



GluR0

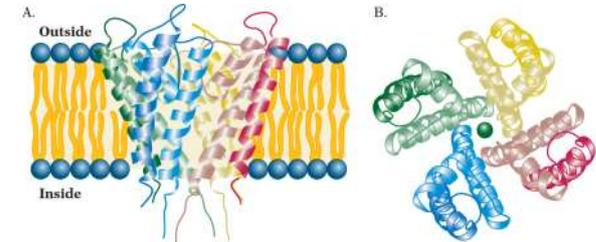
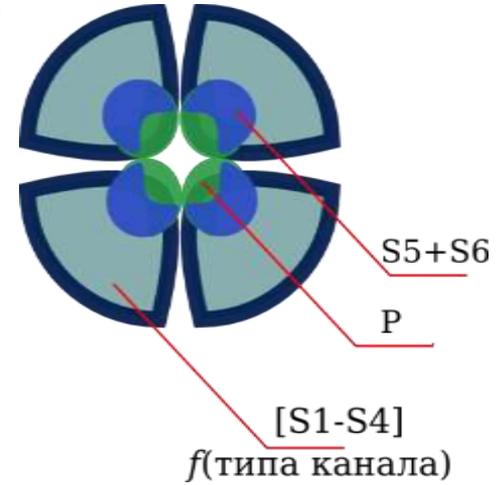


Figure 2. K-channel homology models: KcsA, Shaker, Kir6.2 and GluR0. Each model is viewed from the filter-end mouth (i.e. the extracellular mouth for the K channels and the intracellular mouth for GluR0) down the pore. Acidic residues are coloured red, basic blue and others grey.

Центральная полость

296

M.S.P. Sansom et al. / Biochimica et Biophysica Acta 1565 (2002) 294–307

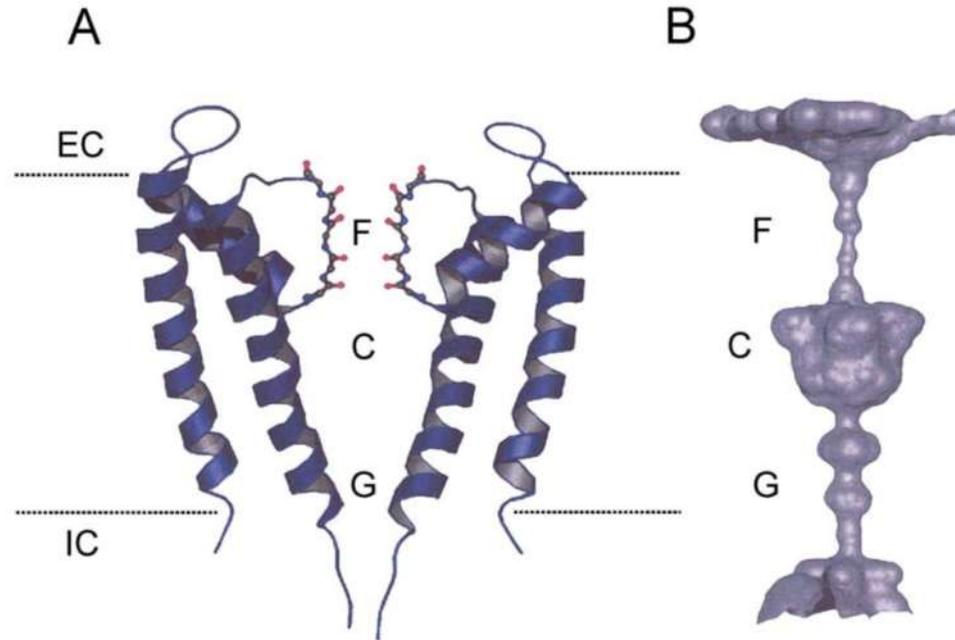
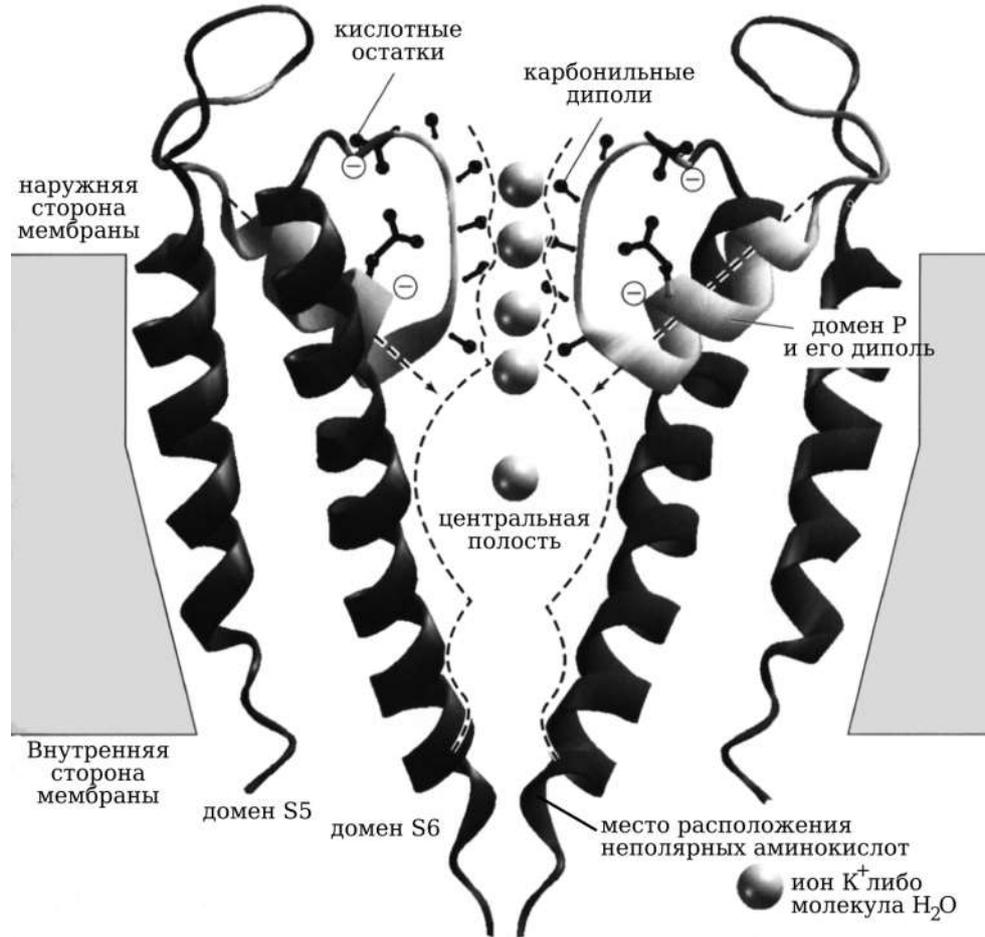


Fig. 2. KcsA fold and pore. (A) Two of the four subunits of KcsA, viewed down a perpendicular to the pore axis. The helices are shown as ribbons; all backbone atoms of the selectivity filter are shown in ball-and-stick format. The lipid bilayer is indicated by the horizontal dotted lines. IC= intracellular; EC= extracellular. (B) The pore-lining surface of KcsA (calculated using HOLE [107,108]) aligned with the fold diagram in (A) and showing the filter (F), cavity (C) and gate (G) regions. Diagrams generated using VMD [109] and Povray.

Стабилизация ионов внутри канала



Воротный механизм

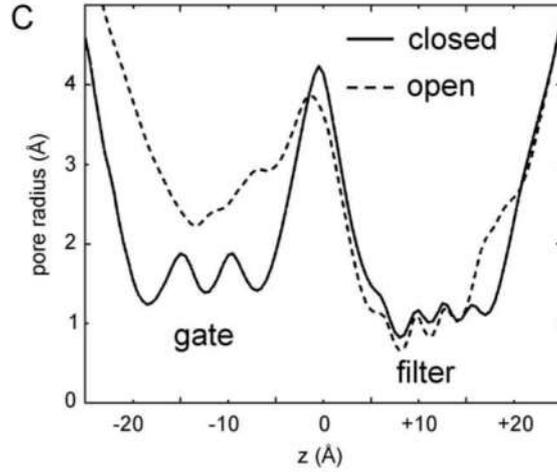
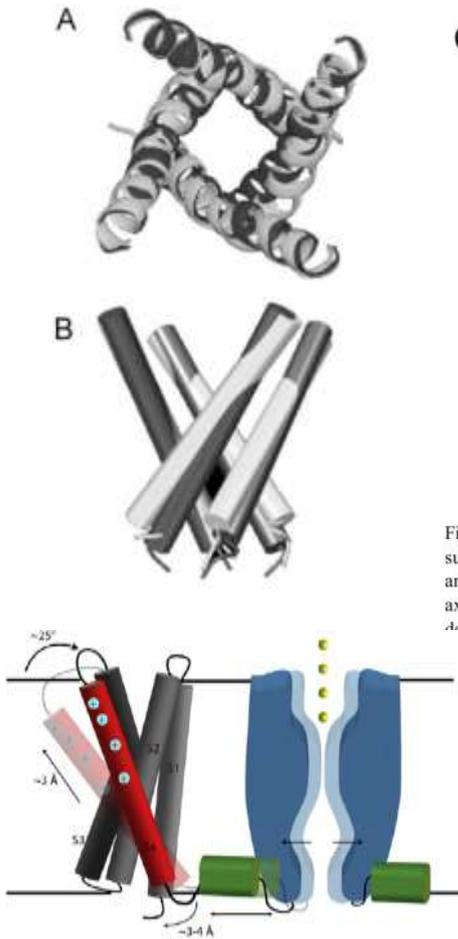
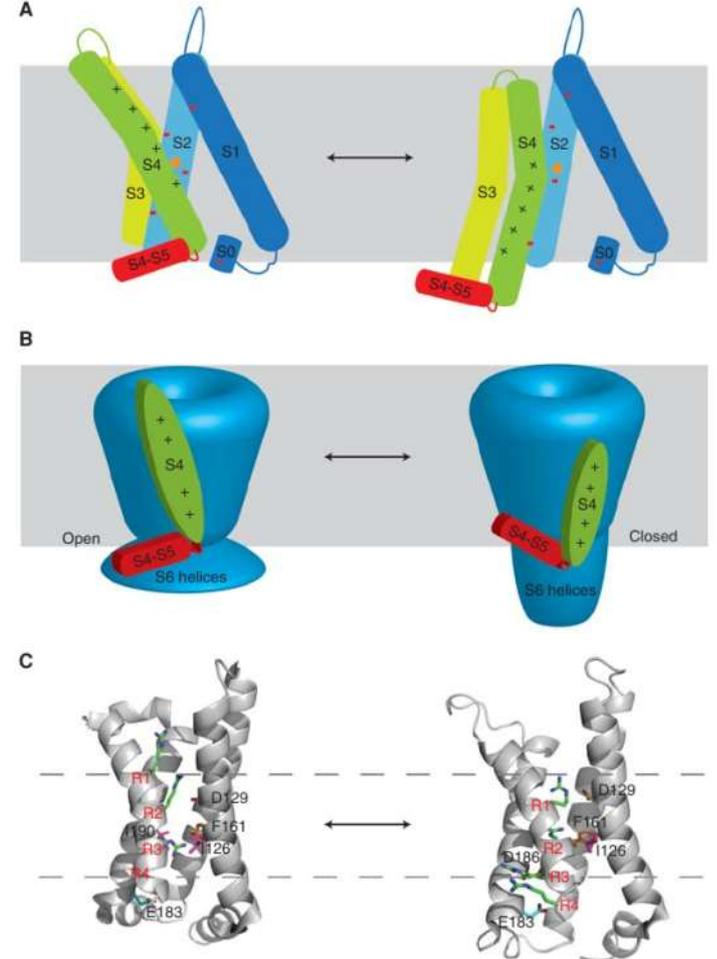
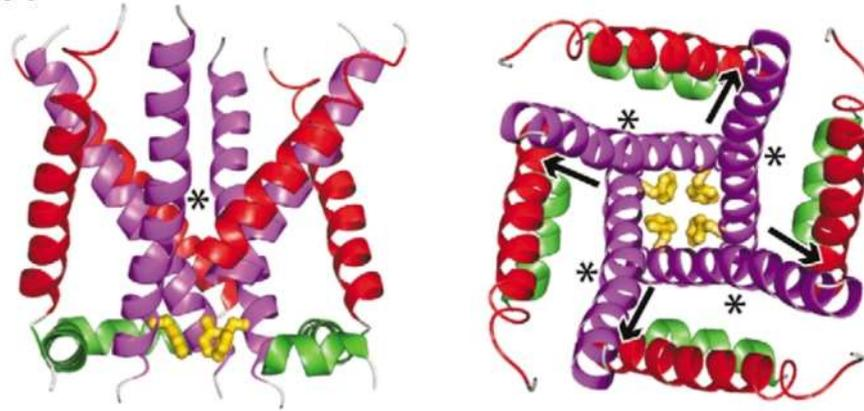


Fig. 8. Modelling the open state of KcsA. The two upper diagrams show a superimposition of the M2 helices from the closed structure (dark grey) and an open state model (light grey) of KcsA. (A) View looking down the pore axis from the filter towards the intracellular mouth of the channel. (B) View shown a perpendicular to the pore axis, the extracellular (filter) end of the helices at the top and the intracellular (gate) end of the helices at the bottom. (C) Pore radius profiles for closed (solid line) and open (broken line) state models of the KcsA channel. Both profiles are averages derived from simulations (see Ref. [61] for details).

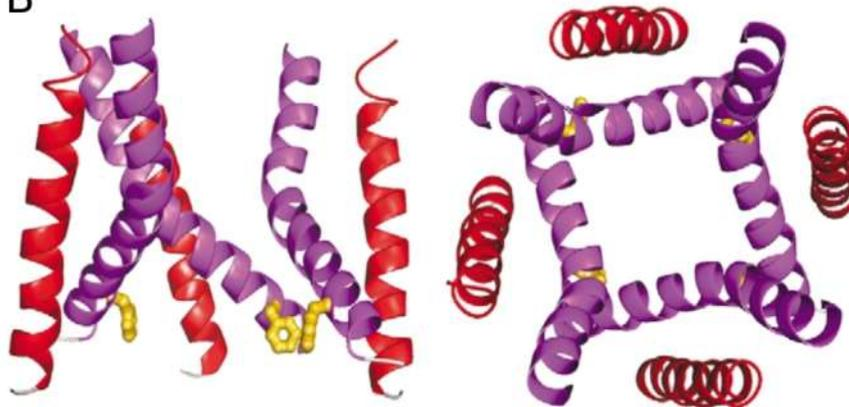


Воротный механизм

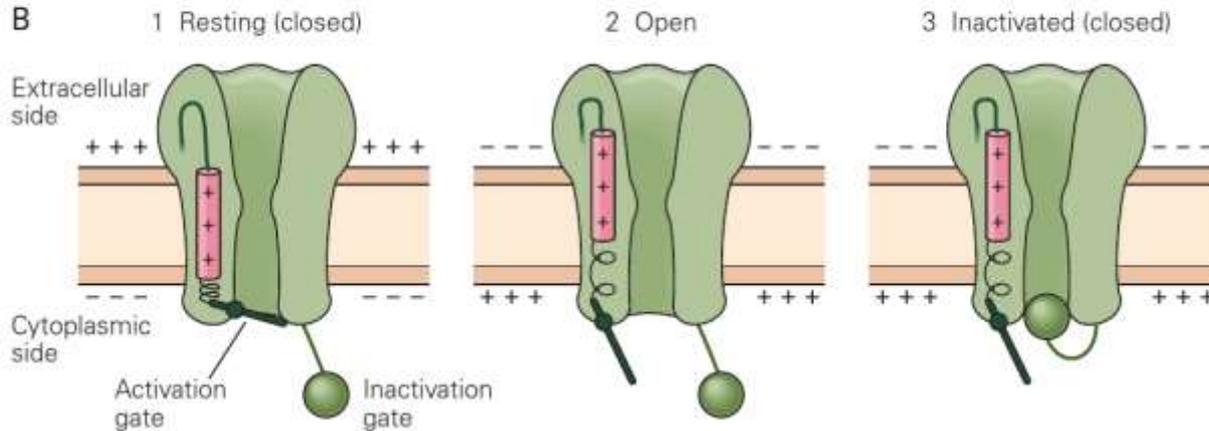
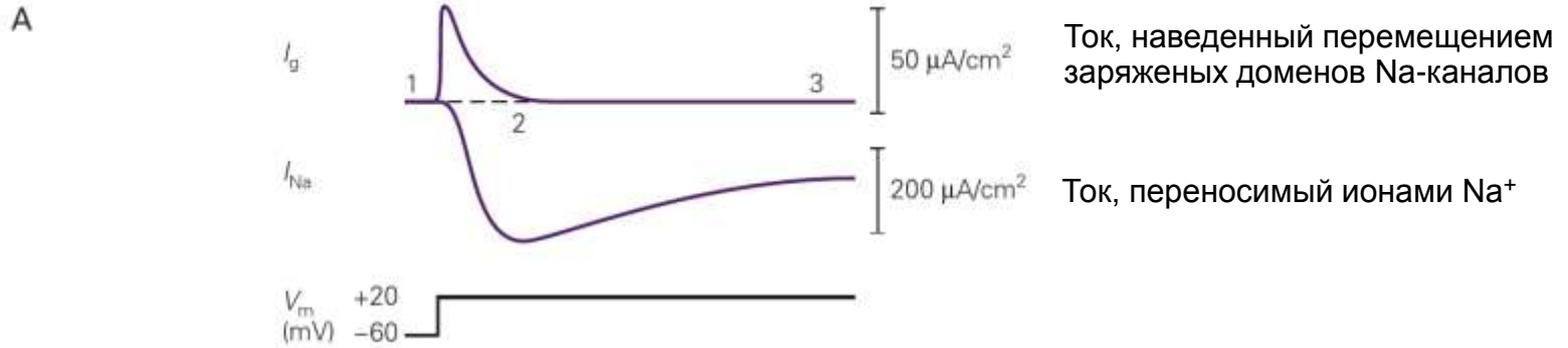
А

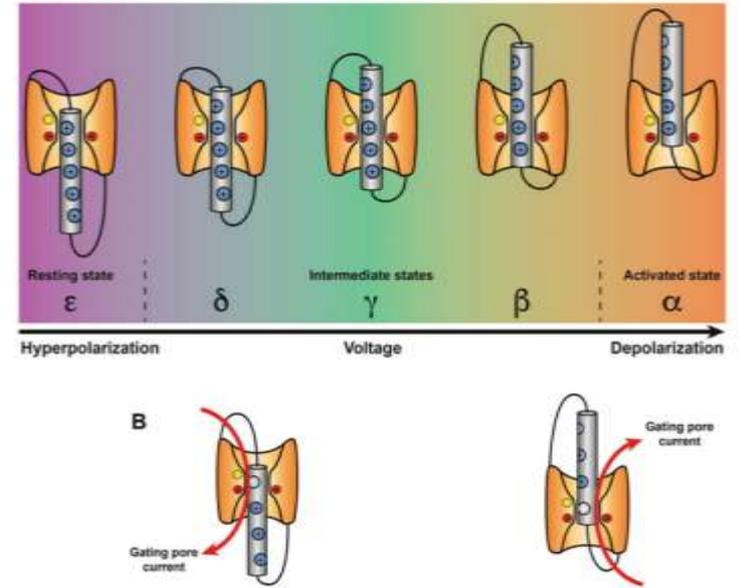
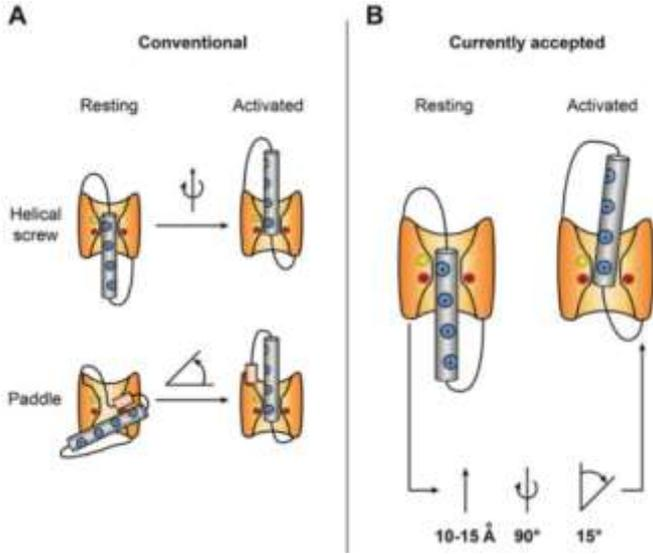


Б



Конформационные изменения каналов и воротные ТОКИ

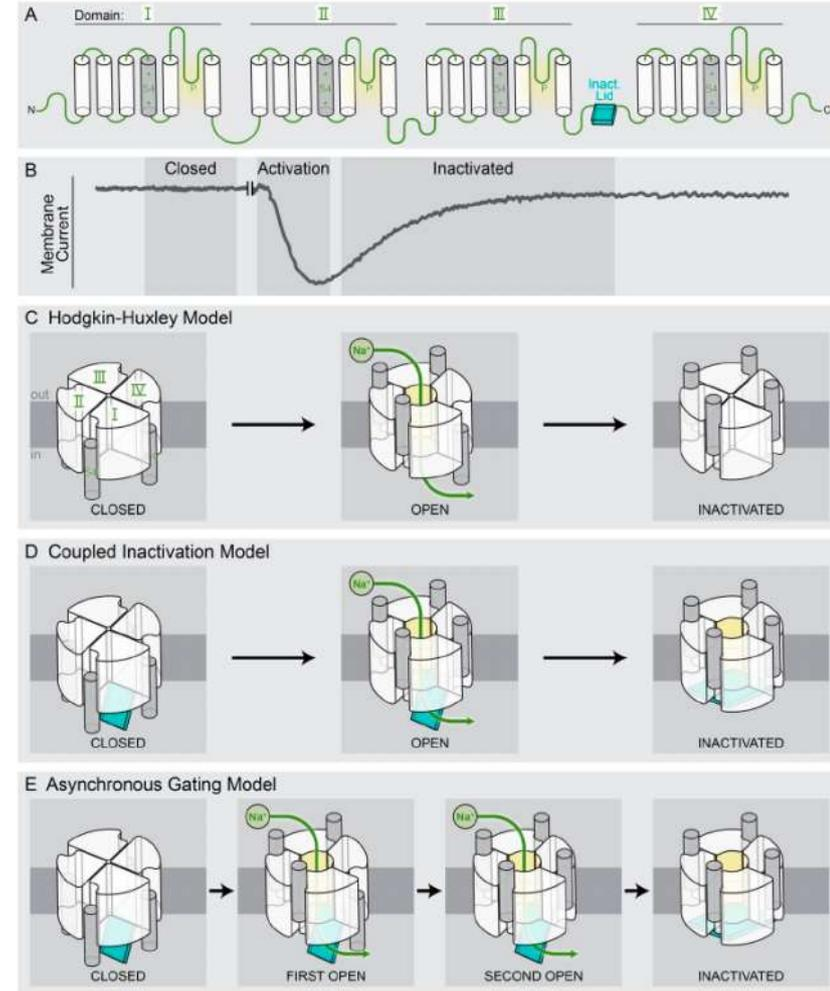
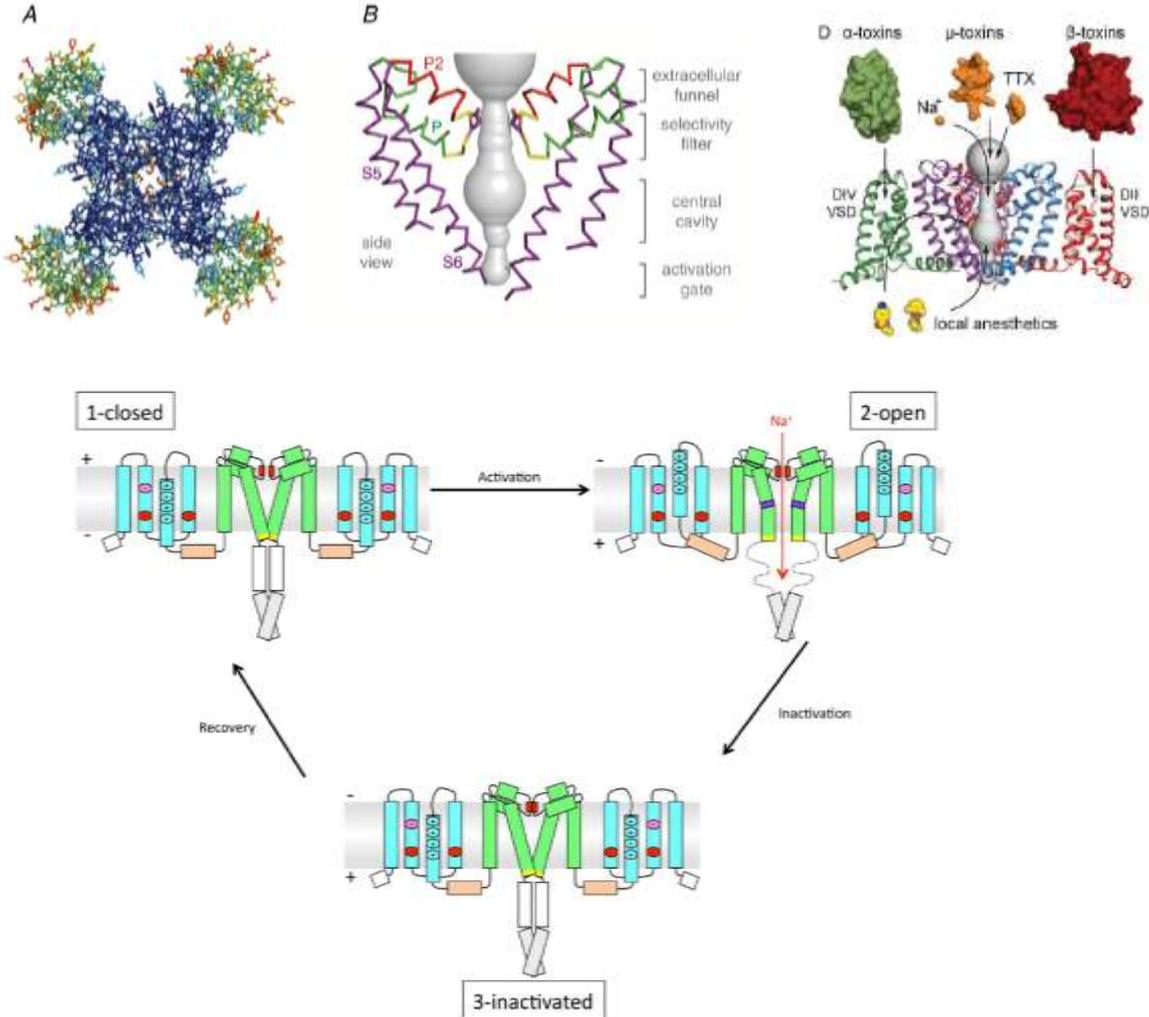




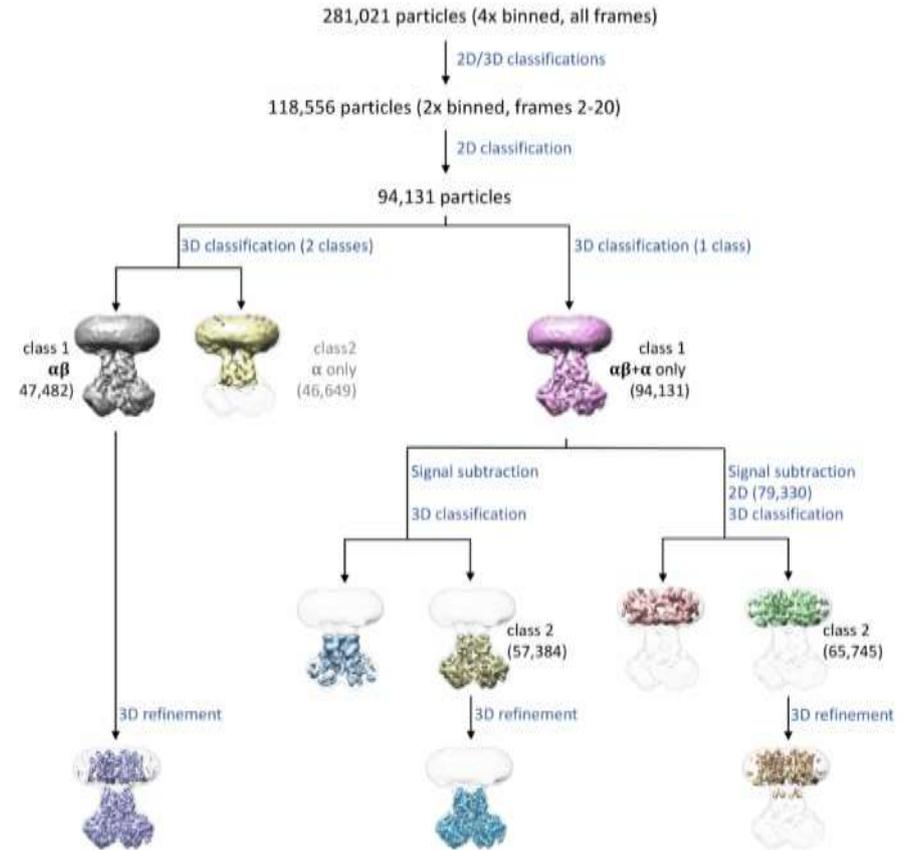
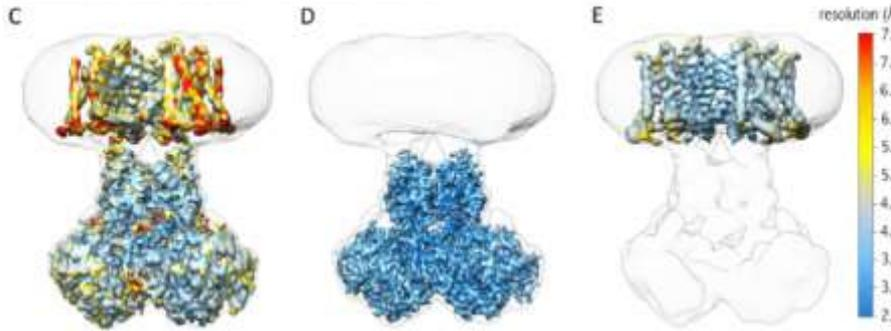
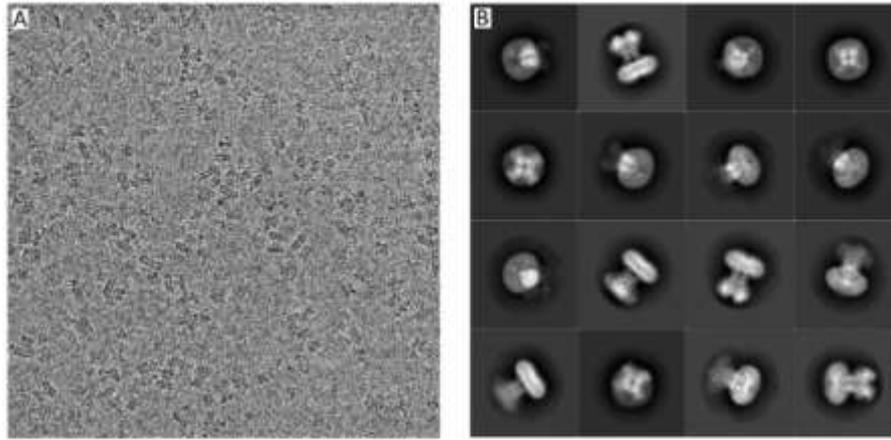
Groome et al 2017

© Springer International Publishing AG 2017
 M. Chahine (ed.), *Voltage-gated Sodium Channels: Structure, Function and Channelopathies*, Handbook of Experimental Pharmacology 246,
https://doi.org/10.1007/164_2017_54

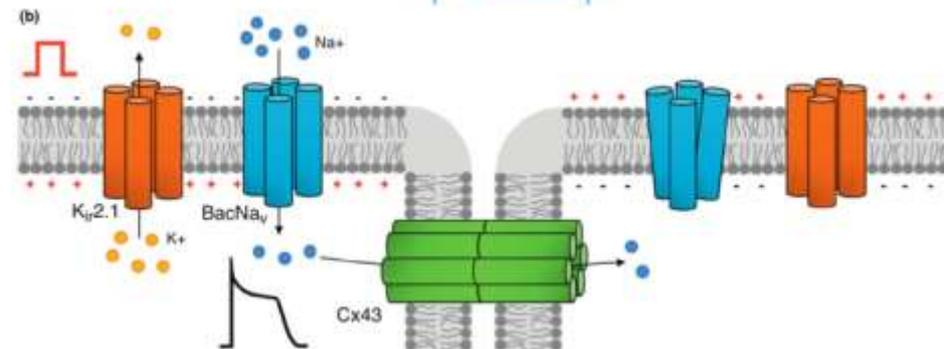
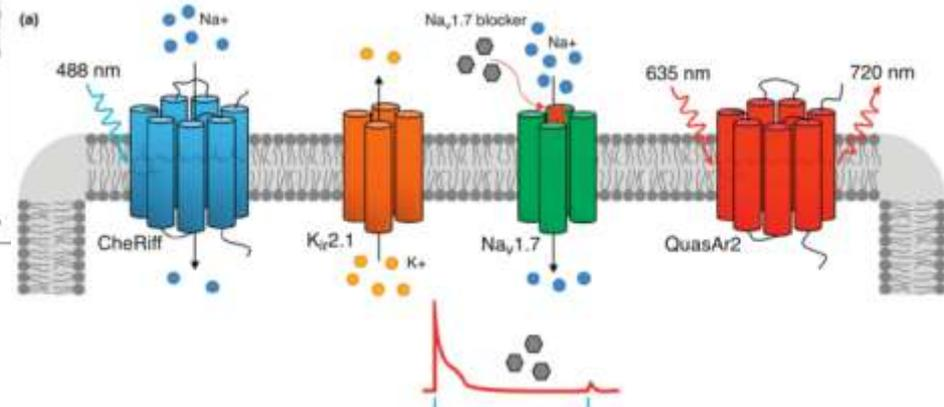
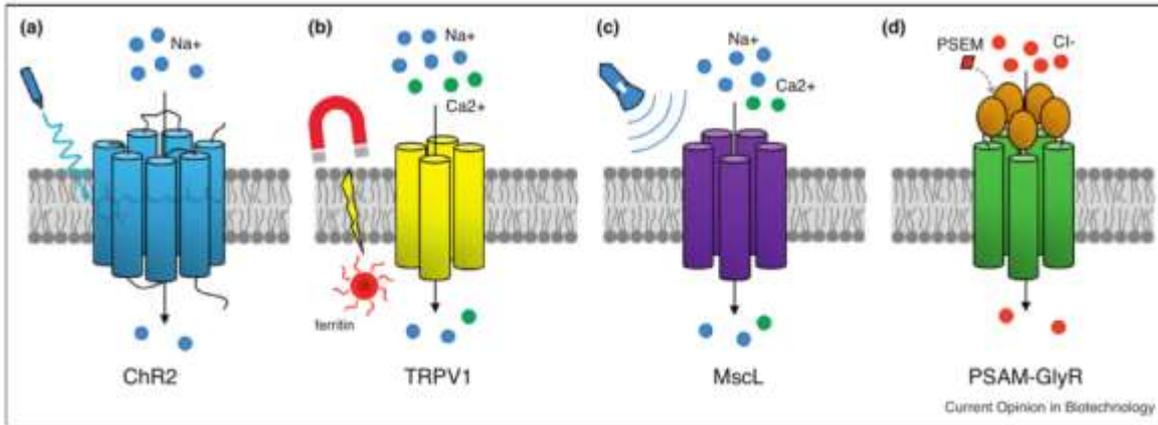
Na_v-каналы: инактивация



Методы исследования структуры каналов: CryoEM



Создание каналов с новыми свойствами



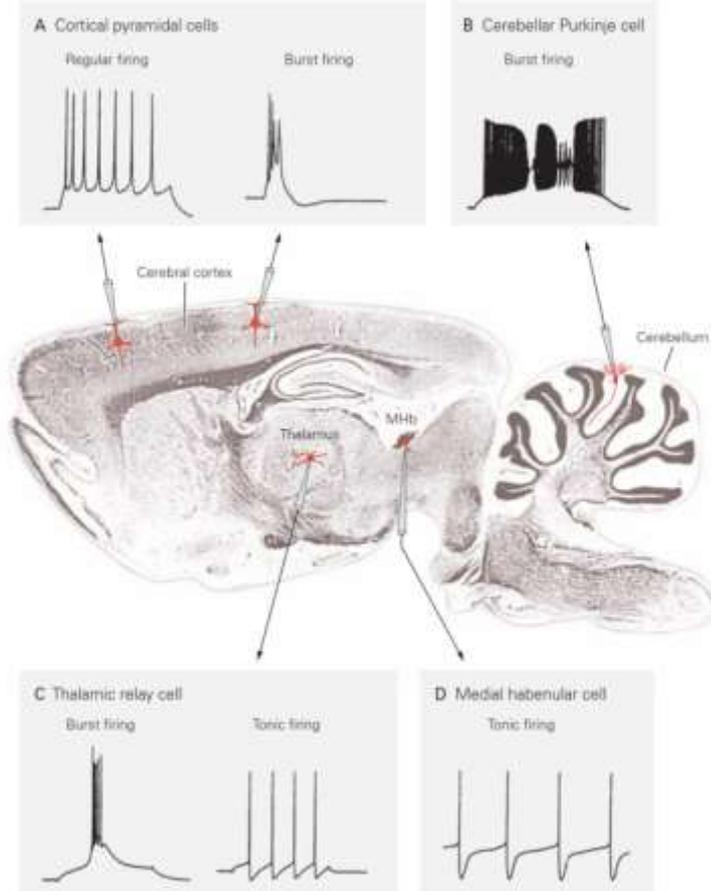
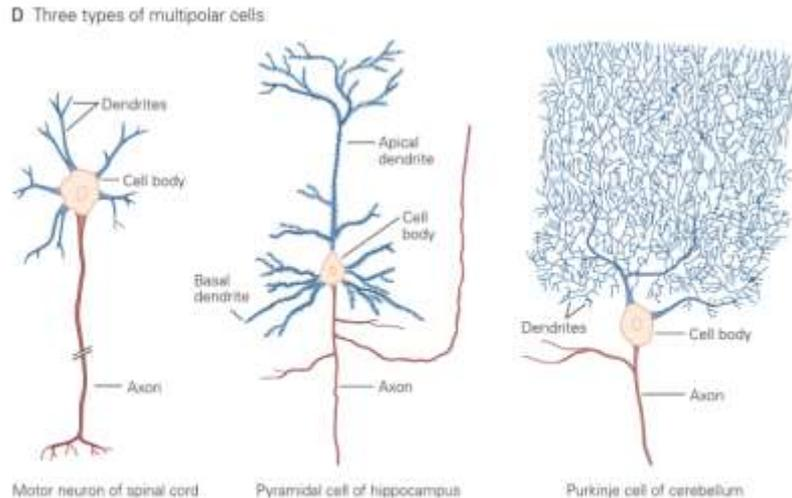
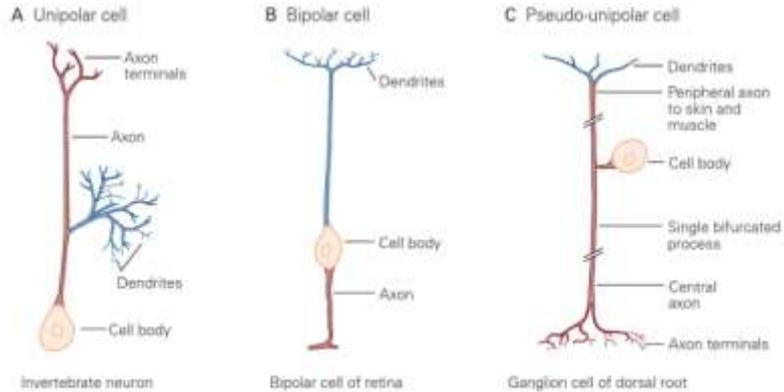
Ion channel engineering for modulation and *de novo* generation of electrical excitability

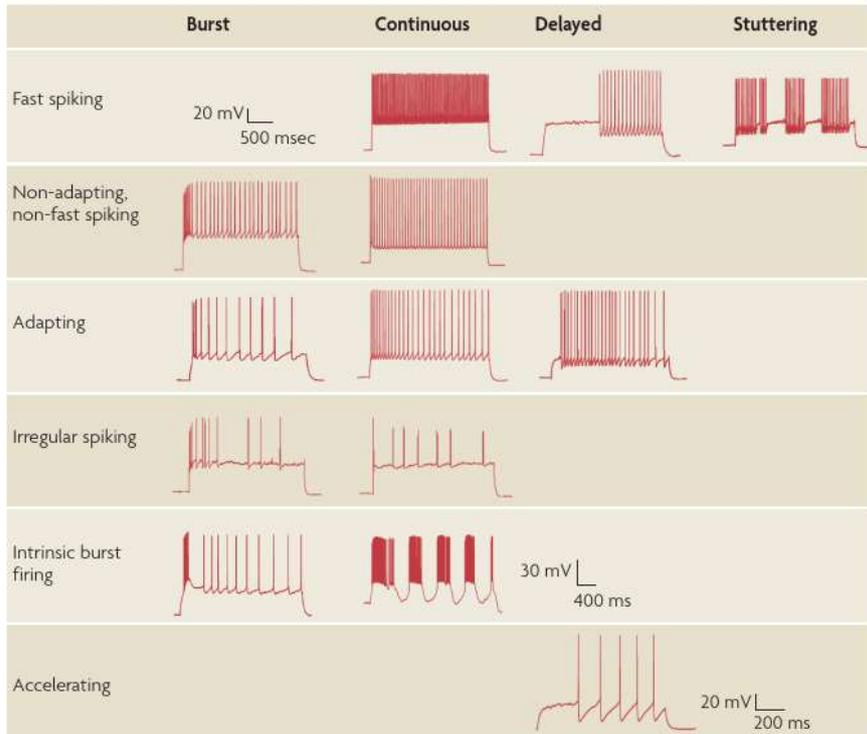
Hung X Nguyen and Nenad Bursac

Current Opinion in Biotechnology 2019, 58:100–107

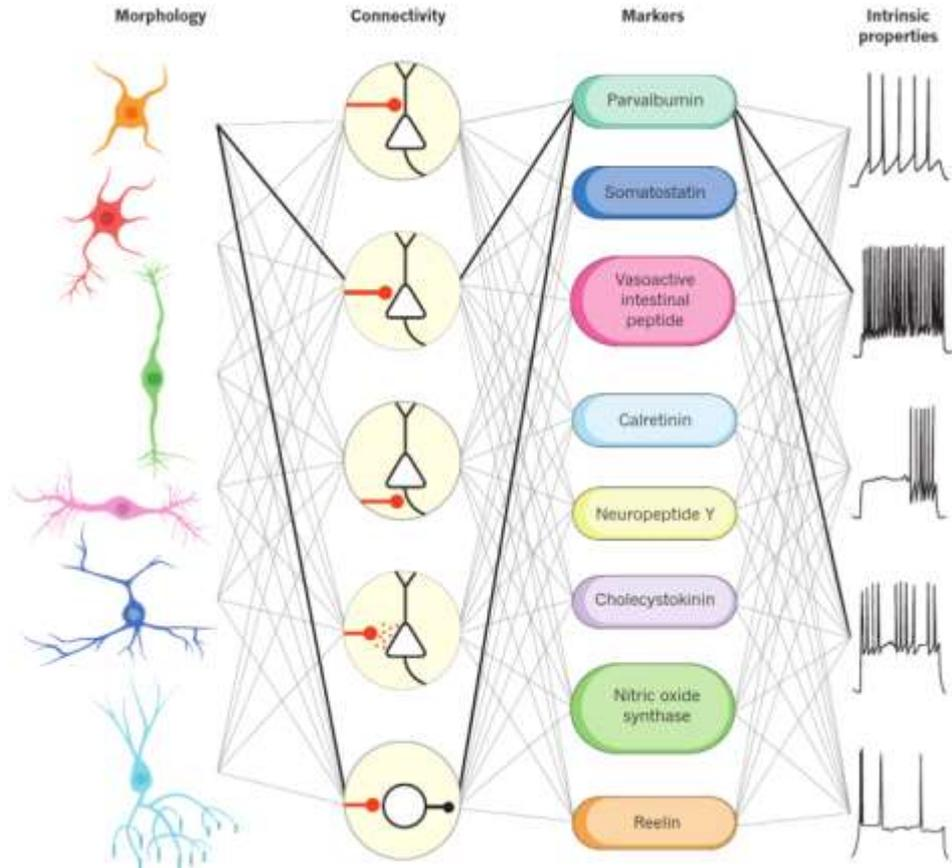
Возбудимость нервных клеток

Разные типы нейронов по-разному отвечают на деполяризацию



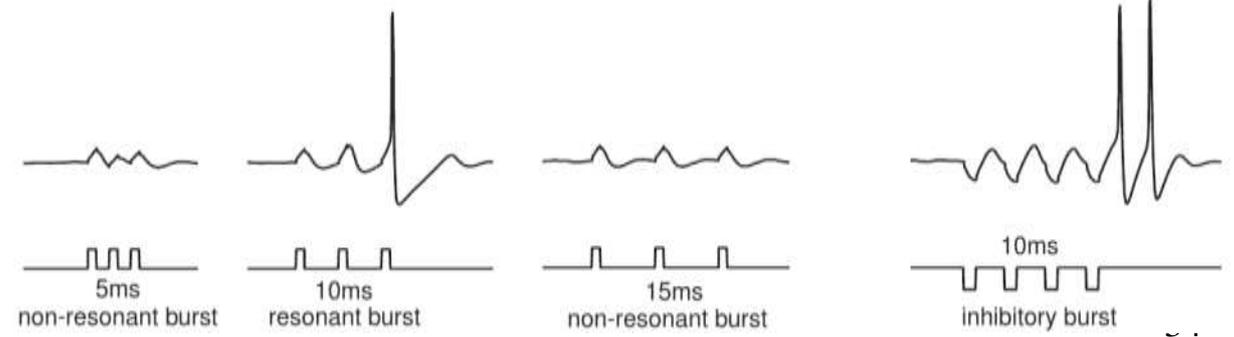
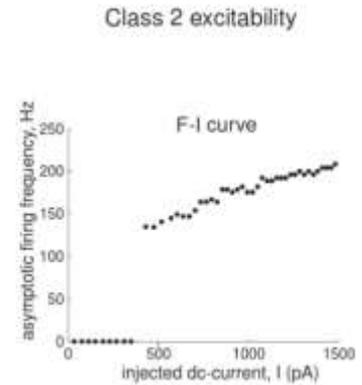
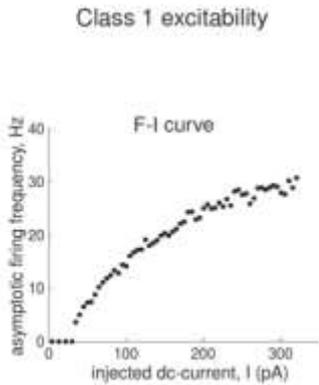
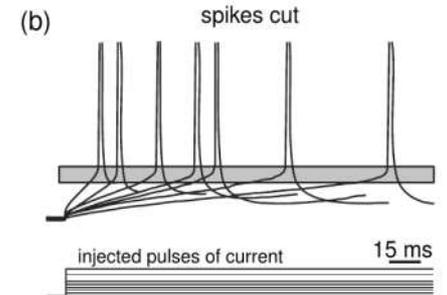
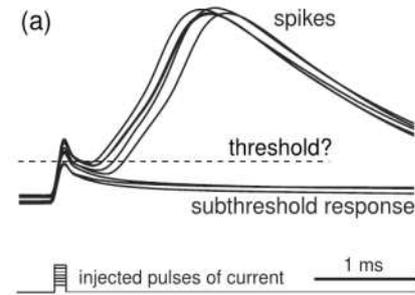
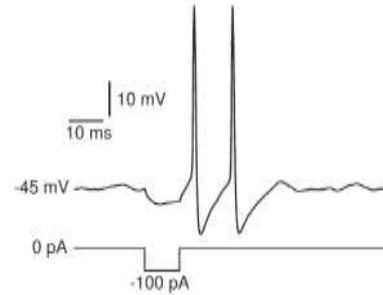
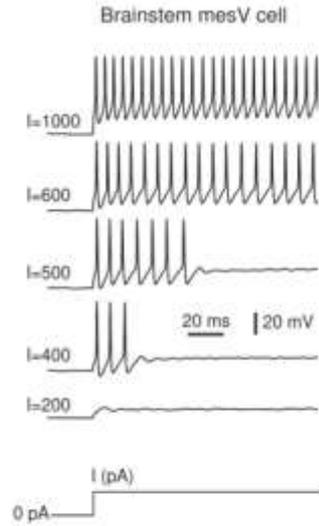
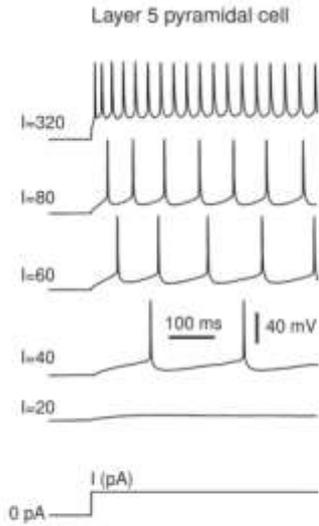


Ascoli et al *Nat neurosci* 2008

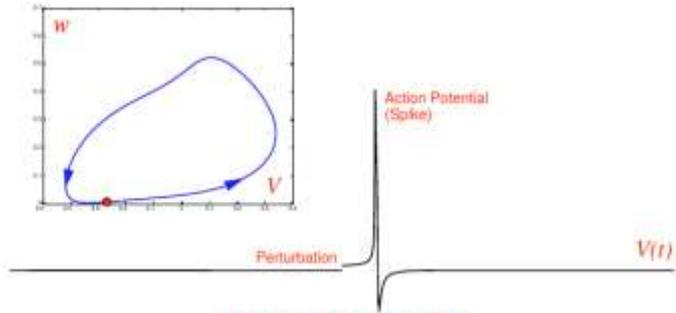


Kepecs & Fishell *Nature* 2014

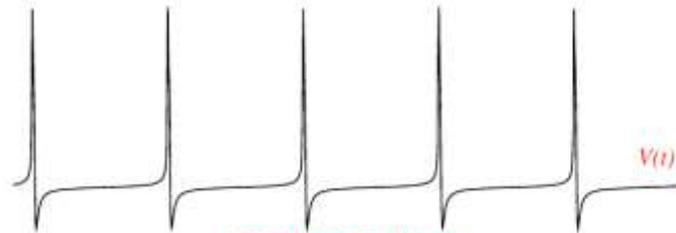
Особенности возбудимости нейронов



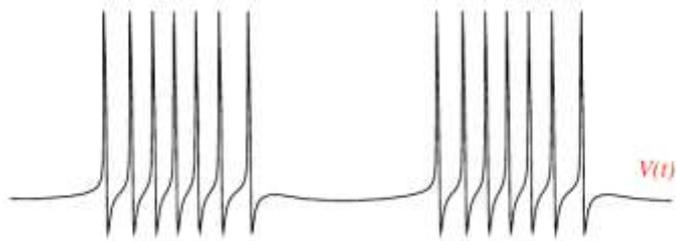
Возбудимость, ритмический и пачечный ответ



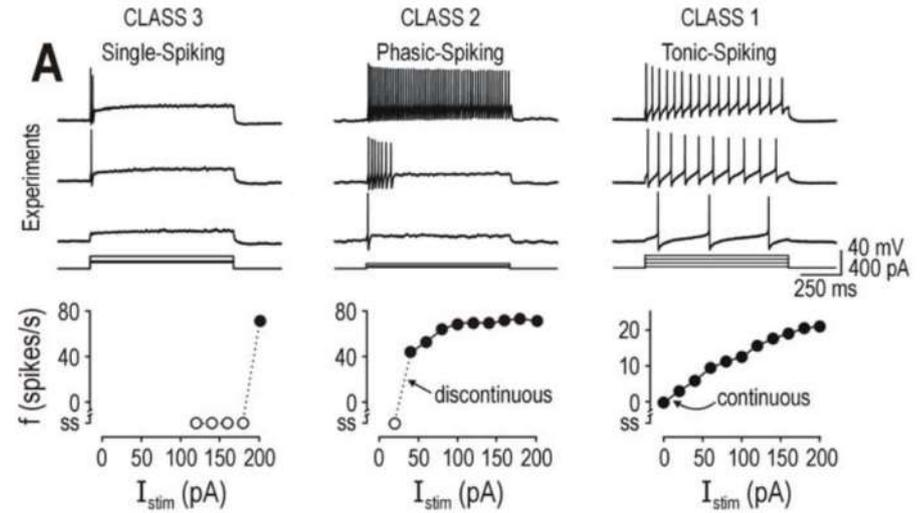
Neural Excitability



Periodic Spiking



Periodic Bursting

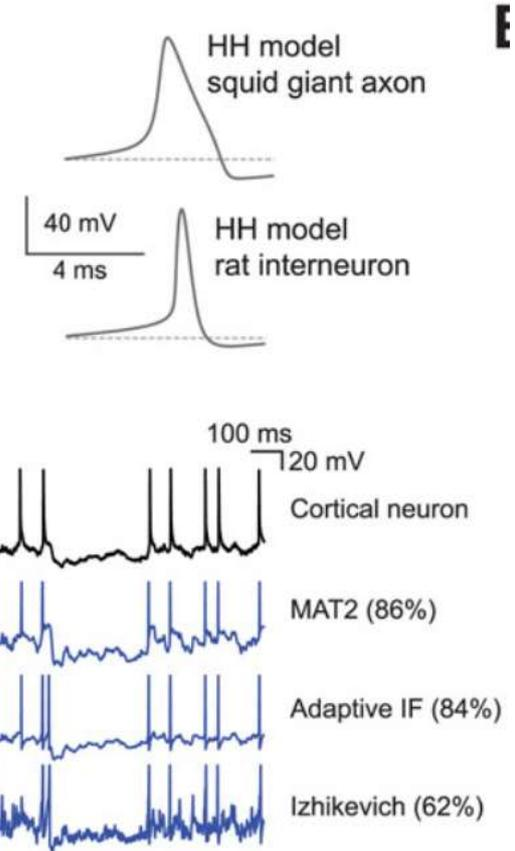
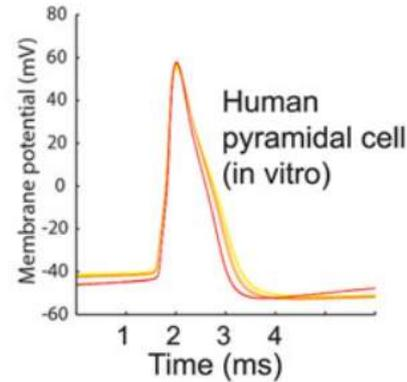
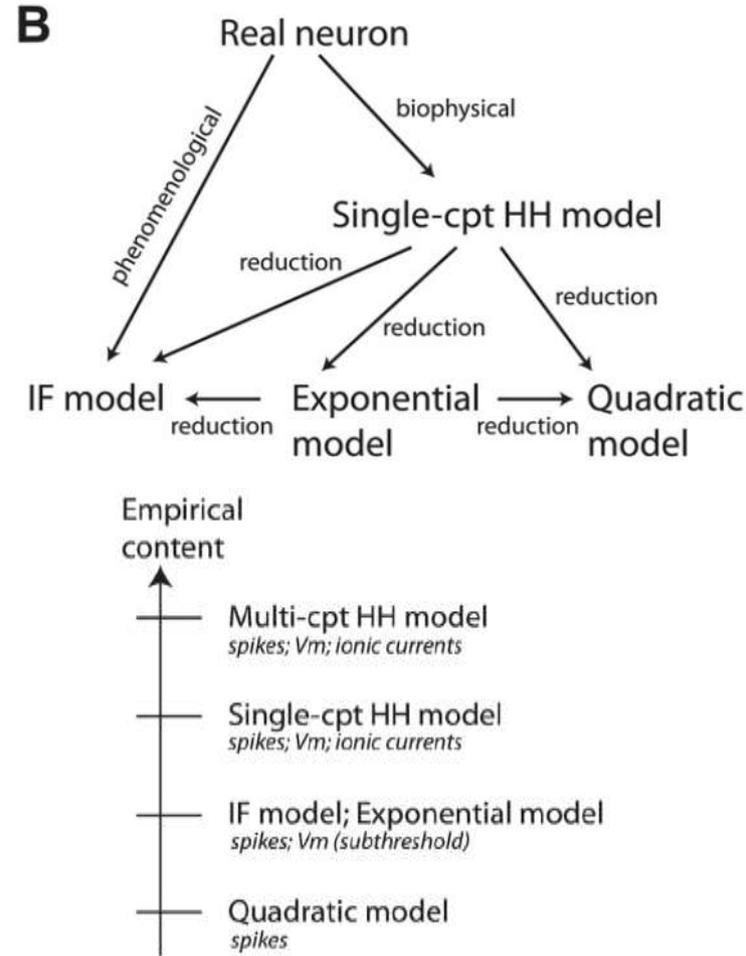


Prescott SA, De Koninck Y, Sejnowski TJ (2008)
PLoS Comput Biol 4(10): e1000198.
 doi:10.1371/journal.pcbi.1000198

Что такое хорошая модель?



Что такое хорошая модель нейрона?

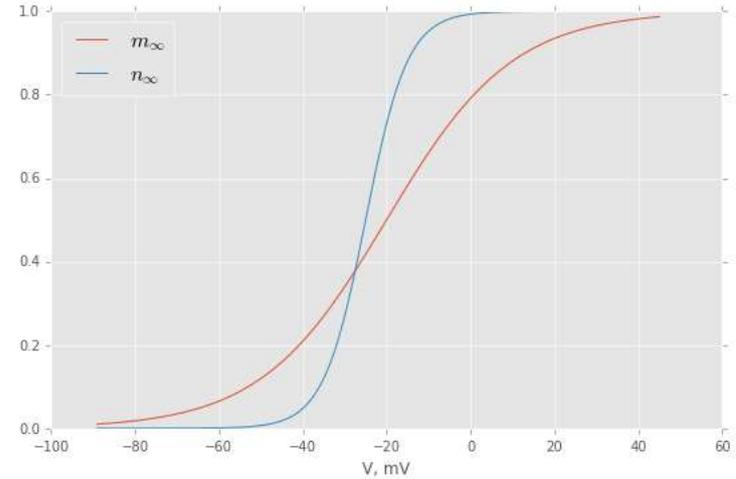


$I_{Na,p} + I_K$ -модель:

$$C\dot{V} = I - \bar{g}_K n(V - E_K) - \bar{g}_{Na} m_\infty(V)(V - E_{Na}) - g_l(V - E_l)$$

$$\tau_n \dot{n} = (n_\infty(V) - n)$$

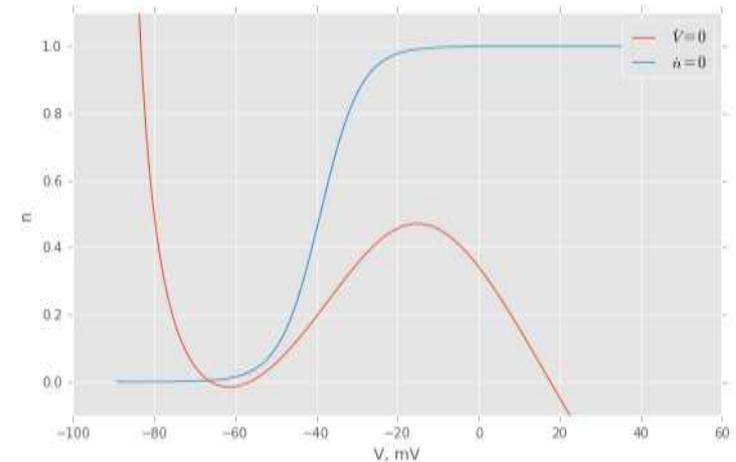
$$x_\infty = \frac{1}{1 + \exp\left(\frac{V_x^{0.5} - V}{k_x}\right)}$$



Нульклины:

$$\dot{V} = 0 \rightarrow n(V) = \frac{I - \bar{g}_{Na} m_\infty(V - E_{Na}) - g_l(V - E_l)}{\bar{g}_k(V - E_k)}$$

$$\dot{n} = 0 \rightarrow n(V) = n_\infty(V)$$

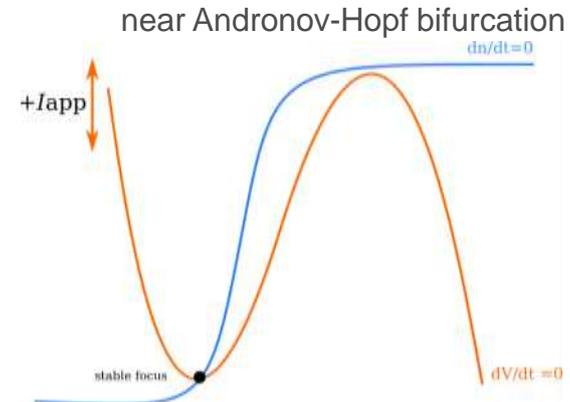
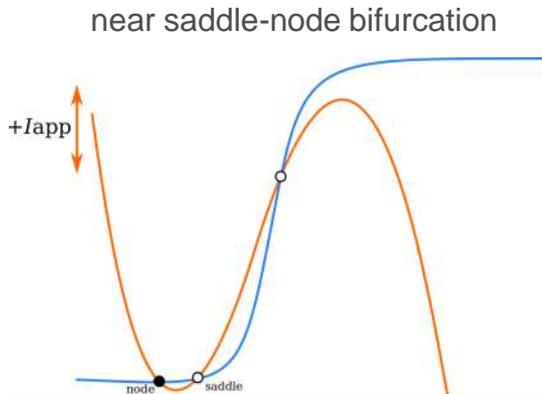


Бифуркации стационарного состояния

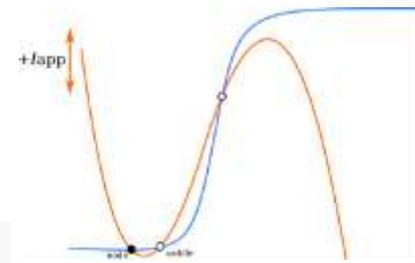
- Седлоузловая
- Седлоузловая на инвариантной окружности
- Суперкритическая бифуркация Андронова-Хопфа
- Субкритическая бифуркация Андронова-Хопфа

integrators

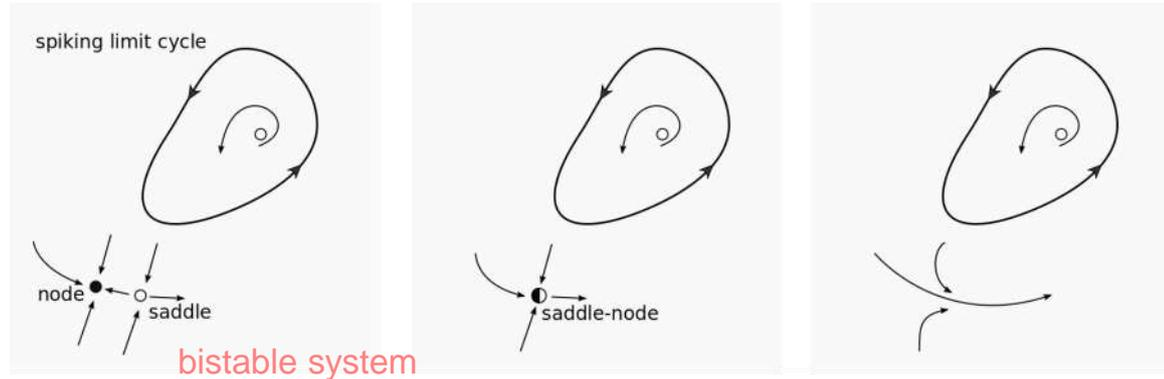
resonators



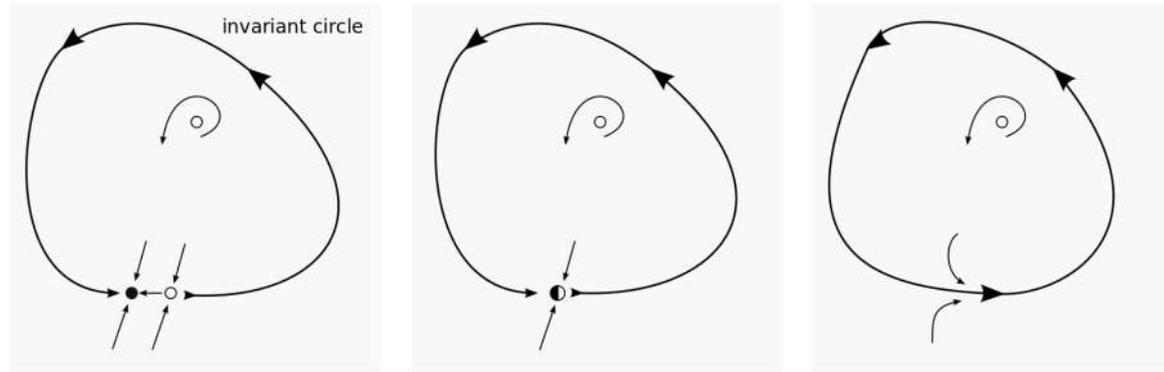
Седлоузловая бифуркация



Saddle-node



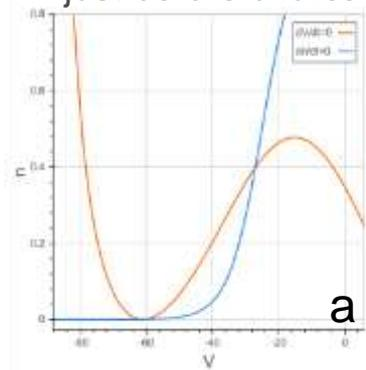
SNIC



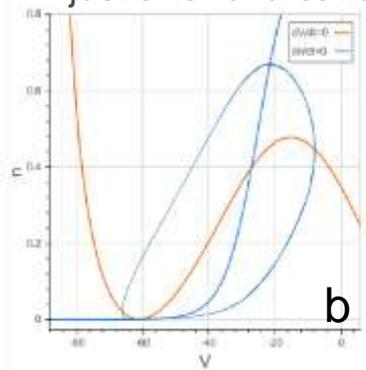
Increasing applied current \rightarrow

Example of SNIC in $I_{Na,p} + I_K$ model

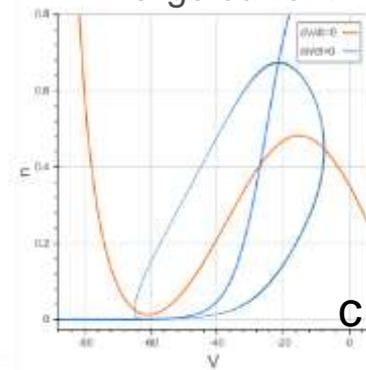
just before bifurcation



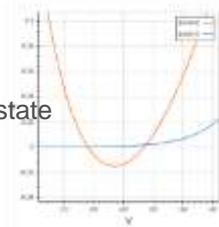
just after bifurcation



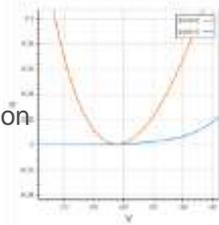
large current



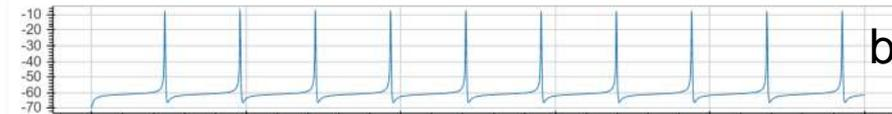
at resting state



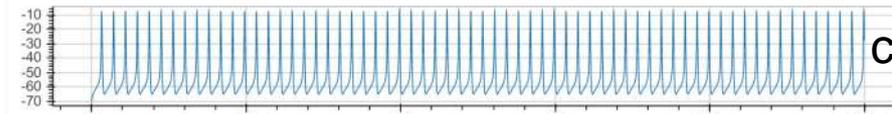
at bifurcation



a



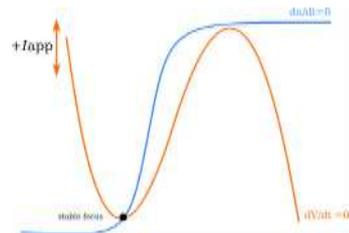
b



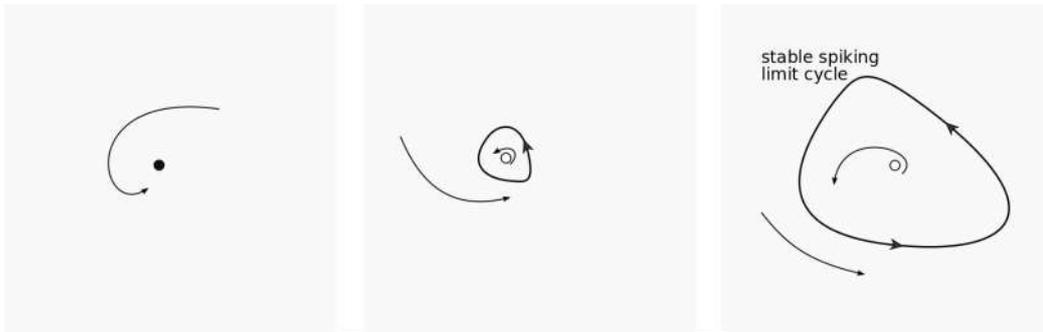
c

time, ms

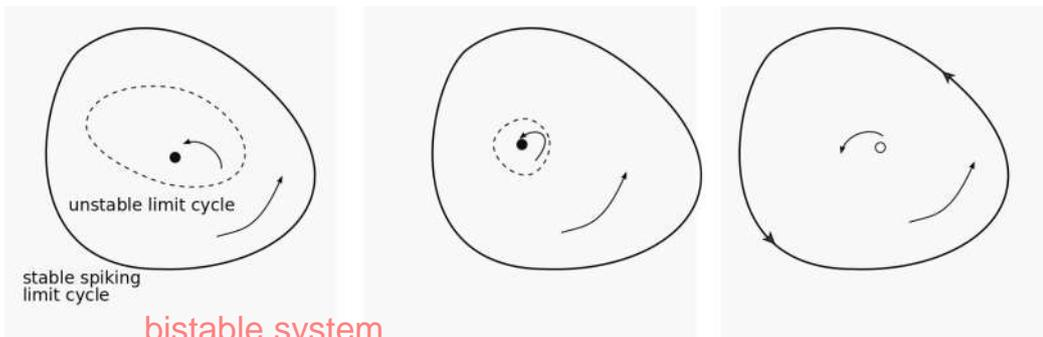
Бифуркации Андронова-Хопфа



supercritical

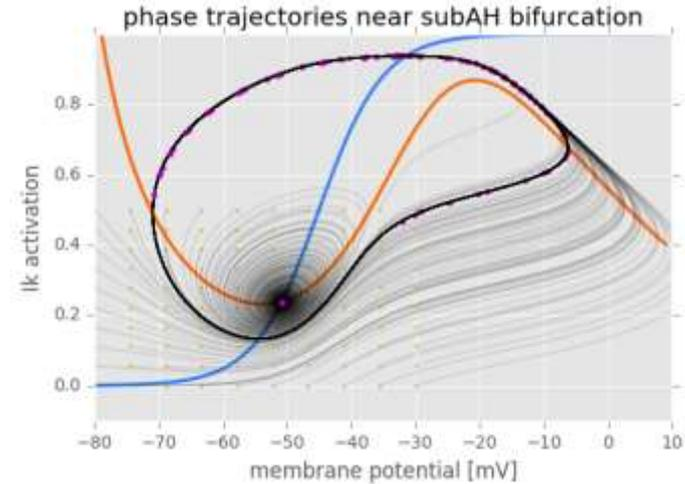
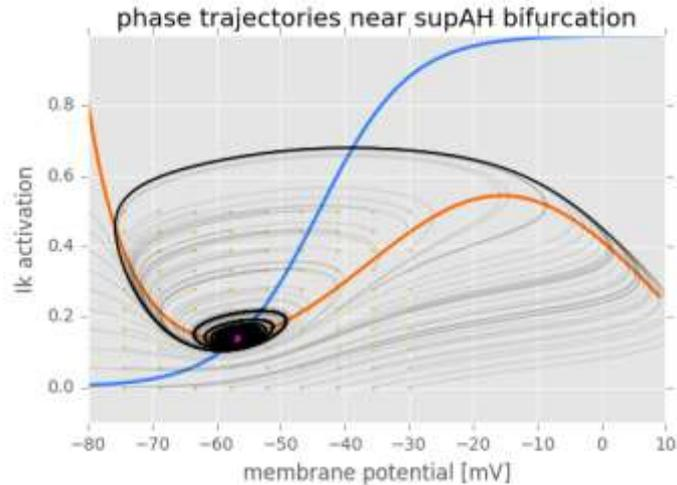
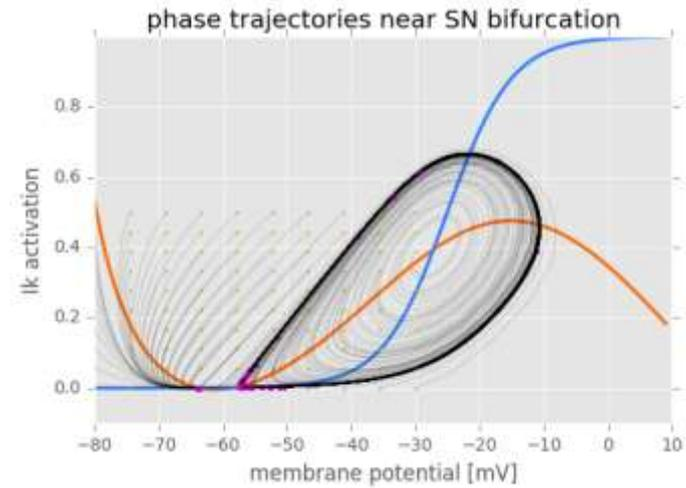
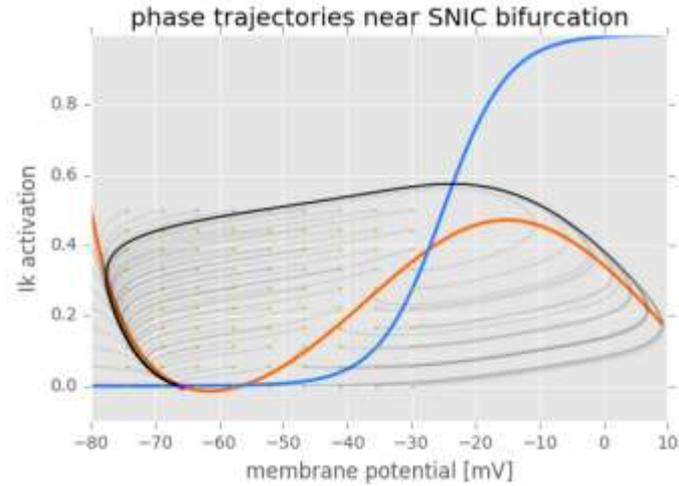


subcritical

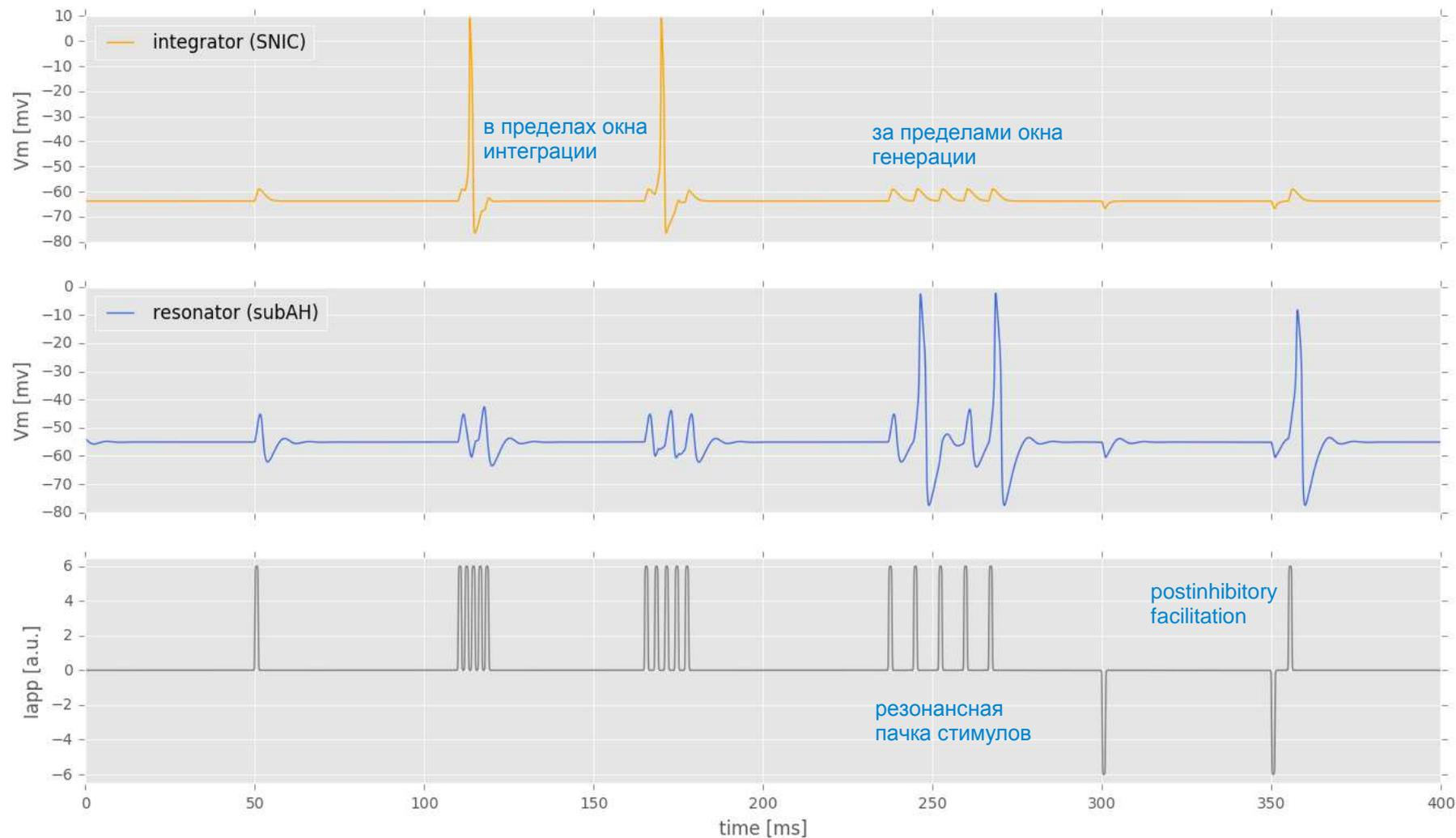


Increasing applied current →

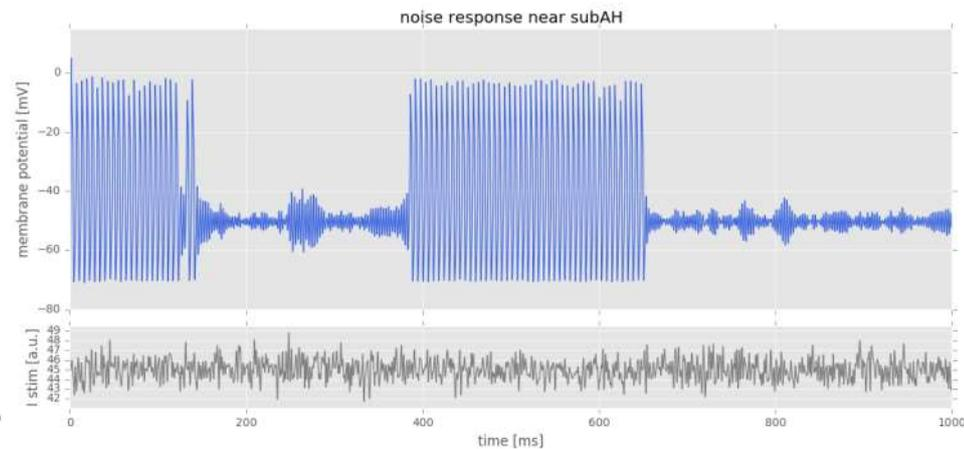
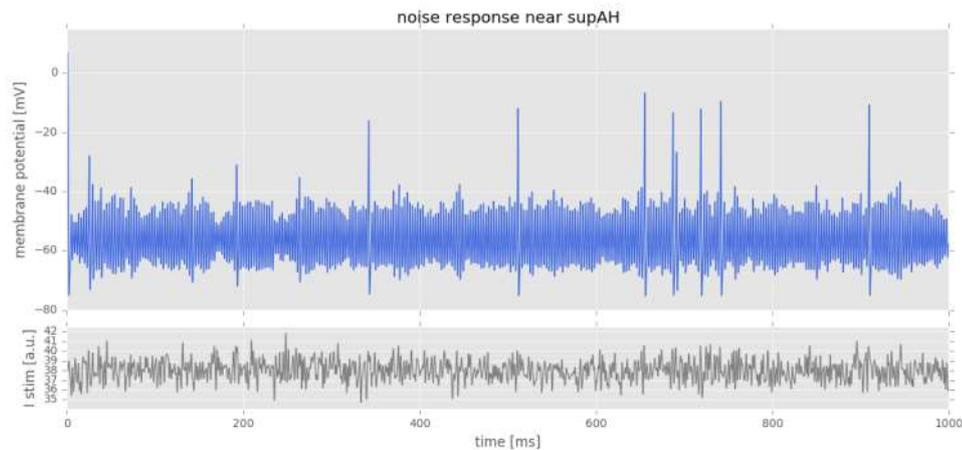
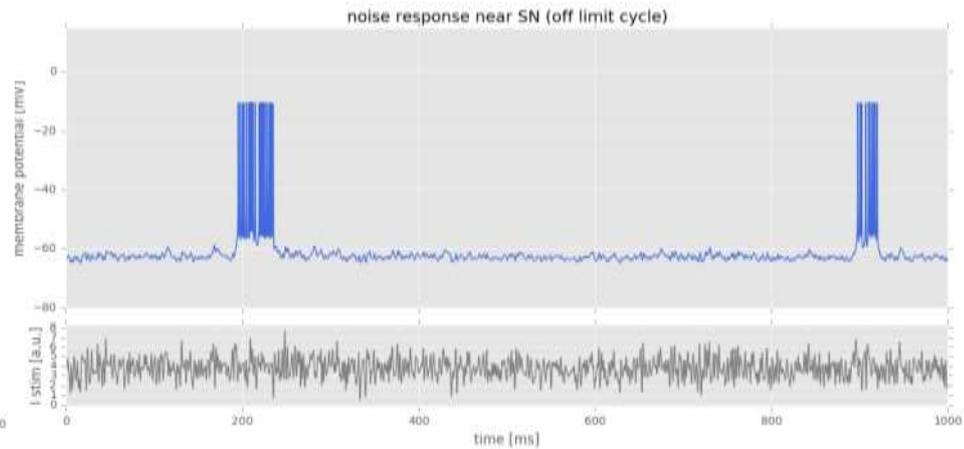
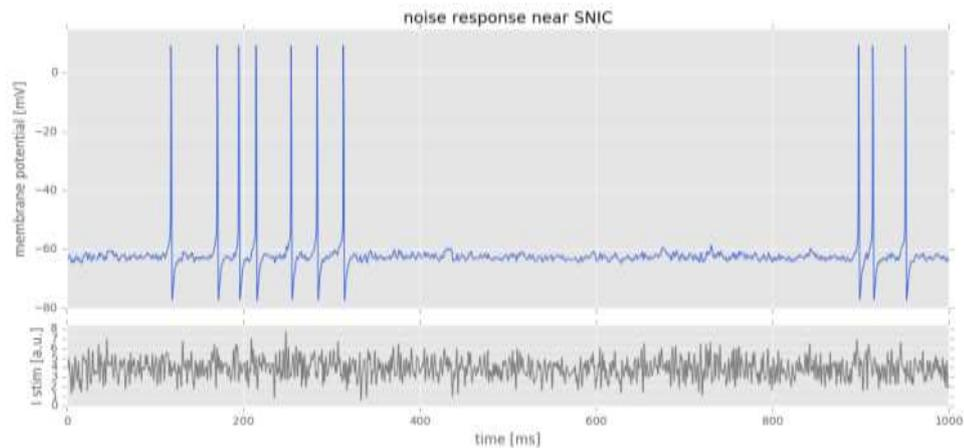
Возбудимость и бистабильность $I_{Na,p} + I_K$ -модели вблизи 4-х типов бифуркации стац. состояния



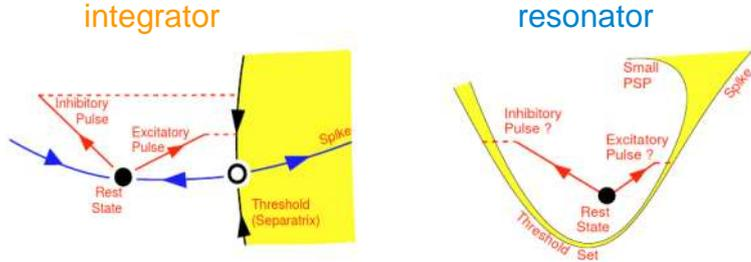
Ответы на короткие стимулы: интеграторы vs резонаторы



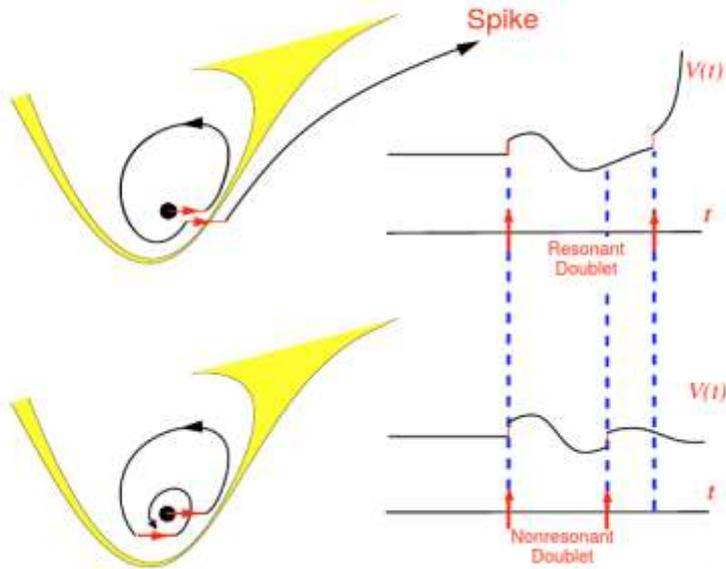
Ответы на стохастическую стимуляцию



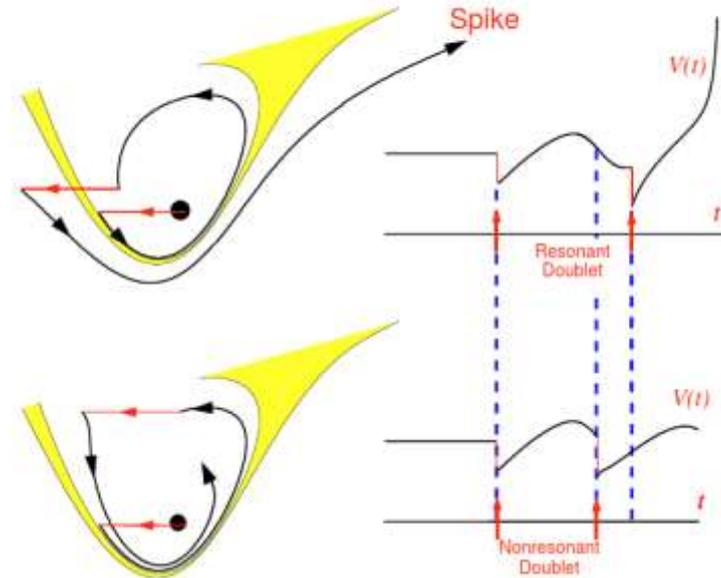
Implications of subthreshold oscillations: excitation by hyperpolarization



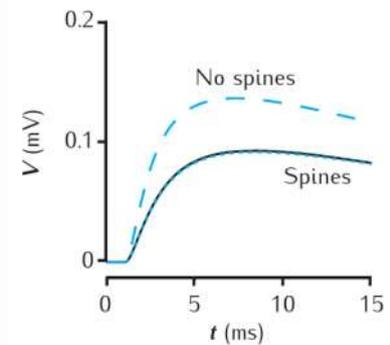
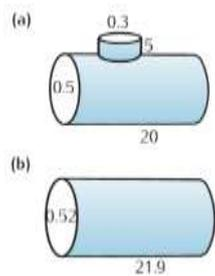
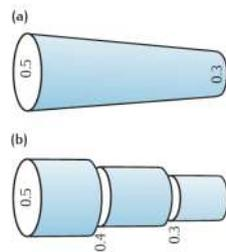
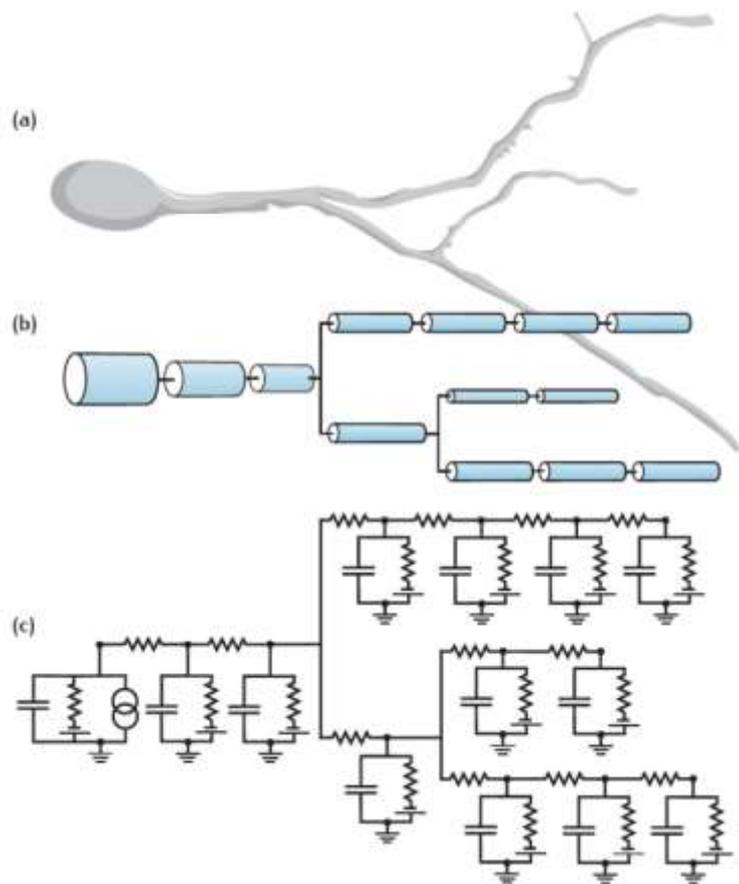
"Excitatory" Pulses



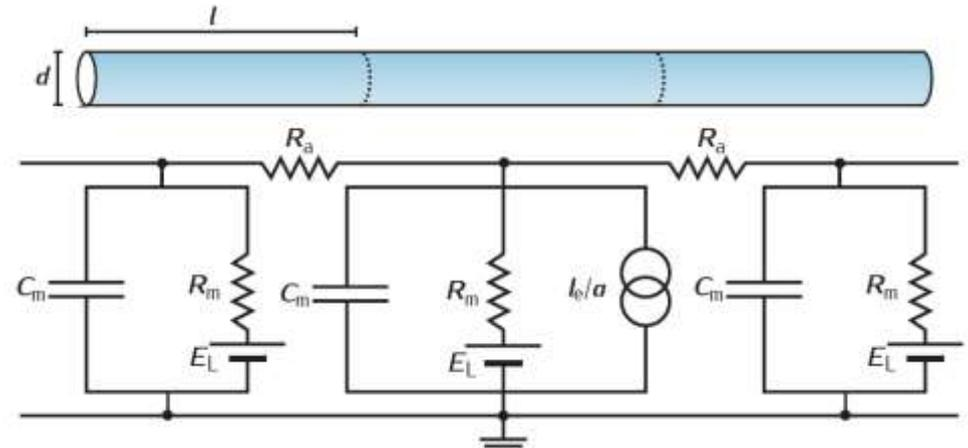
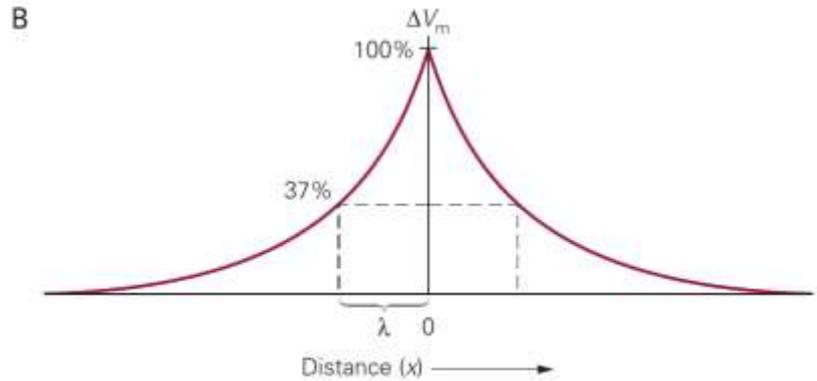
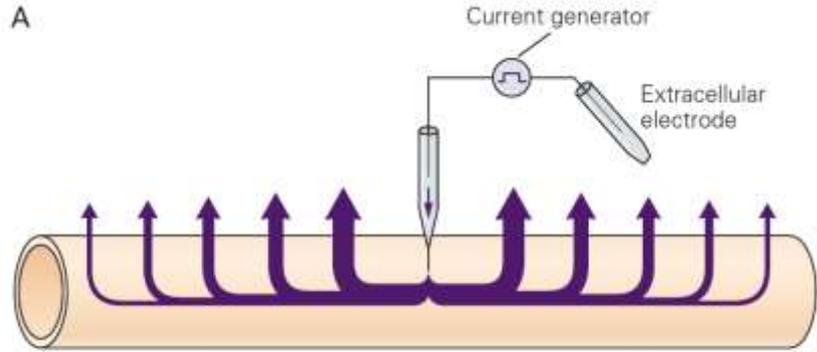
"Inhibitory" Pulses



Модели с реконструкцией морфологии



Кабельные свойства нервного волокна

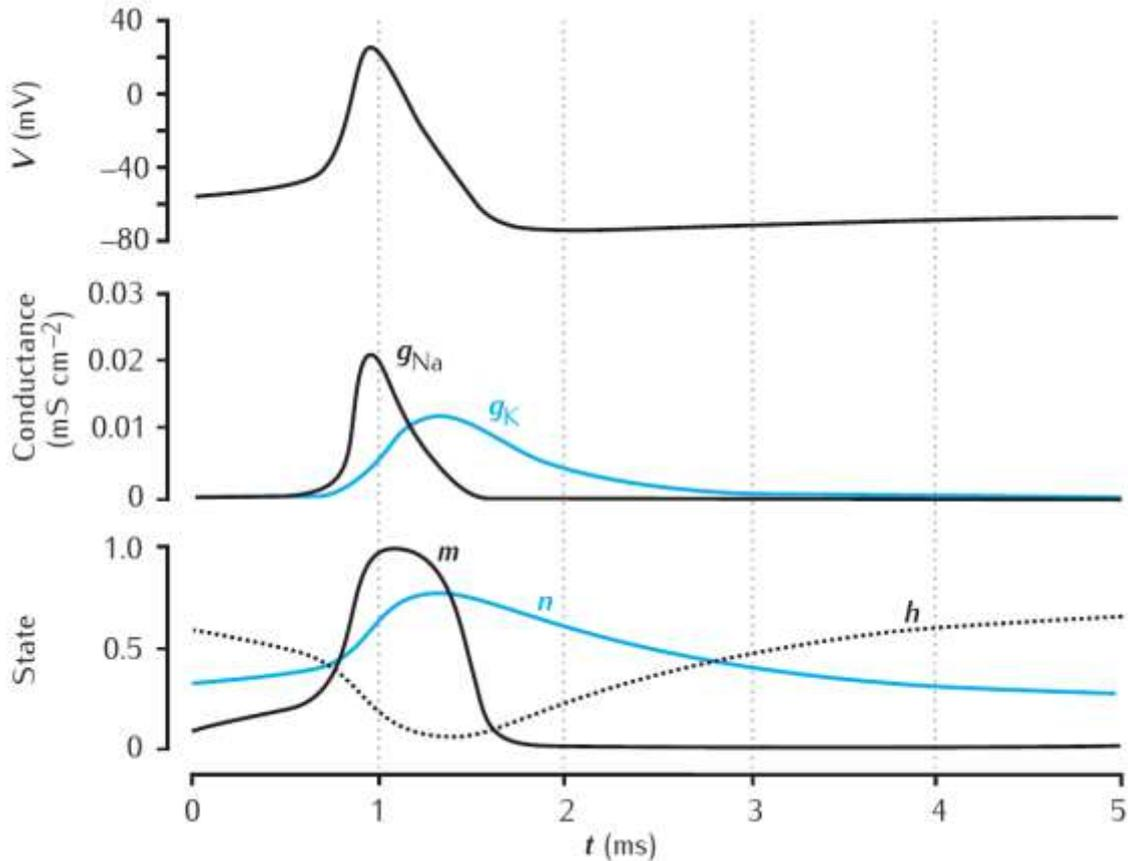


$$C_m \frac{\partial V}{\partial t} = \frac{E_m - V}{R_m} + \frac{d}{4R_a} \frac{\partial^2 V}{\partial x^2} + \frac{I_c}{\pi d}$$

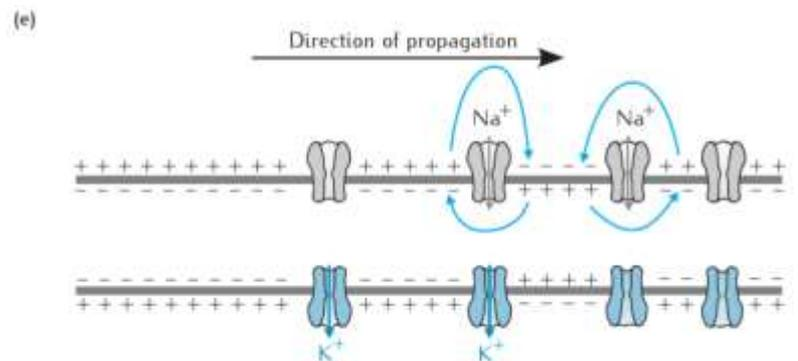
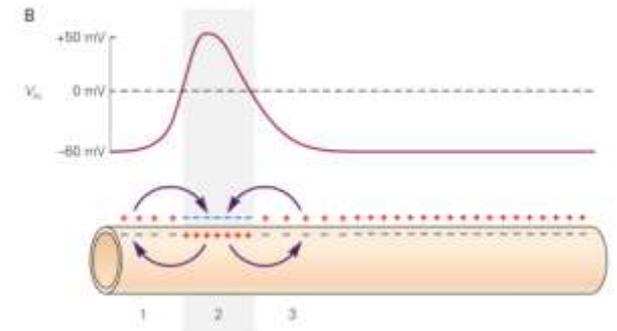
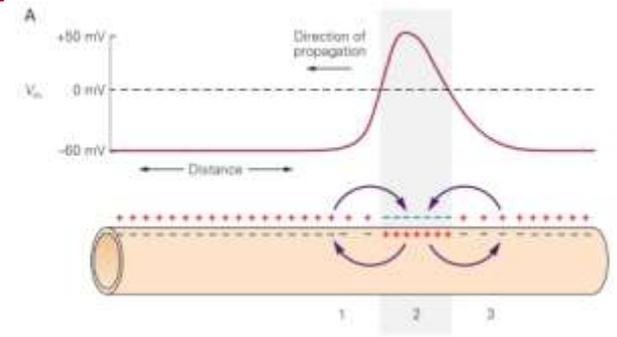
$$V(x) = E_m + R_\infty I_c e^{-x/\lambda}$$

$$\lambda = \sqrt{\frac{R_m d}{4R_a}} = \sqrt{\frac{r_m}{r_a}}$$

Генерация и проведение ПД в нервном волокне кальмара

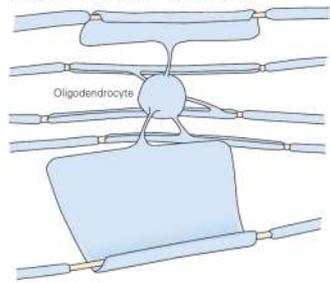


$$C_m \frac{dV}{dt} = I_{electrode} - \bar{g}_L(V - E_L) - \bar{g}_{Na} m^3 h (V - E_{Na}) - \bar{g}_K n^4 (V - E_K)$$

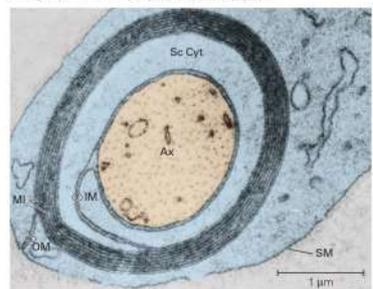


Проведение в миелинизированных волокнах

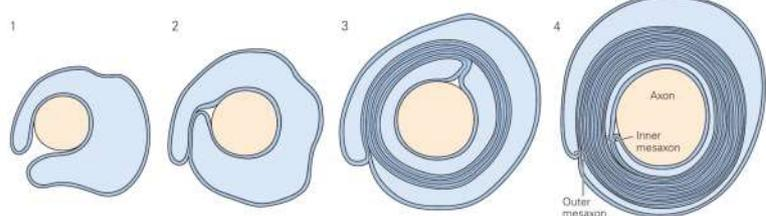
A Myelination in the central nervous system



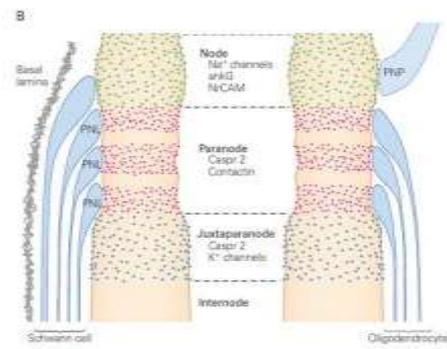
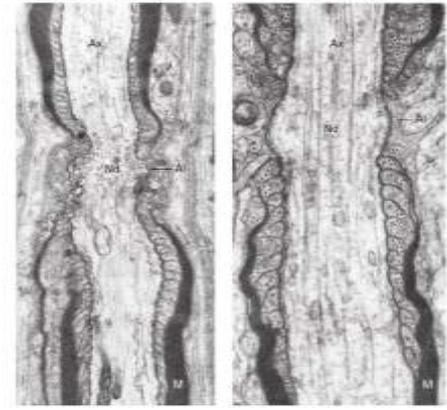
B Myelination in the peripheral nervous system



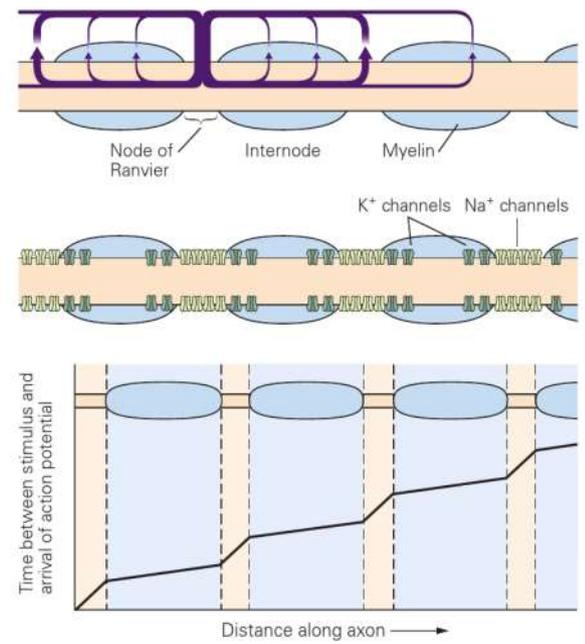
C Development of myelin sheath in the peripheral nervous system



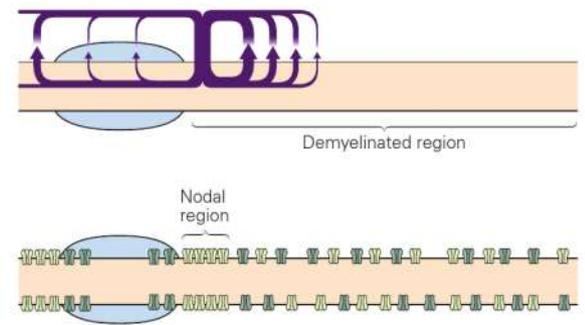
A Peripheral nervous system Central nervous system



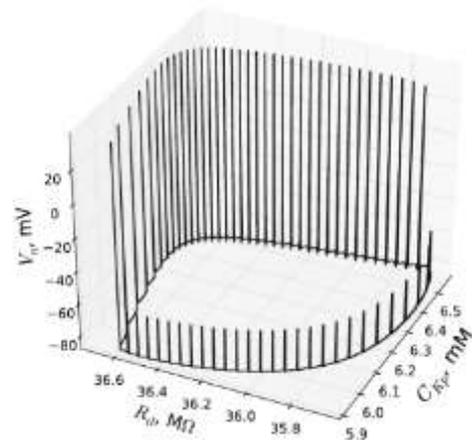
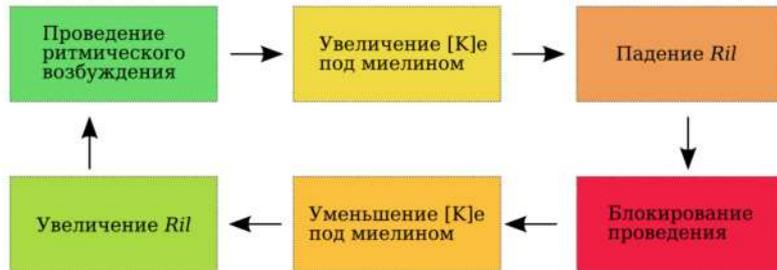
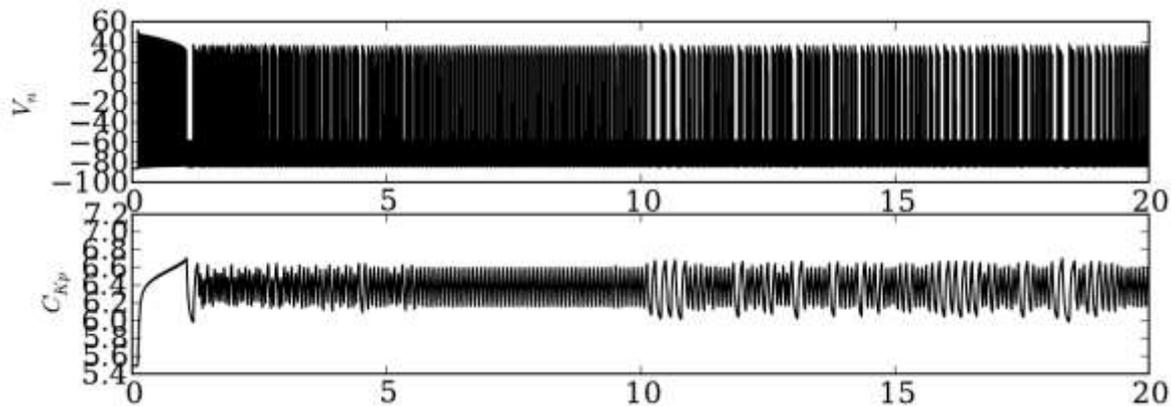
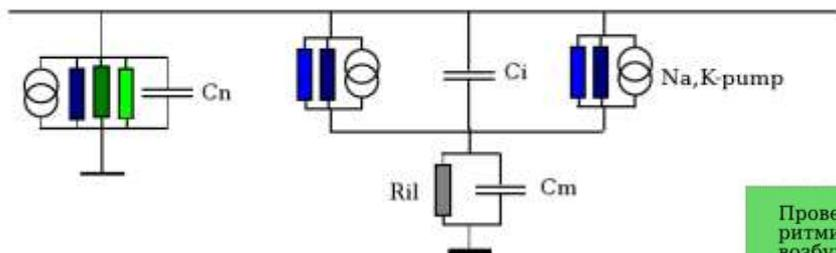
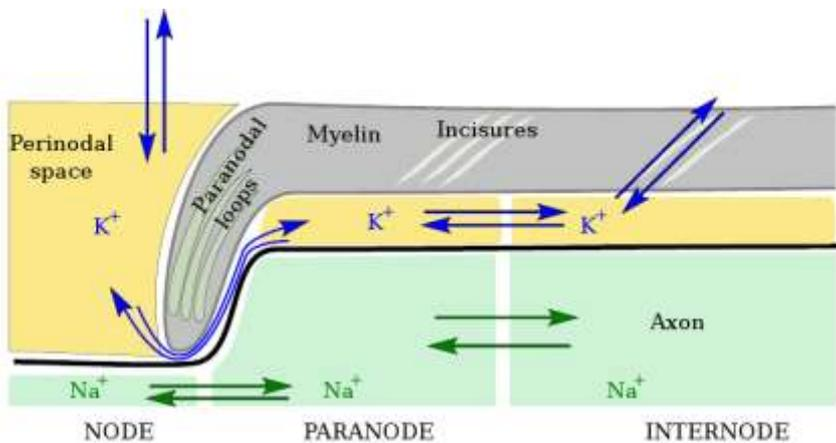
A Normal axon



B Demyelinated axon

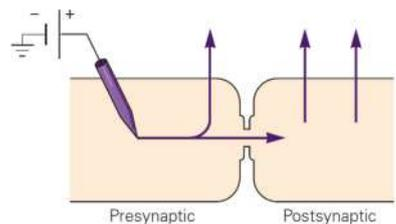


Влияние проведения серий ПД на возбудимость

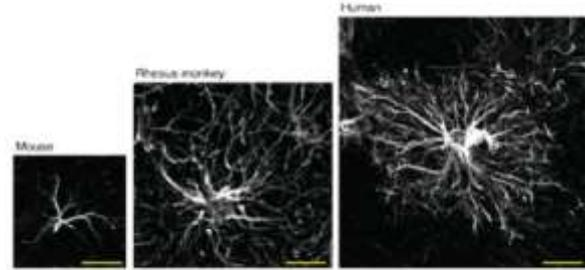
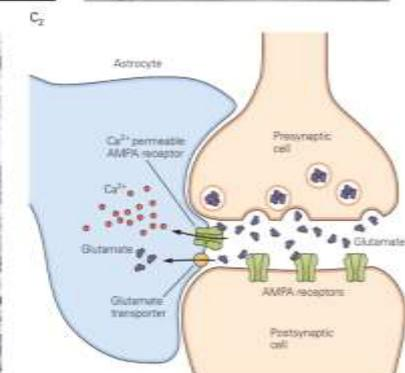
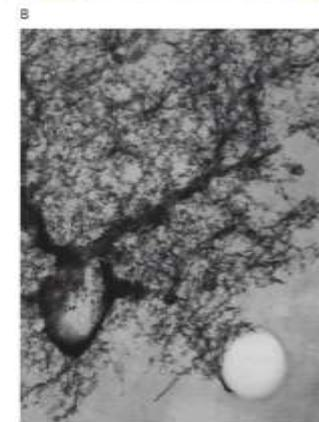
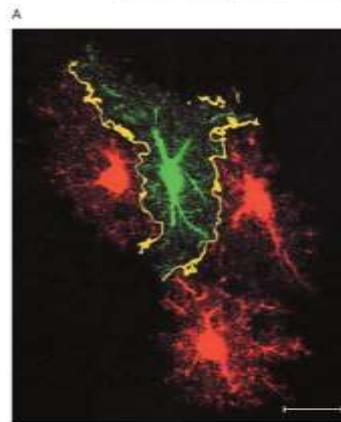
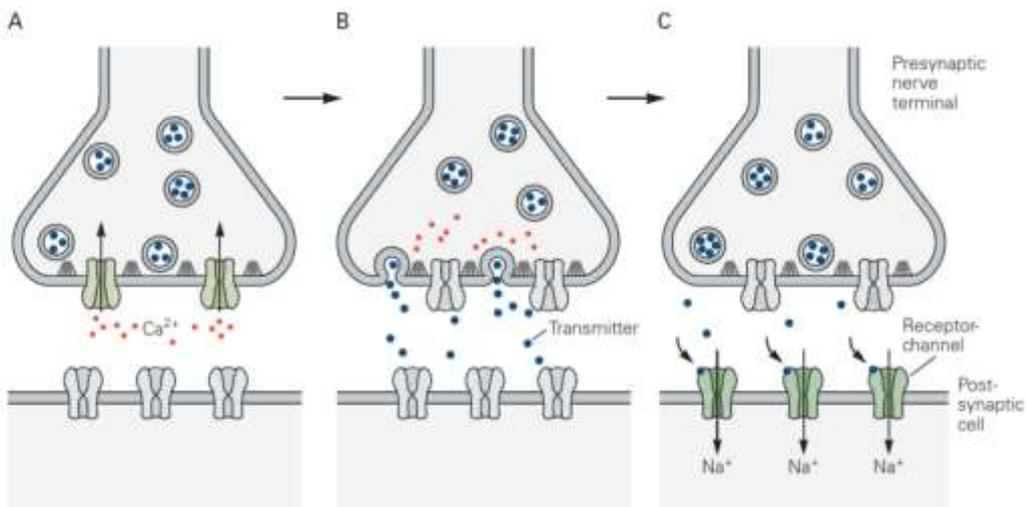
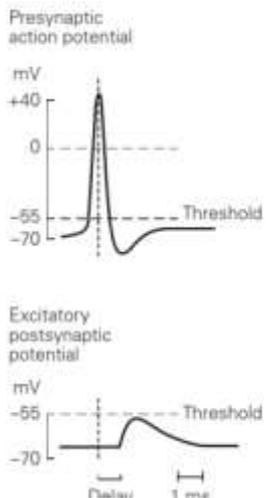
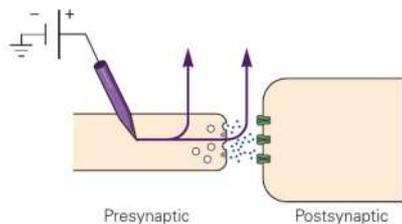


Синаптическая передача

A Current pathways at electrical synapses

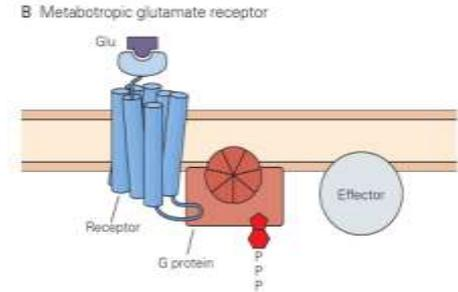
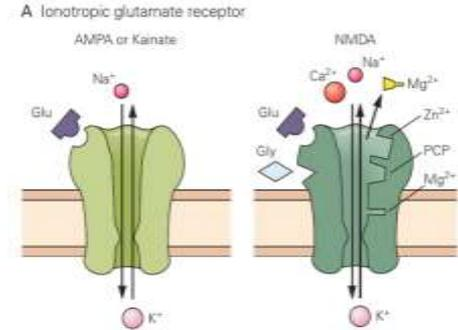
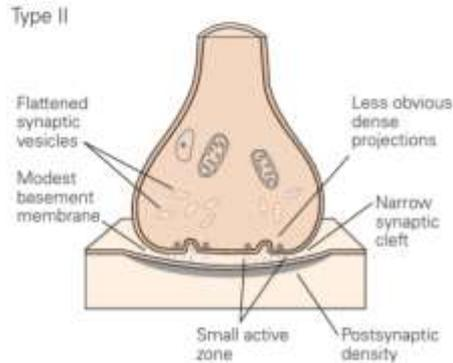
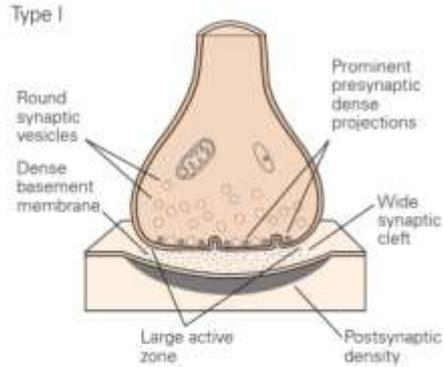
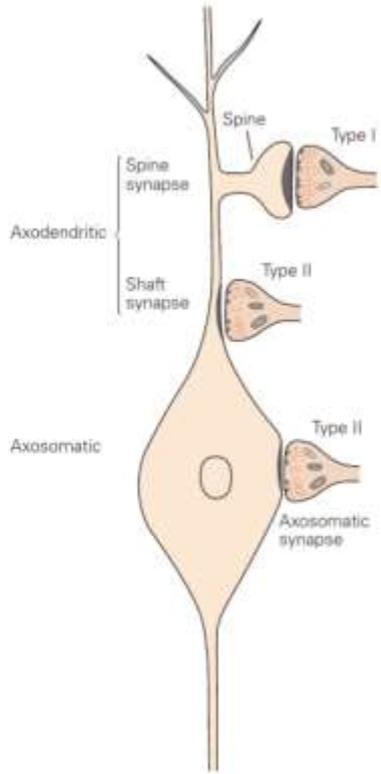


B Current pathways at chemical synapses



Типы синапсов

Figure 10-3 The two most common morphological types of synapses in the central nervous system are Gray type I and type II. Type I is usually excitatory, exemplified by glutamatergic synapses; type II is usually inhibitory, exemplified by GABAergic synapses. Differences include the shape of vesicles, prominence of presynaptic densities, total area of the active zone, width of the synaptic cleft, and presence of a dense basement membrane. Type I synapses typically contact specialized projections on the dendrites, called spines, and less commonly contact the shafts of dendrites. Type II synapses often contact the cell body and dendritic shaft.



Рецепторы к глутамату

| Ionotropic glutamate receptors (iGluRs) | | | |
|---|---------|---------|--------|
| AMPA | Kainate | NMDA | Delta |
| GluA1 | GluK1 | GluN1* | GluD1 |
| GluA2 | GluK2 | GluN2A | GluD2* |
| GluA3 | GluK3 | GluN2B | |
| GluA4 | | GluN2C | |
| | | GluN2D | |
| | GluK4 | GluN3A* | |
| | GluK5 | GluN3B* | |

- гетеротетрамеры
- пре- и пост-трансляционные модификации

Строение AMPA-рецепторов

Synaptic Neurotransmitter-Gated Receptors

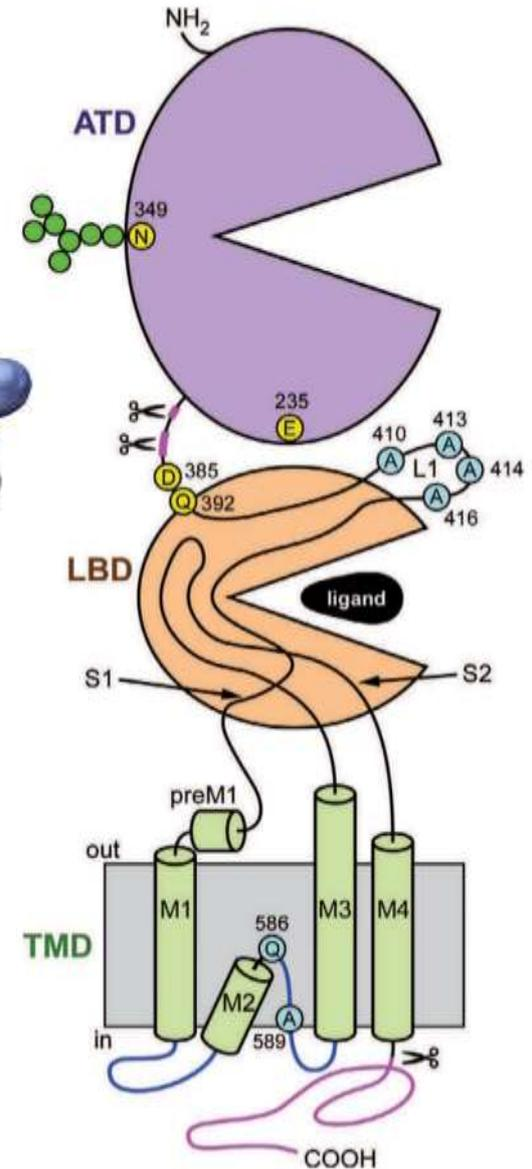
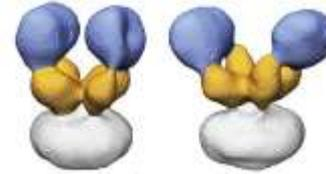
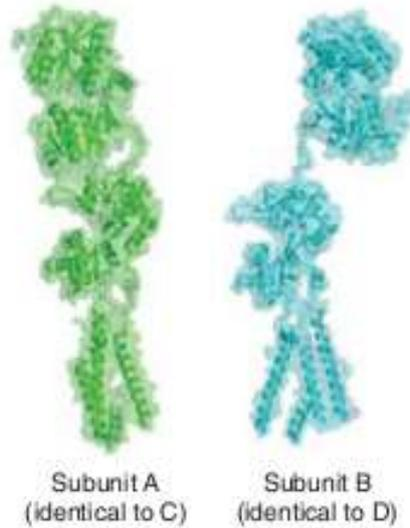
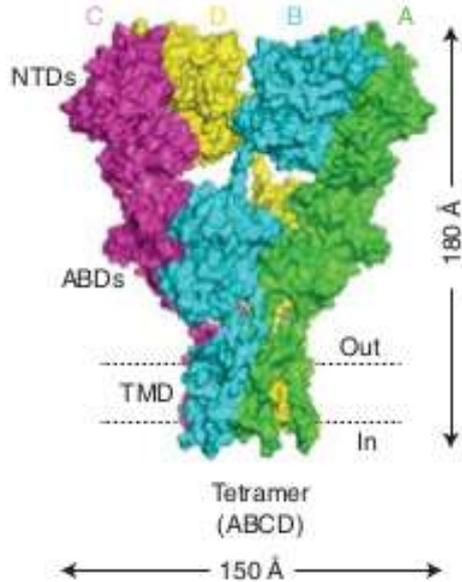


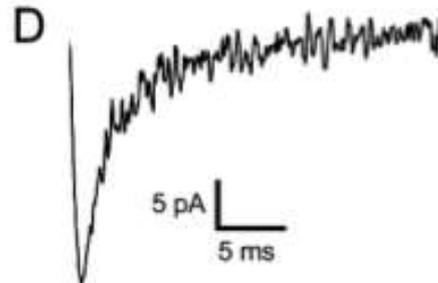
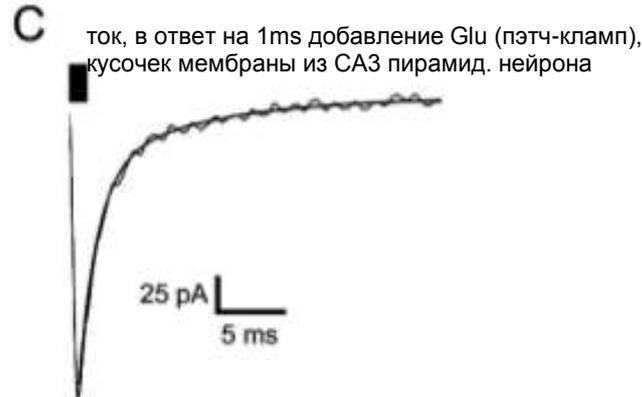
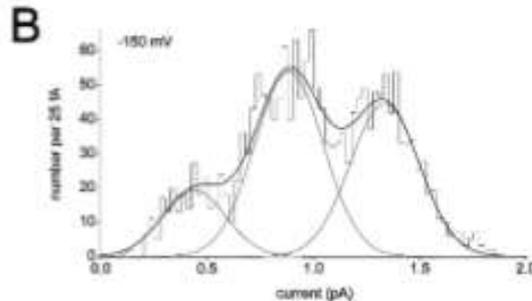
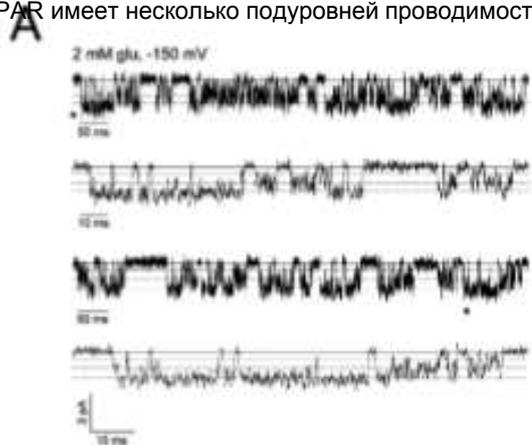
Figure 6. The tetrameric structure of the AMPA GluA2 receptor. (*Left*) X-ray crystal structure of the AMPA GluA2 homotetrameric receptor (Sobolevsky et al. 2009). Each subunit is in a different color. The tetramer shows a typical layer organization with at the “top” the amino-terminal domains (ATDs or NTDs), at the “bottom” the transmembrane domain (TMD) where the ion channel sits, and sandwiched between the two the agonist-binding domains (ABDs or S1S2 domains) binding glutamate (or glycine/D-serine). (*Right*) Subunit non-equivalence. α -Carbon traces of subunit A and subunit B with the ABDs similarly oriented. Note the striking difference in overall domain orientation between the two subunits.

Проводимость и кинетика AMPA-рецепторов

AMPA Receptors

11

AMPA имеет несколько подуровней проводимости



Миниатюрный постсинаптический ток в
интернейроне коры

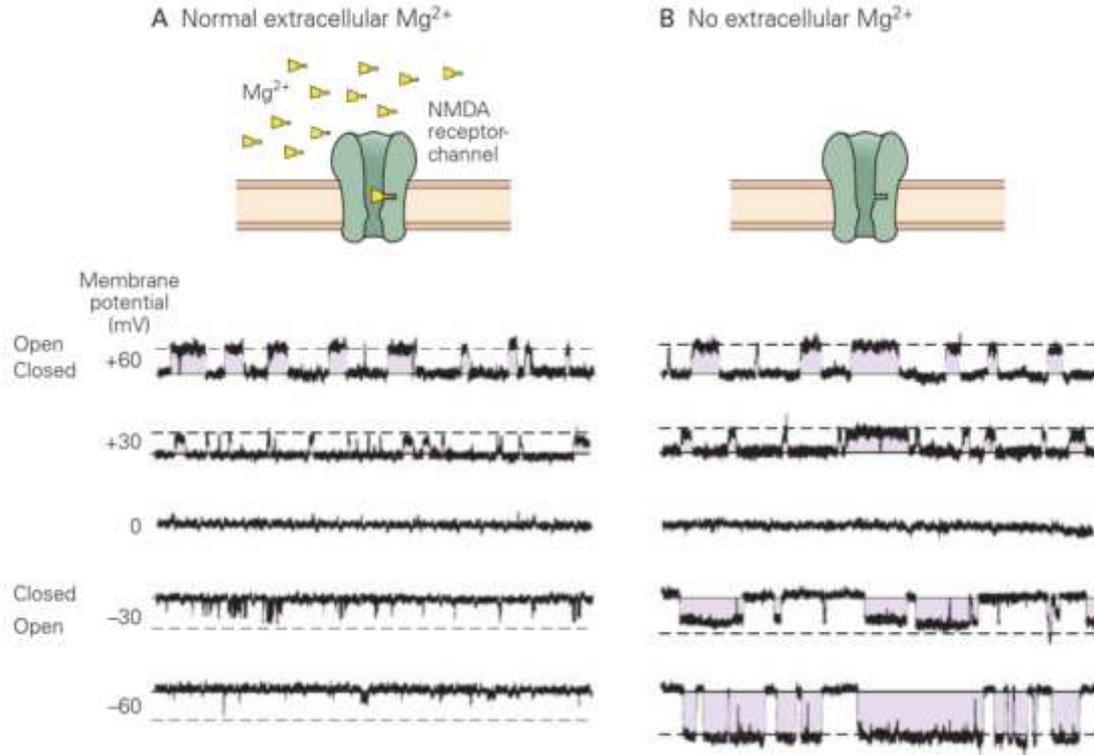
AMPA

- $\langle g \rangle \sim 12 \text{ pS}$
- $V_0 \sim 0 \text{ mV}$
- проводят: Na, K, но не Ca (у взрослых, если есть GluA₂)
- NB: сайт ORN
- быстро десенситизируются
- основной тип GluR

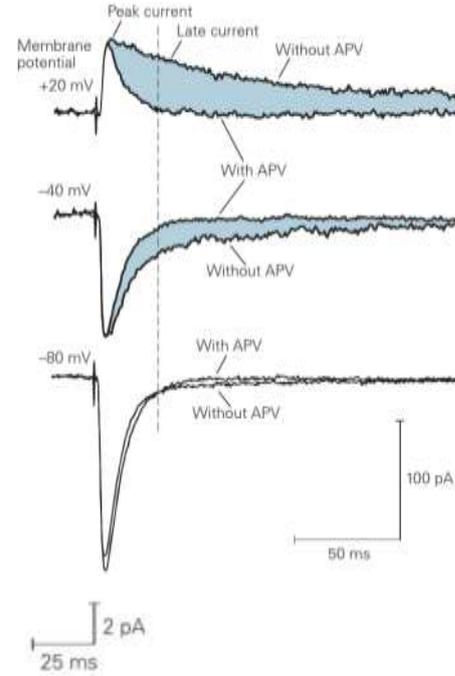
NMDAR

- хорошо проводят Ca, 15% входящего тока
- участвуют в обр. памяти
- блокируются Mg^{2+} (зав. от потенциала)
- для открывания нужно связать 2 Glu и 2 {Gly | D-Ser}

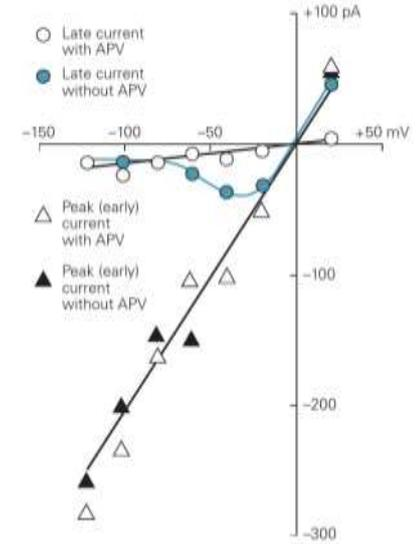
NMDA-рецепторы (Glu-эргические синапсы)



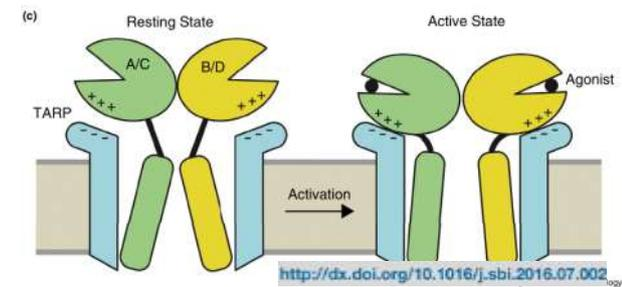
A Early and late components of synaptic current



B Current-voltage relationship of the synaptic current



Связывание лиганда, воротный механизм и аллостерическая модуляция



T.G. Smart and P. Paoletti

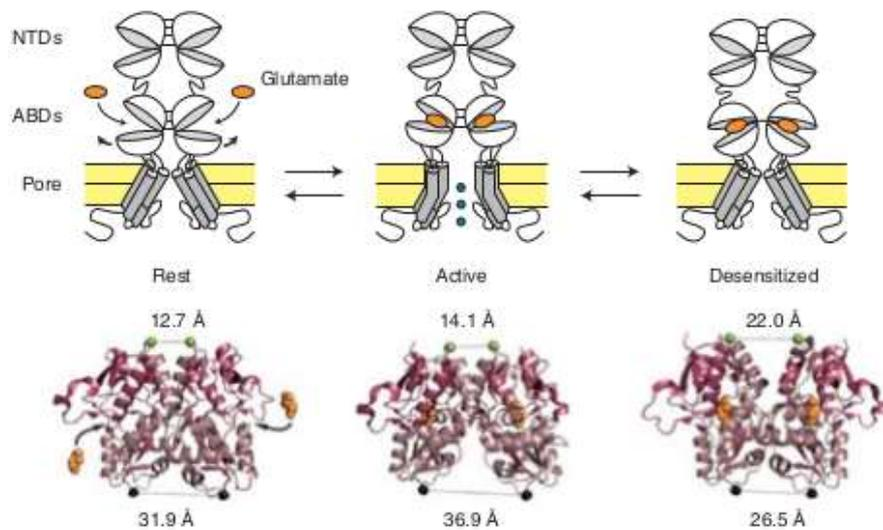


Figure 7. Structural mechanism of iGluR activation and desensitization. A single dimer is represented; a full receptor is a tetramer made of two such dimers. (Below) The crystal structures of the GluA2 ABD dimer in conformations that correspond to the resting state (no ligand bound; pdb code 1FT0), the active state (glutamate-bound; pdb code 1FT1), and the desensitized state (pdb code 2I3V). The distances between the two protomers, at the top of the upper lobes (green spheres; dimer interface) and at the bottom of the lower lobes (black spheres; connections to the transmembrane segments), are indicated (Armstrong et al. 2006).

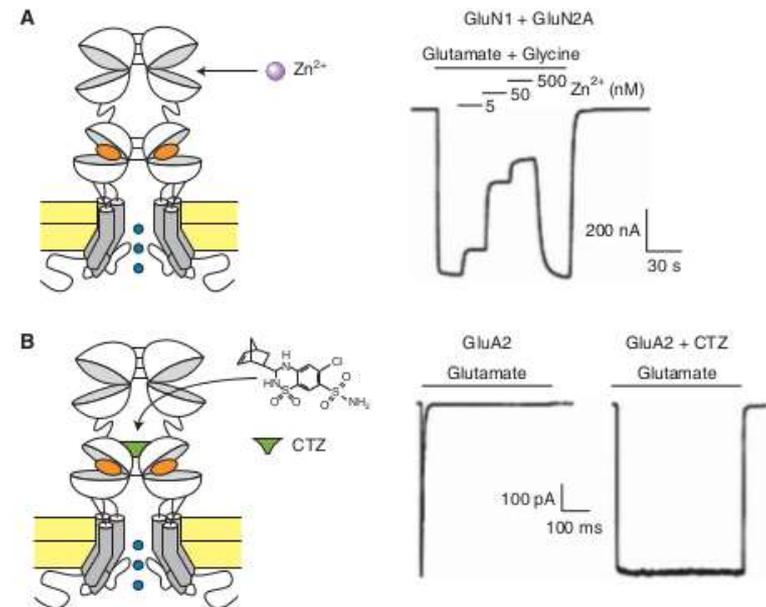
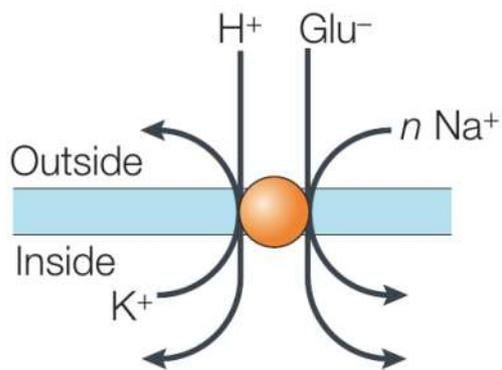


Figure 8. Allosteric modulation of iGluRs. (A) Negative allosteric modulation of NMDARs by extracellular zinc. The GluN2A and GluN2B NTDs form subunit-specific inhibitory zinc-binding sites. (Right) Inhibition by nanomolar zinc concentrations of GluN1/GluN2A responses (adapted from Paoletti et al. 2000). (B) Positive allosteric modulation of AMPARs by cyclothiazide (CTZ). CTZ binds and stabilizes the ABD dimer interface. (Right) CTZ blocks desensitization of GluA2 receptors (Sun et al. 2002).

Стехиометрия захвата Glu⁻ астроцитами

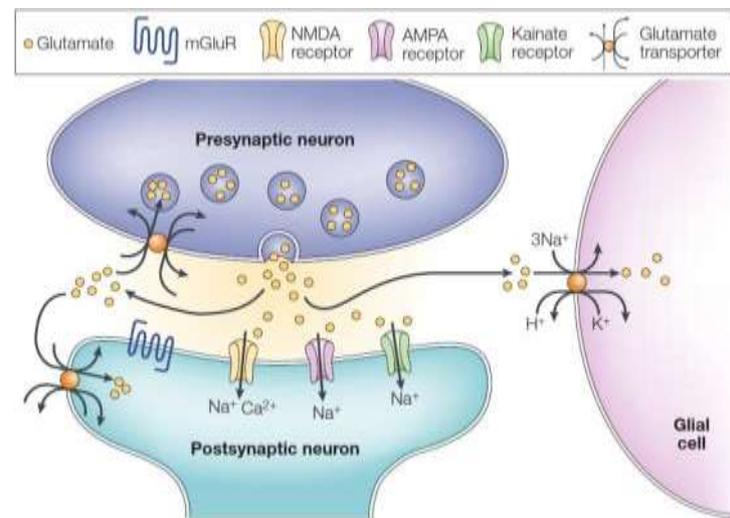


$$[\text{Glu}]_o = [\text{Glu}]_i (\text{Na}^+_i / [\text{Na}^+]_o)^n ([\text{H}^+]_i / [\text{H}^+]_o) ([\text{K}^+]_o / [\text{K}^+]_i) e^{(n-1)VF/RT}$$

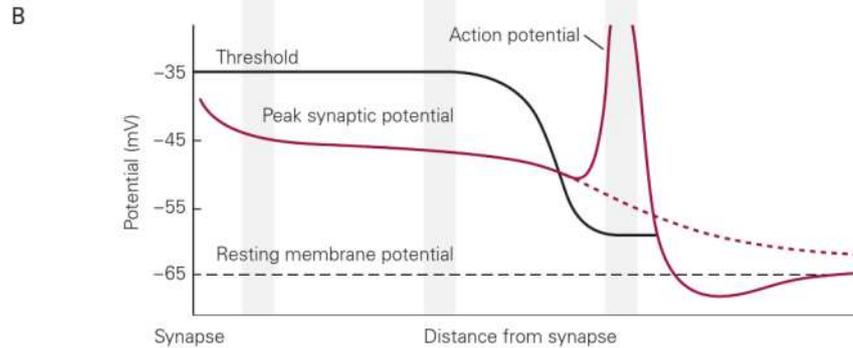
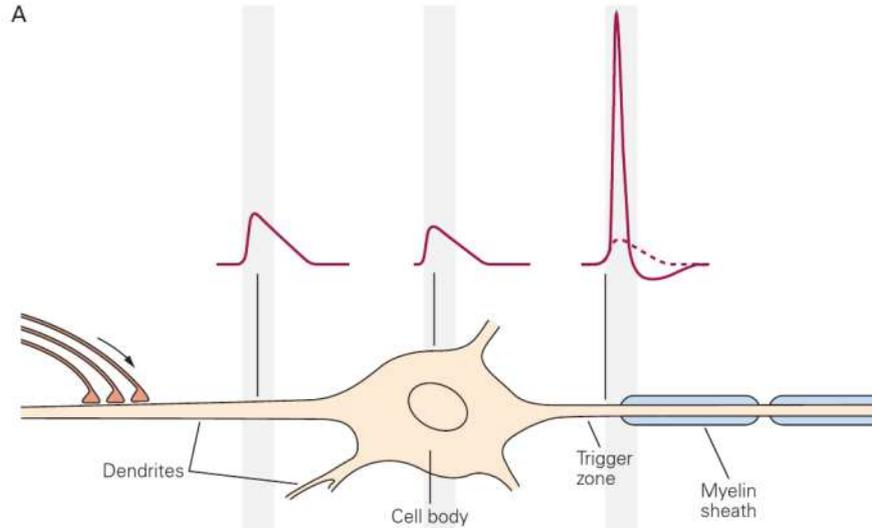
| n | $[\text{Glu}]_o$ | % of NMDA p_{max} (steady state) |
|-----|----------------------|---|
| 1 | 21 μM | 99% |
| 2 | 0.18 μM | 13% |
| 3 | 0.0016 μM | 0.002% |

Перенос 3-х ионов Na⁺ необходим для достаточно полного удаления Glu из синаптической щели

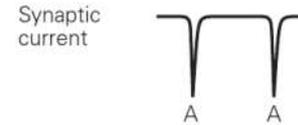
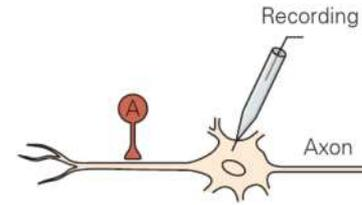
Перенос **каждого** из ионов, кроме Glu, энергетически выгоден



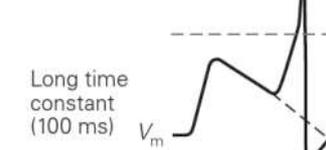
Обработка информации на дендритах



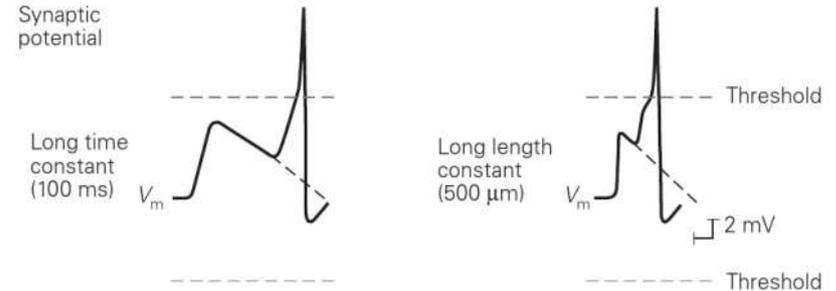
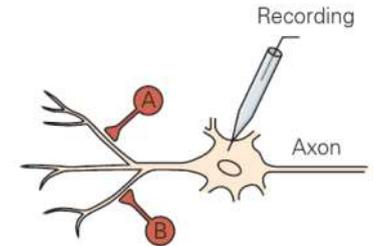
A Temporal summation



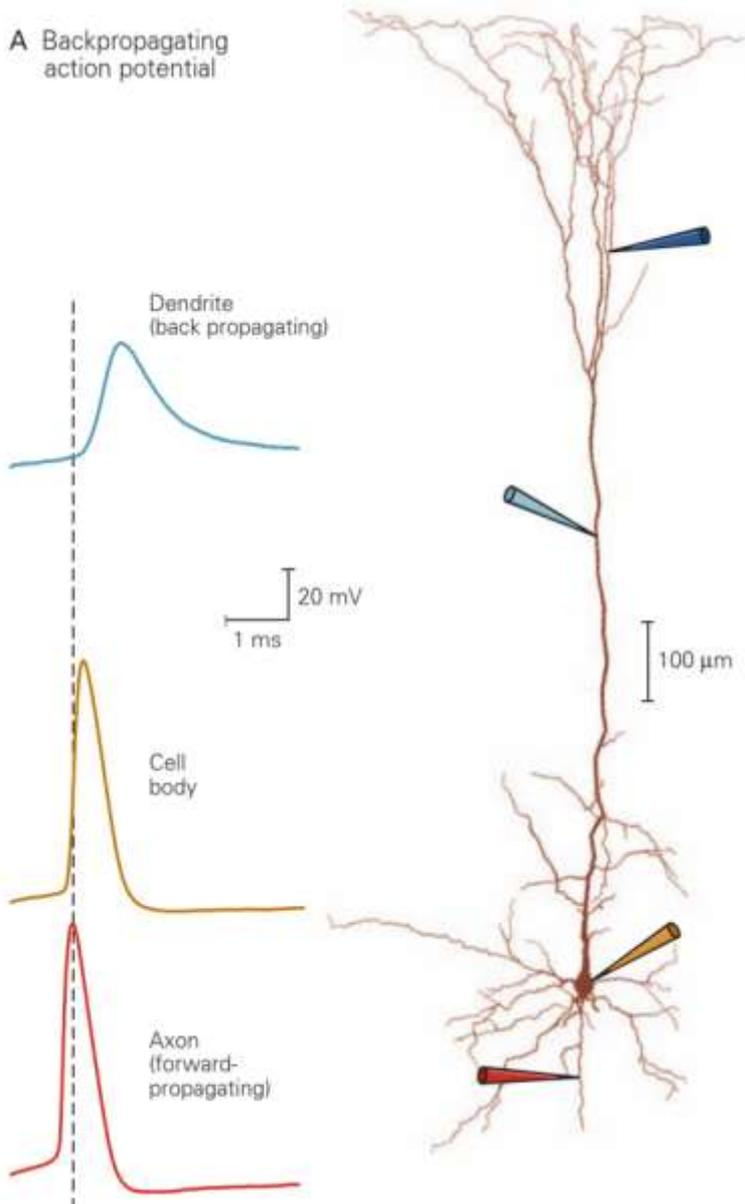
Synaptic potential



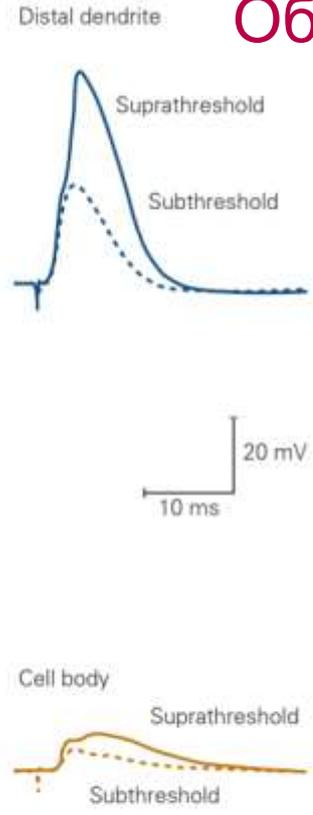
B Spatial summation



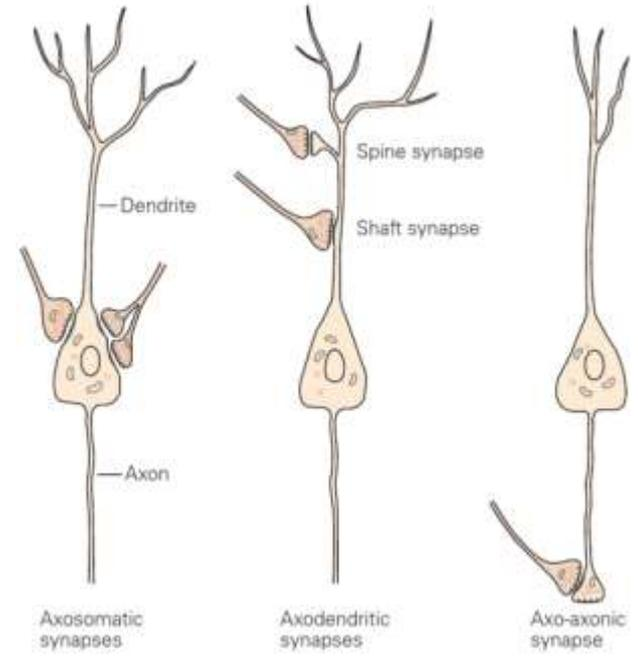
A Backpropagating action potential



B Action potential propagating from dendrite

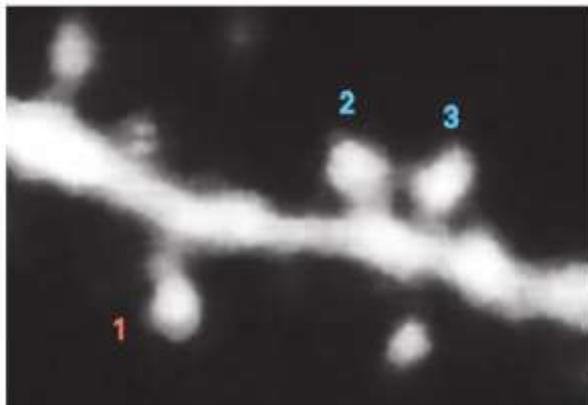


Обратное распространение ПД

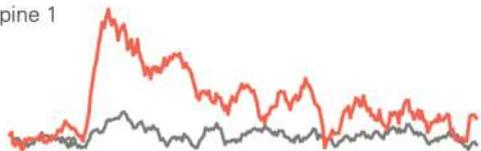


Дендритные шипики и динамика $[Ca^{2+}]$

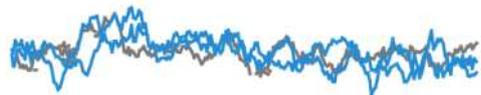
A



Spine 1



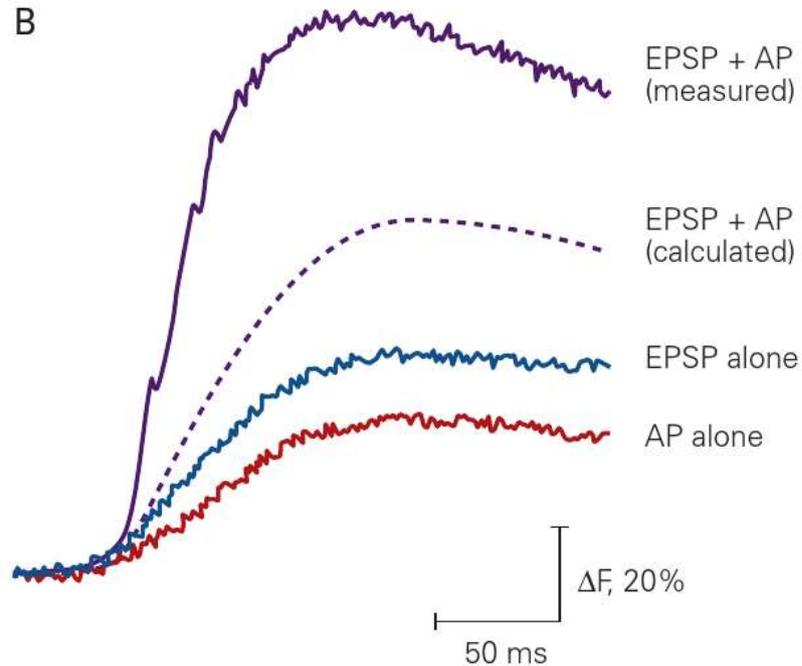
Spines 2 and 3



ΔF , 30%

100 ms

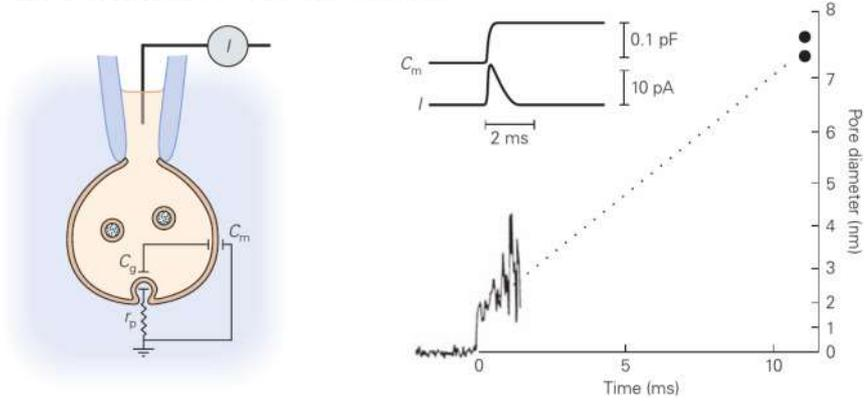
B



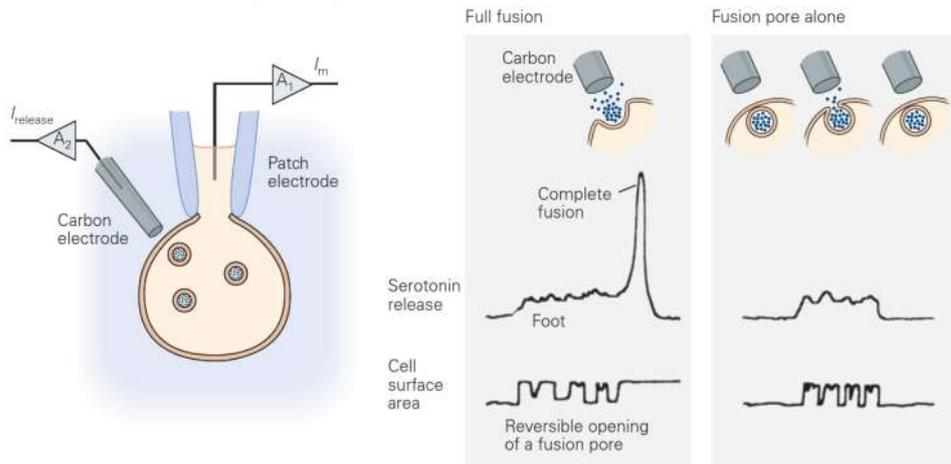
Генерация ПД усиливает вход Ca^{2+}

Механизмы выброса медиатора

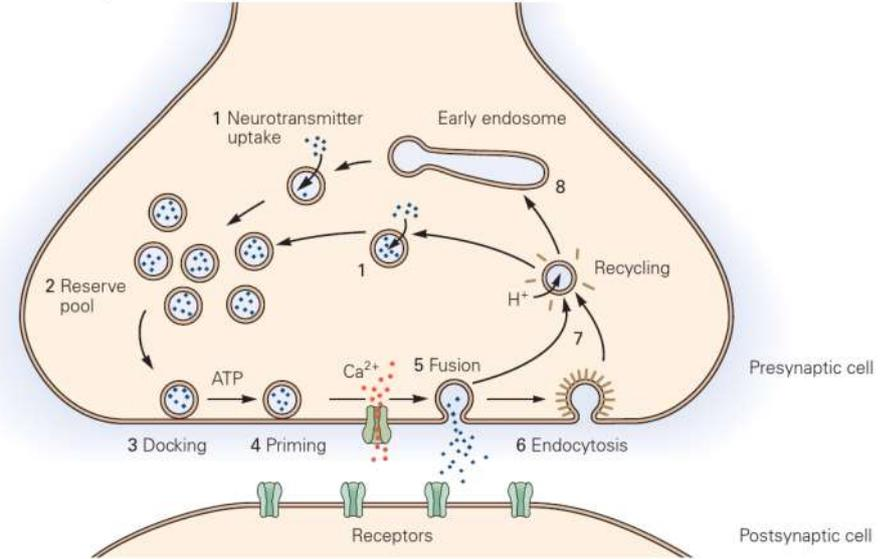
A Electrical events associated with opening of fusion pore



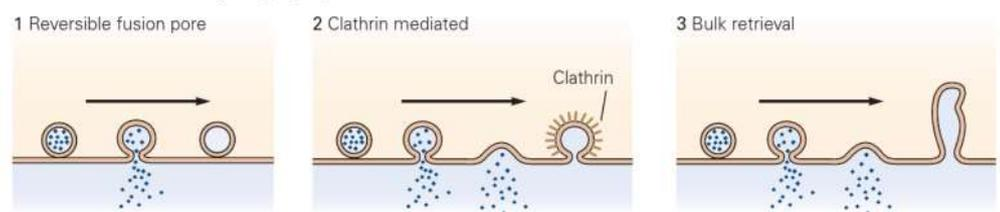
B Transmitter release through fusion pore



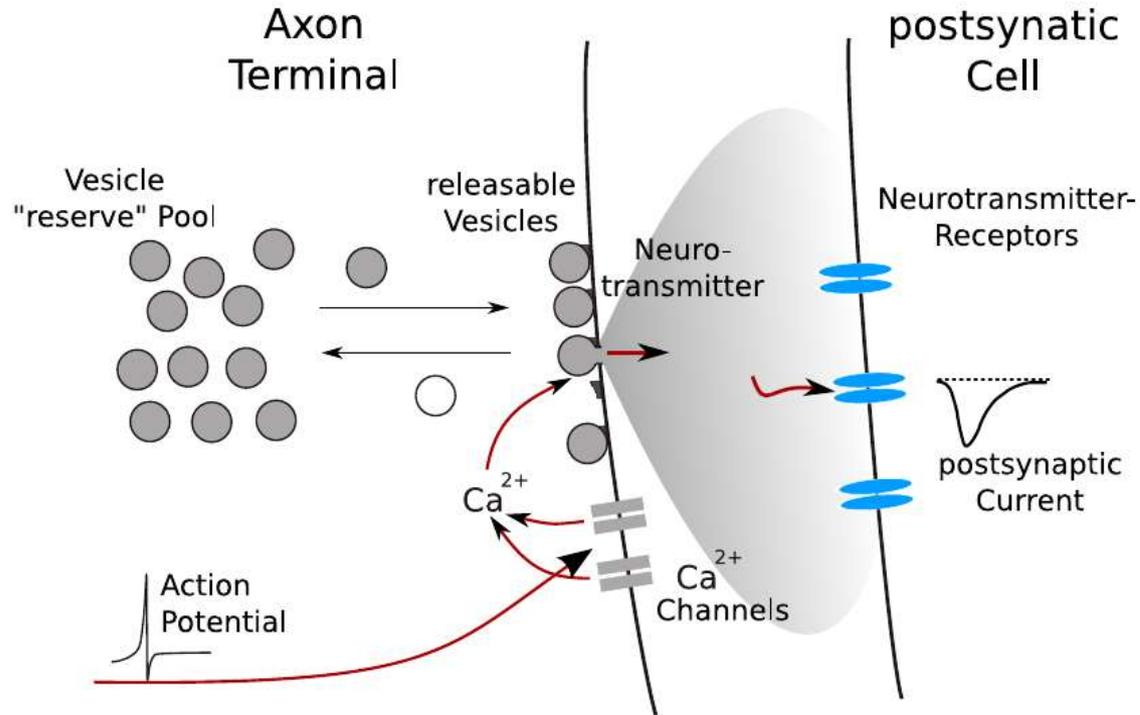
A Synaptic vesicle cycle



B Mechanisms for recycling synaptic vesicles

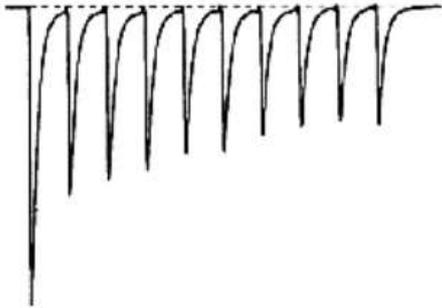


Short-time plasticity (presynaptic membrane)



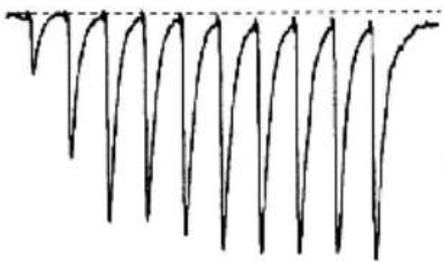
Types of short-time plasticity

Climbing Fibre to Purkinje Cell



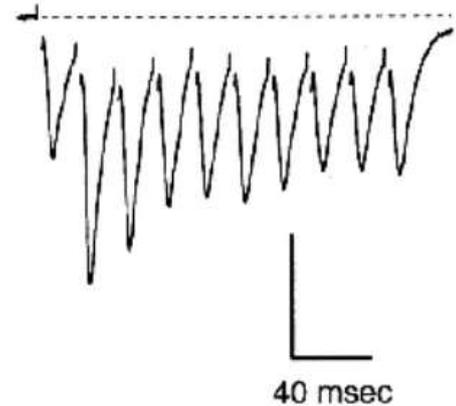
depression

Parallel Fibre to Purkinje Cell



facilitation

Schaffer Collateral



mixed

Dittman et al., 2000 (10 Stimuli at 50 Hz)

Depletion/facilitation model

$$\frac{dn(t)}{dt} = \underbrace{\frac{1-n(t)}{\tau_r}}_{\text{refilling}} - \underbrace{\sum_j \delta(t-t_j) \cdot p \cdot n(t)}_{\text{release}},$$

$$\frac{dp(t)}{dt} = \frac{p_0 - p}{\tau_f} + \sum_j \delta(t-t_j) \cdot f \cdot (1-p(t)),$$

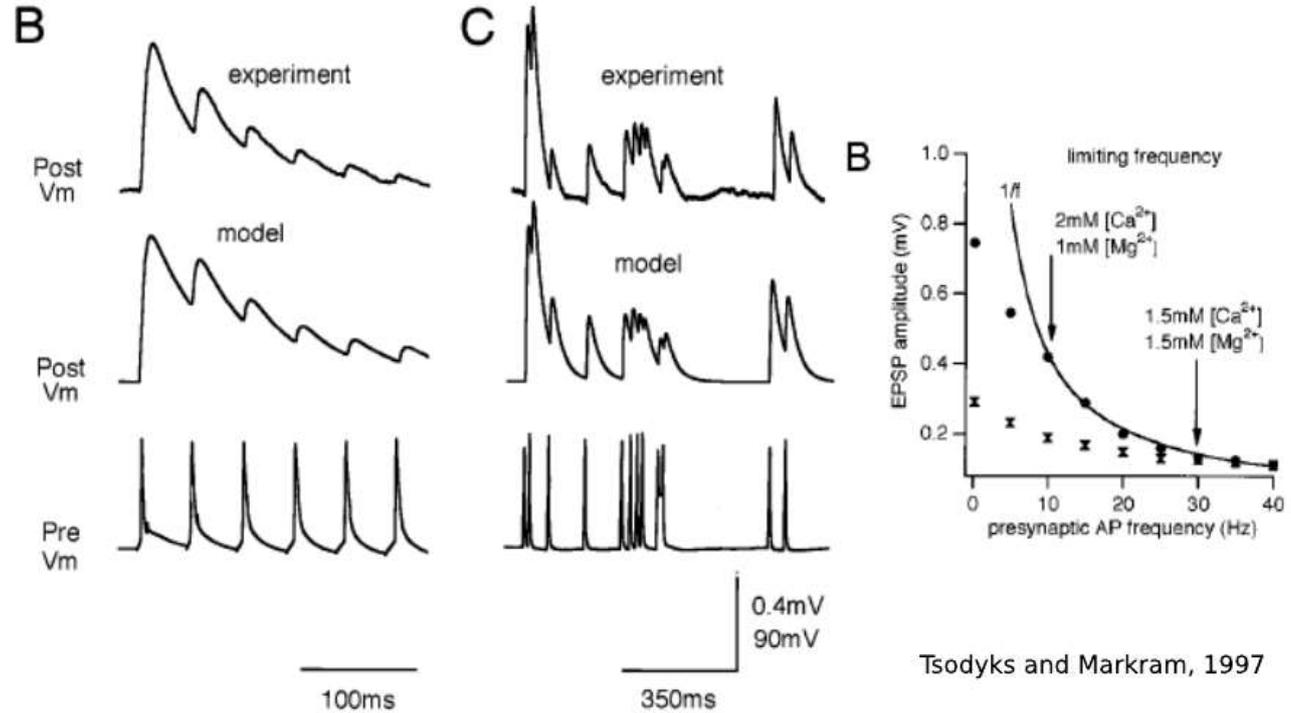


Fig. 8: Modelling synaptic depression with a simple depletion model (neocortical pyramidal cells, compiled from [Tsodyks and Markram 1997](#)).

Рецепторы с цистеиновой петлей (Cys-loop)

- nAChR
- 5-HT₃R
- GABA_{A/C}R
- GlyR
- Zn²⁺-activated cationic ch.
- Бесп: анионные 5-HTR и GluR
- Бесп: катионные GABAR

- Гетеропентамеры:
 - αβγδε...
 - 2:2:1 α:β:γ (GABAR)
 - α₂βεδ (nAChR)
- Консервативная петля из дисульф. связи, соединяющая цистеины, фланкирующие короткую консервативную последовательность из 13 амк между канальной и рецепторной частями белка

Ацетилхолиновый рецептор: nAChR

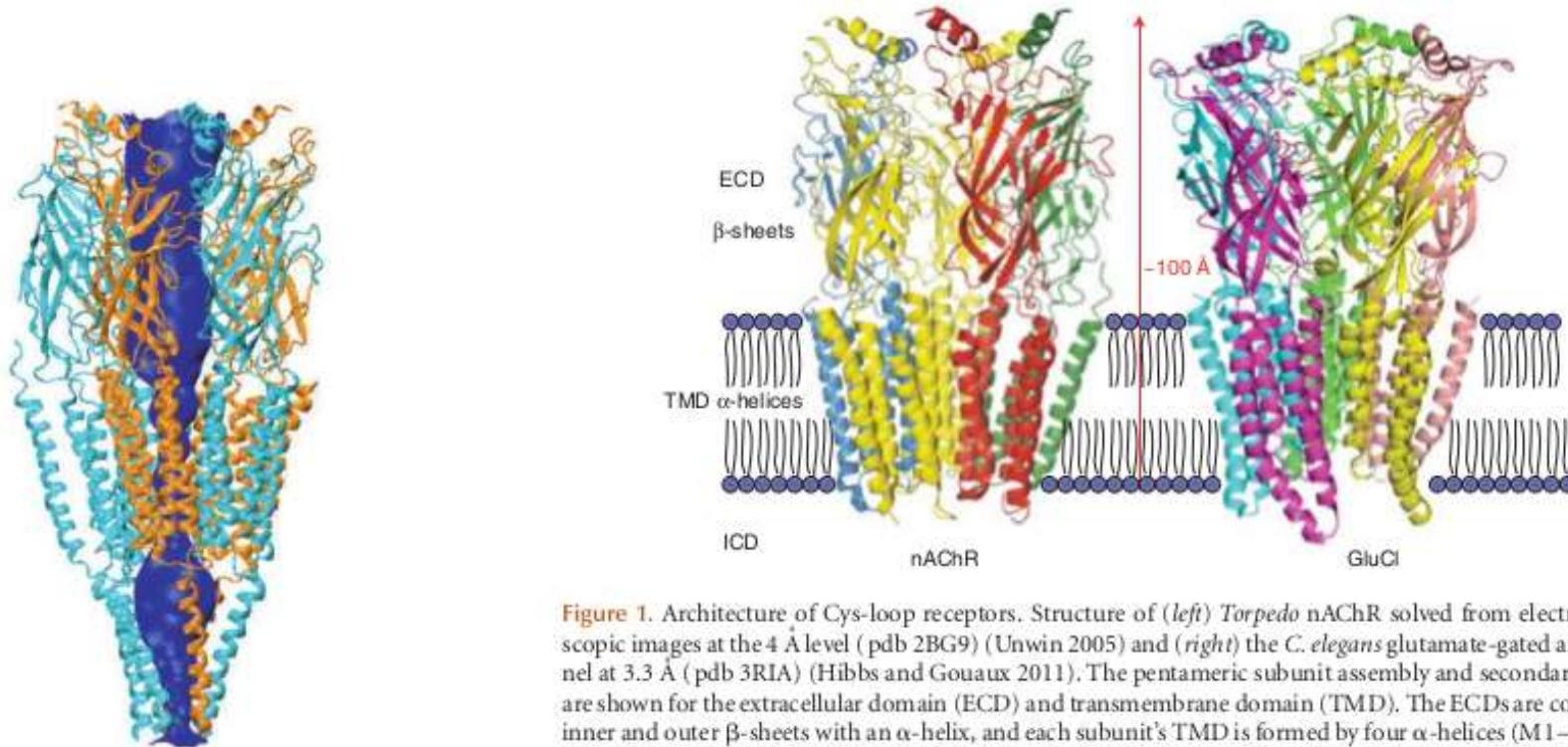


Figure 1. Architecture of Cys-loop receptors. Structure of (left) *Torpedo* nAChR solved from electron microscopic images at the 4 Å level (pdb 2BG9) (Unwin 2005) and (right) the *C. elegans* glutamate-gated anion channel at 3.3 Å (pdb 3RIA) (Hibbs and Gouaux 2011). The pentameric subunit assembly and secondary structure are shown for the extracellular domain (ECD) and transmembrane domain (TMD). The ECDs are composed of inner and outer β -sheets with an α -helix, and each subunit's TMD is formed by four α -helices (M1–M4). Note that for nAChR, the intracellular (MA) helices preceding M4 are omitted, whereas the M3–MA stretch is disordered and is thus not included in the structure. For the GluCl structure, the M3–M4 domain is replaced by a tripeptide, A-G-T (Hibbs and Gouaux 2011).

Связывание лигандов

Synaptic Neurotransmitter-Gated Receptors

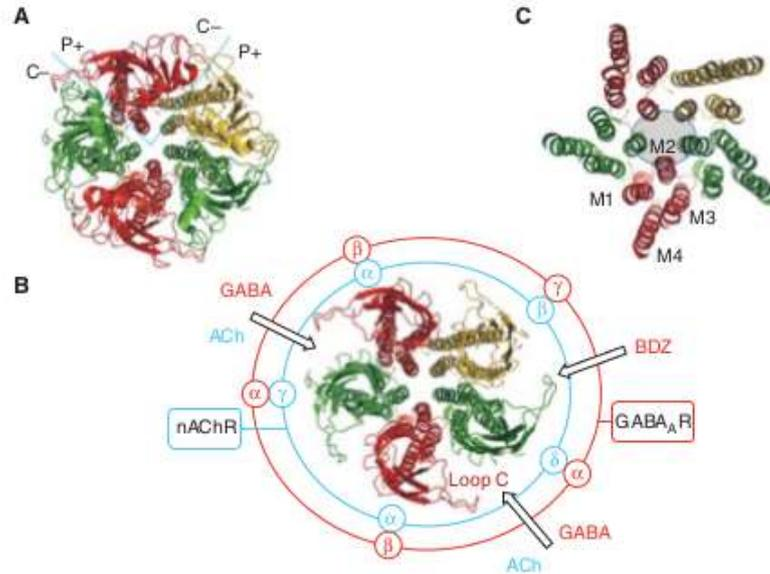


Figure 2. Synaptic view of a Cys-loop receptor. Looking across from the presynaptic terminal over to the post-synaptic membrane, an image of the structure for a typical Cys-loop receptor is shown. This is generated from the atomic resolution structure for AChBP (pdb 2BYQ) (Hansen et al. 2005) for the ECD, linked to the trans-membrane domains taken from images of GLIC (Bocquet et al. 2009). (A) The five subunits form a pseudo-symmetrical ring with interfacial binding sites between principal (P, +) and complementary (C, -) binding faces. Note the central aqueous pathway for ion conduction. (B) A cut-away slab from A depicts the loop C structures on each subunit and the relative stoichiometry for a muscle nAChR and neuronal GABA_AR. The identity of the subunits and neurotransmitter-binding sites are illustrated. (C) Further cut-away to reveal the tops of the TMDs showing M2 lining the ion channel and the support formed by M1, M3, and M4.

Конформационные изменения при связывании ACh

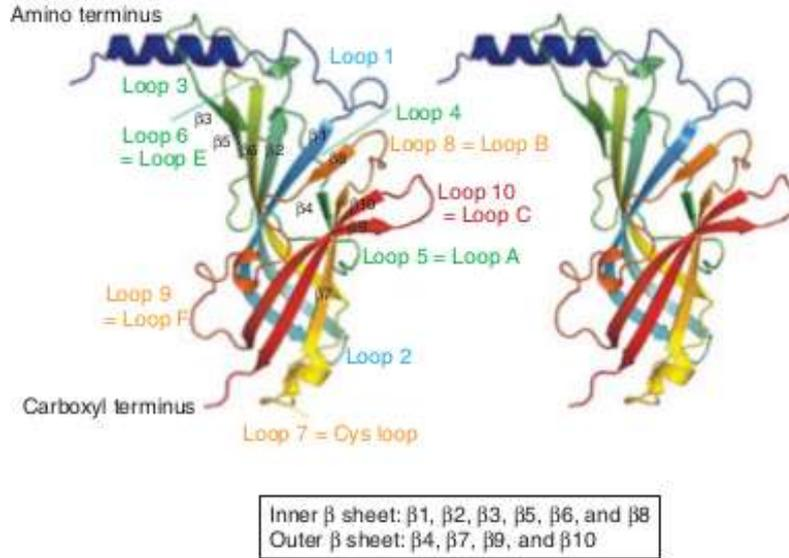
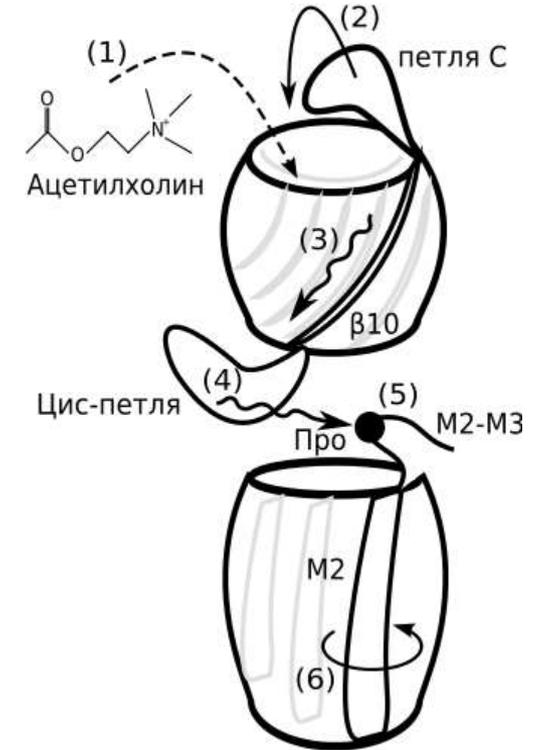
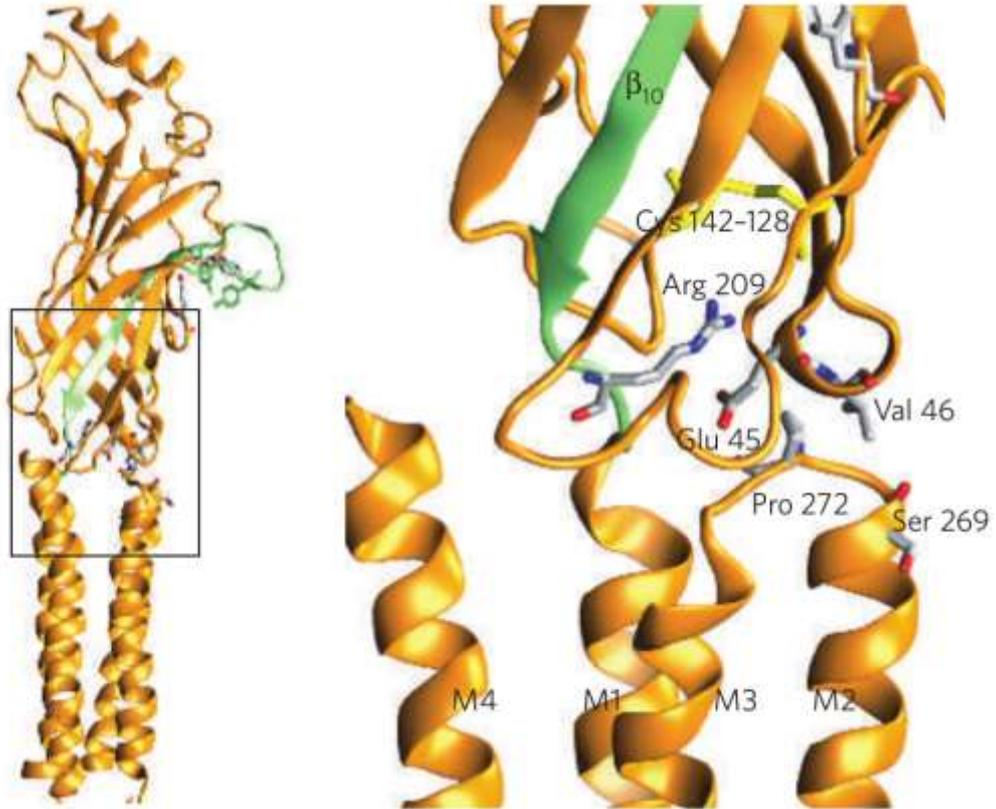


Figure 3. Structure of the extracellular domain. Side view of two adjacent subunits of the AChBP. The positions of the binding loops and other loops from the amino terminus to the carboxyl terminus that adjoins the pre-M1 domain in Cys-loop receptors are shown. β -strands that form the inner and outer β -sheets are also indicated with labeling according to Brejc et al. (2001).

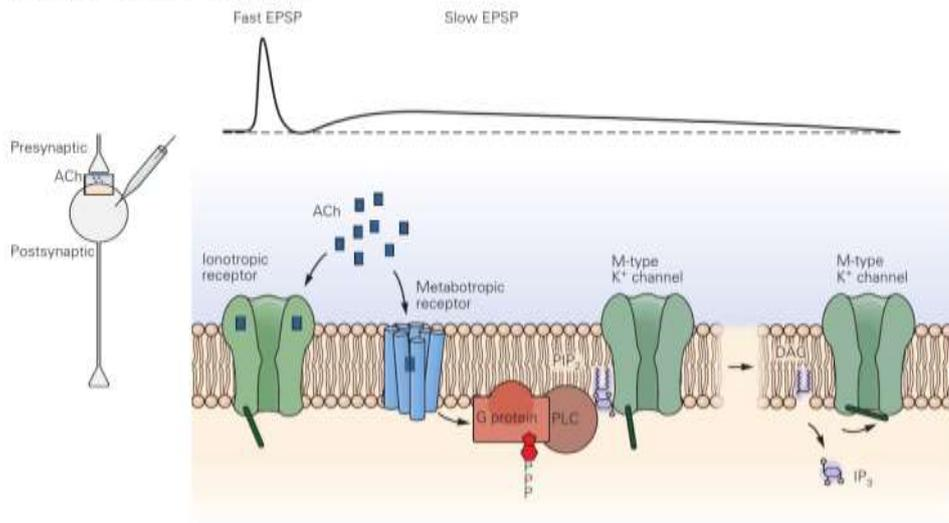


Передача сигнала о связывании к ТМ-части

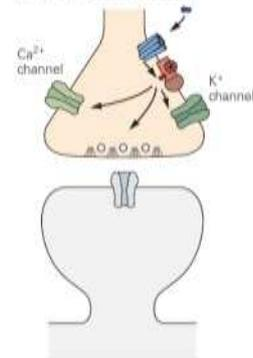


Медленная модуляция синаптической передачи

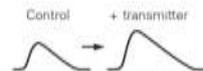
A Fast and slow synaptic transmission



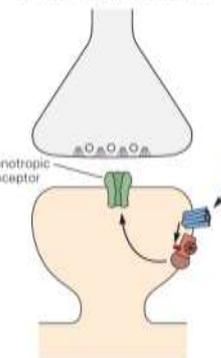
A Presynaptic modulation



Postsynaptic potential



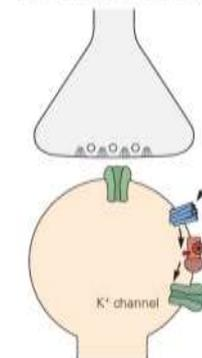
B Postsynaptic modulation



Postsynaptic potential



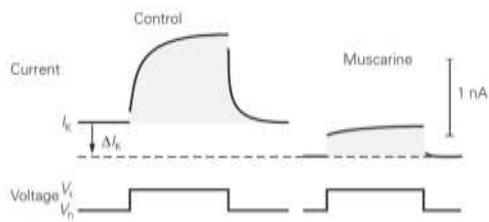
C Modulation in cell body



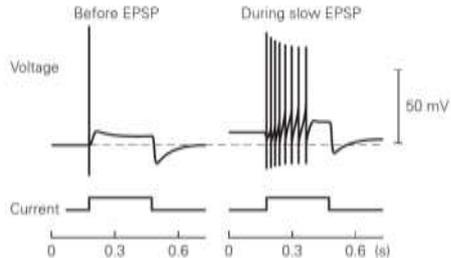
Action potential



B The effect of muscarine on the M-type K⁺ current



C The anti-accommodation effect of M-type K⁺ current inhibition



Подробнее о синапсах

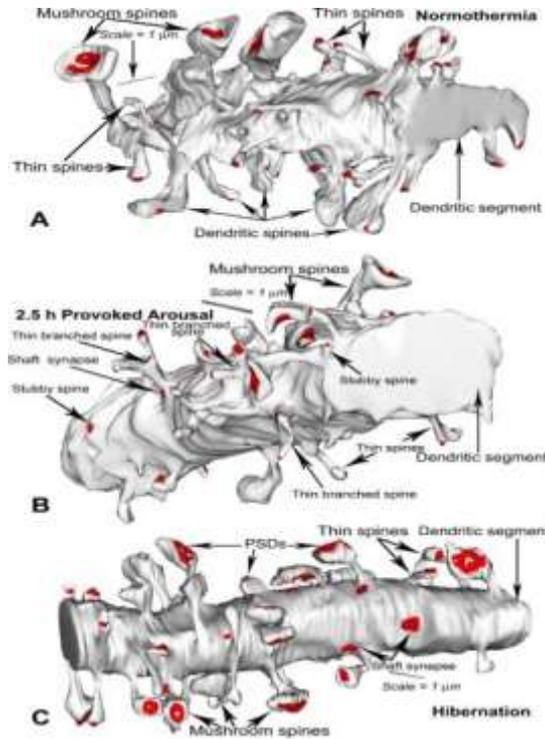


Fig. 6 Typical representatives of 3-D reconstructed dendritic segments in CA1 stratum radiatum of ground squirrels in different functional states: normothermia (A); 2.5 h provoked arousal from hibernation bout (B); and hibernation (C). Twelve dendritic seg...

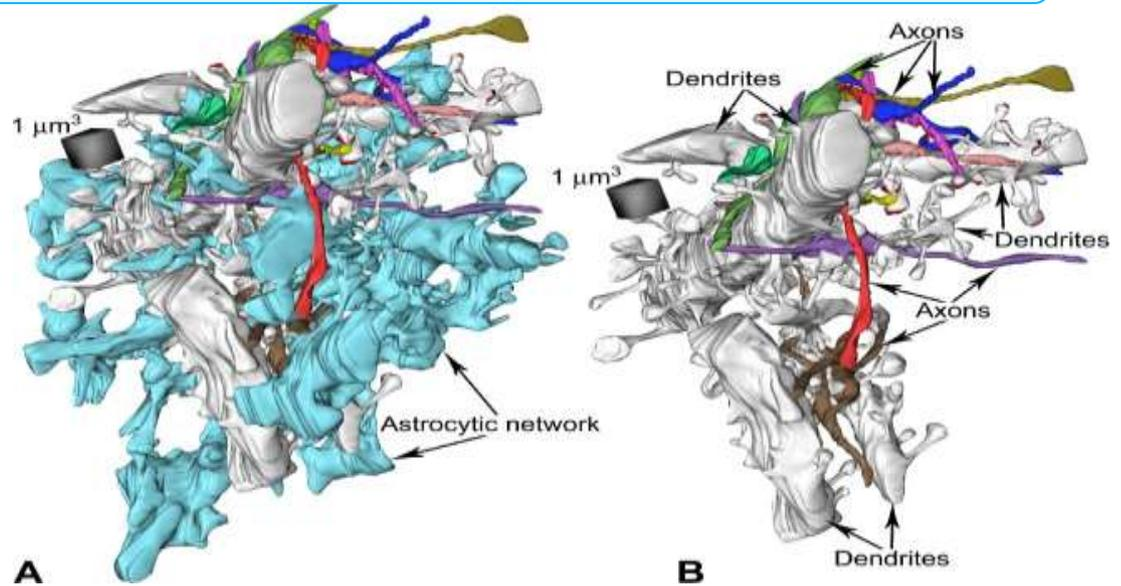


Fig. 8 Examples of spatial geometry of 3-D reconstructions of astrocytic network; dendritic and axonal segments (A) and only six dendritic segments and 10 axonal segments. (B) As (A) but with the astrocyte stripped off leaving dendrites and axons. For hibe...

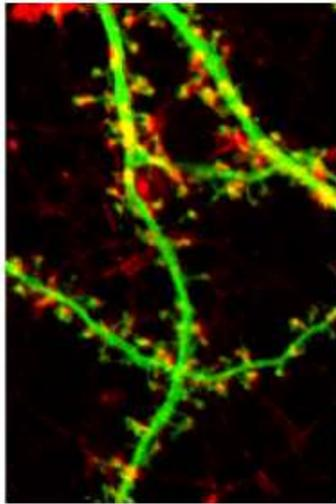
Важные факты:

- один аксон часто дает до 10 синапсов с одним дендритом
- вероятность выделения везикулы медиатора при ПД $p \ll 1$

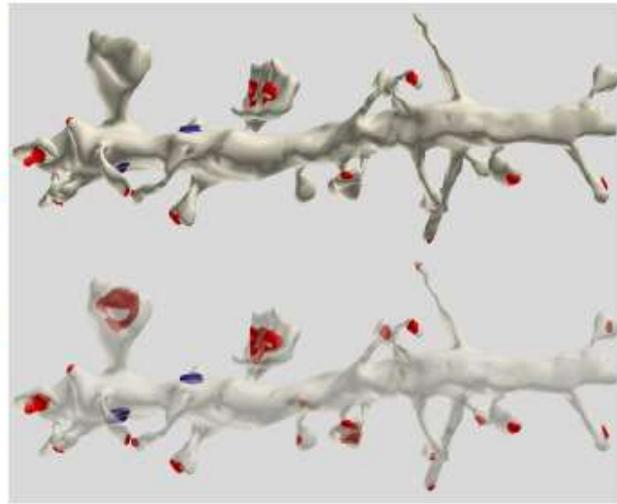
Reversible reduction in dendritic spines in CA1 of rat and ground squirrel subjected to hypothermia–normothermia *in vivo* : A three-dimensional electron microscope study

V.I. Popov , N.I. Medvedev , I.V. Patrushev , D.A. Ignat'ev , E.D. Morenkov , M.G. Stewart

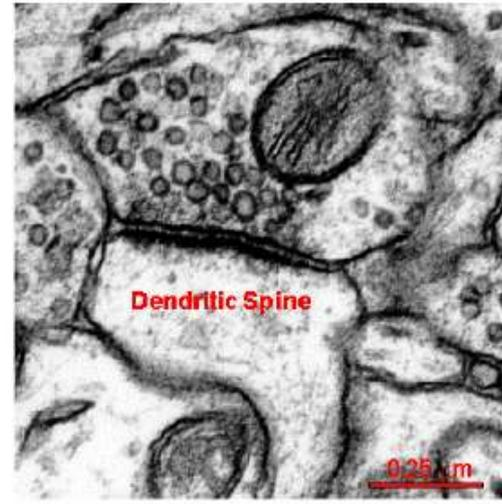
Neuroscience, Volume 149, Issue 3, 2007, 549 - 560
<http://dx.doi.org/10.1016/j.neuroscience.2007.07.059>



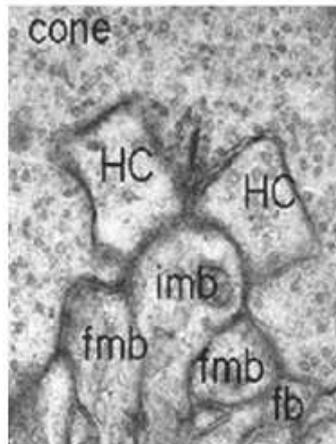
Cultured hippocampal neurons



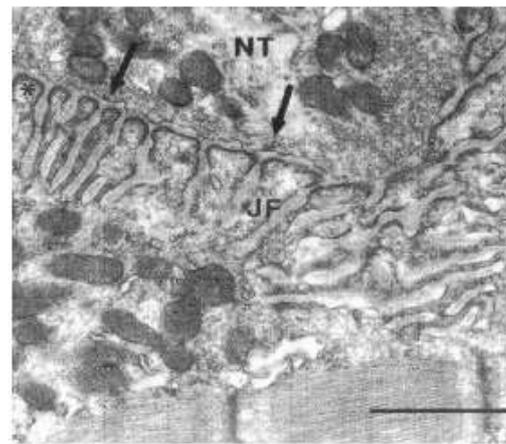
Dendritic spines
(from Synapse Web)



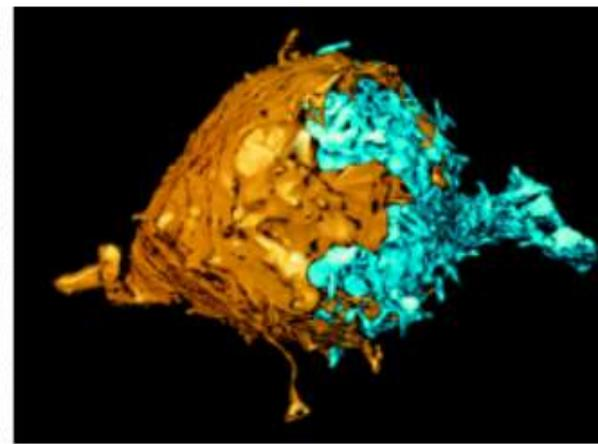
Axon and spine
(from Synapse Web)



Human retinal cone terminal



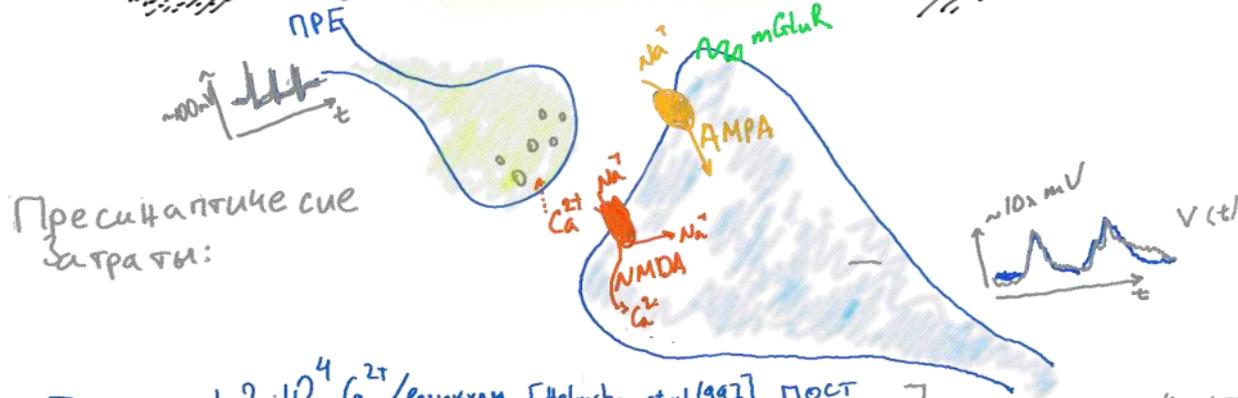
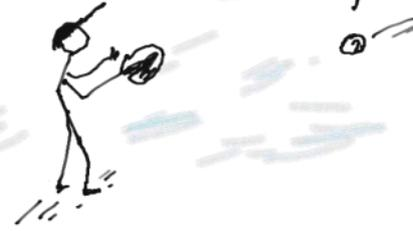
Mouse neuromuscular junction
(Salpeter, 1987)



Calyx of Held in rat auditory brainstem
(Saetzler et al, 2002)



ЗАТРАТЫ НА СИНАПТИЧЕСКУЮ ПЕРЕДАЧУ (2)



Пресинаптические затраты:

$$1 \text{ ПА} \rightarrow \sim 1.2 \cdot 10^4 \text{ Ca}^{2+} / \text{везикулу} \text{ [Helmen et al 1997]} \text{ ПОСТ}$$

$$\rightarrow 1.2 \cdot 10^4 \text{ АТФ} / \text{везикулу}$$

$$- + \sim 500 \text{ АТФ на собств. выдох везикулы}$$

$$+ \text{ обработка } \Gamma_{\text{л}}: \sim 2.67 \cdot 4000 \approx 11 \cdot 10^3 \frac{\text{АТФ}}{\text{ВСП}}$$

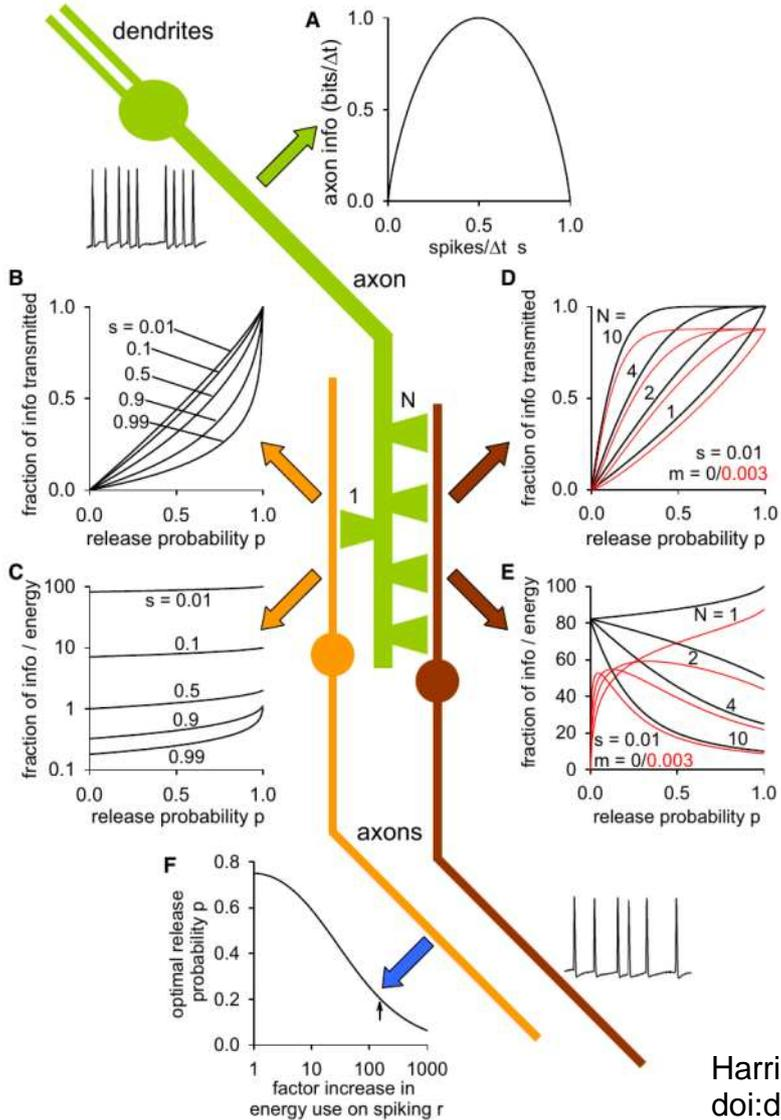
$$\sum_{\text{пре}} = 1.25 \cdot 10^4 \frac{\text{АТФ}}{\text{ВСП}}$$

$$\sum_{\text{пост}} = 14 \cdot 10^4 \frac{\text{АТФ}}{\text{ВСП}}$$

$$\sum_{\text{гл}} = 1.1 \cdot 10^4 \frac{\text{АТФ}}{\text{ВСП}}$$

$$\sum: 1.64 \cdot 10^5 \frac{\text{АТФ}}{\text{ВСП}}$$

Передача информации через синапс и метаболические ограничения



Доля переданной информации / энергозатраты при нескольких синапсах

```

function model_noise_multis(p,N,spnt;verbose=false, Ntrials=100)
% Calculate empirical probabilities
responses = zeros(2,N+1)
for i = 1:Ntrials
    if randi() = 1 % spike arrived
        row,col = 1,1
        for j = 1:N % for each release site
            col = if randi() = p 1 else 0 end
        end
    else
        row,col = 1,1
        for j = 2:N % spontaneous release
            col = if randi() = spnt 1 else 0 end
        end
    end
    responses[row,col] += 1
end

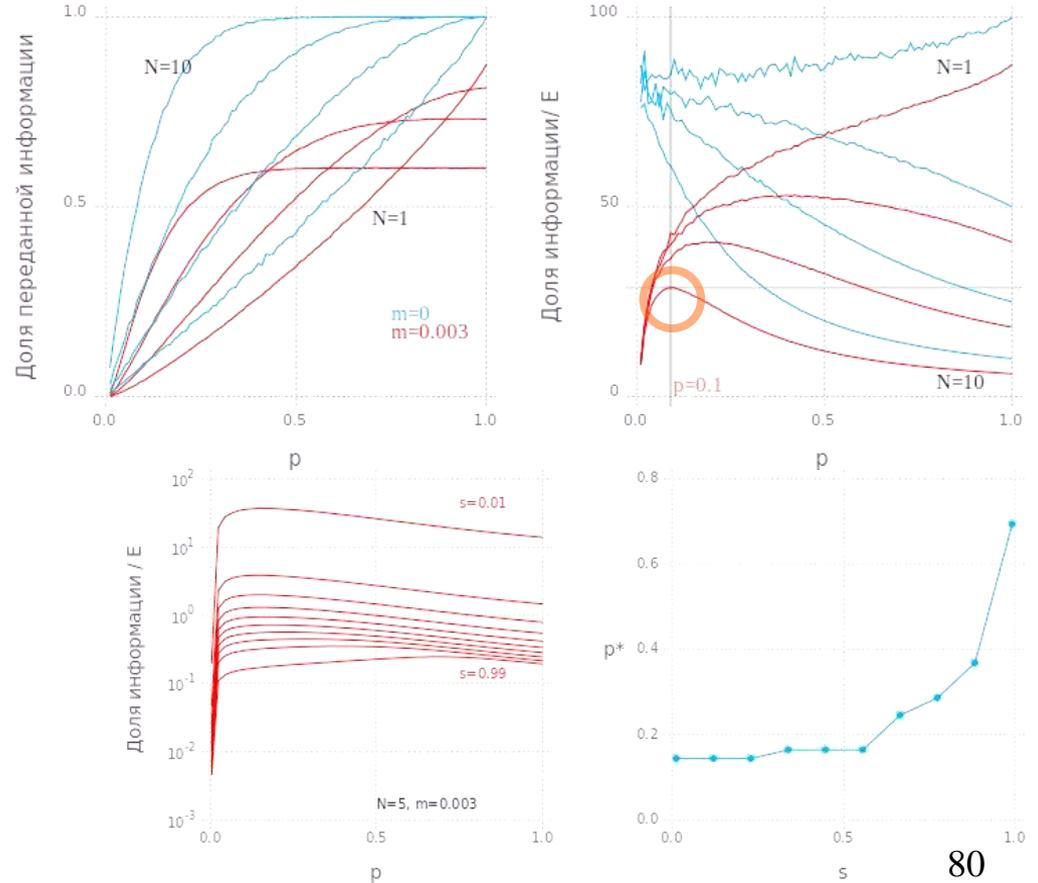
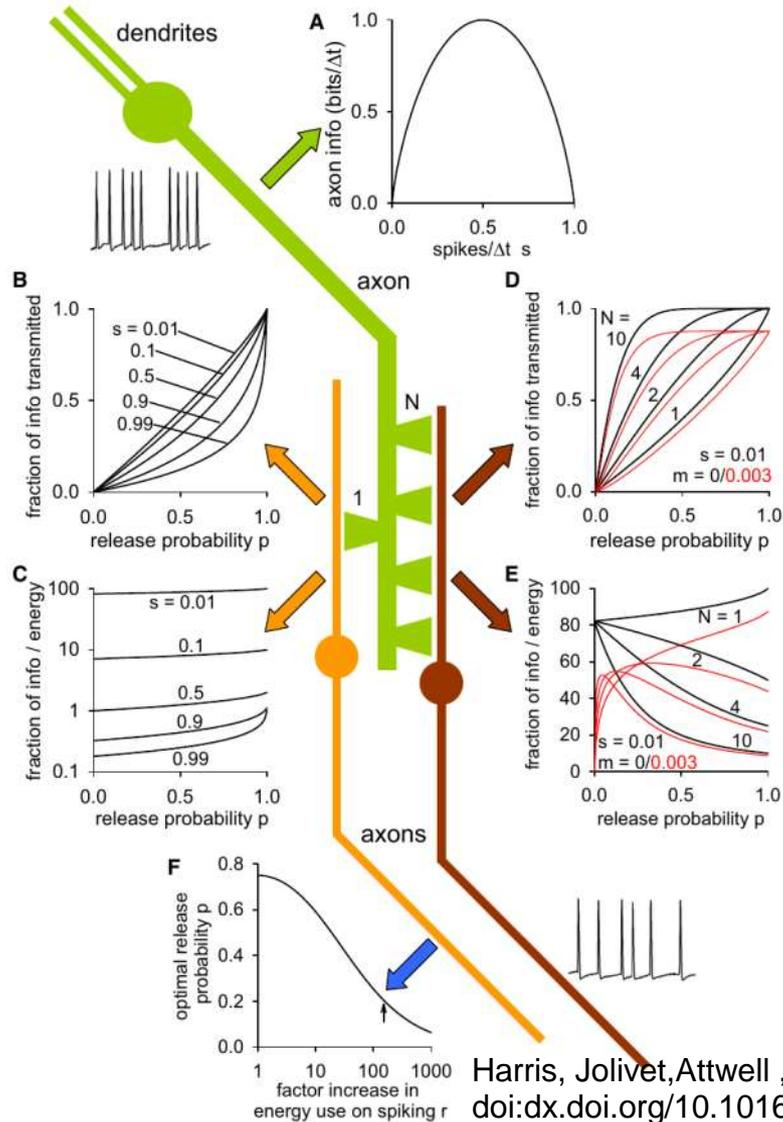
probe = responses/Ntrials
probe = hcat(probe{:},1), sumprobe{:},2:end(2,2))
if verbose printInfoAndProbe(1) end

% calculate information
out = 0
for col in 1:size(probe,2)
    Pr = sumprobe{:},col
    for row in 1,2
        P & r = probe[row,col]/Pr
        if P & r = 0
            out = Pr * s * r * log2(P & r)
        end
    end
end

Ps = sum(probe{:},2)
Iinp = -sum(Ps .* log2(Ps))
return I = out/Iinp
end
    
```

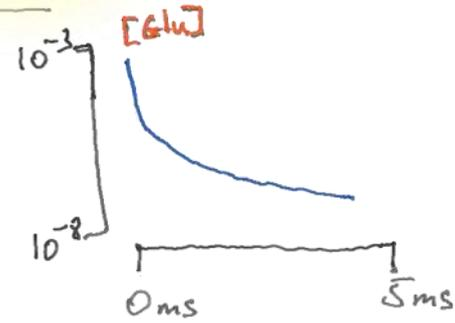
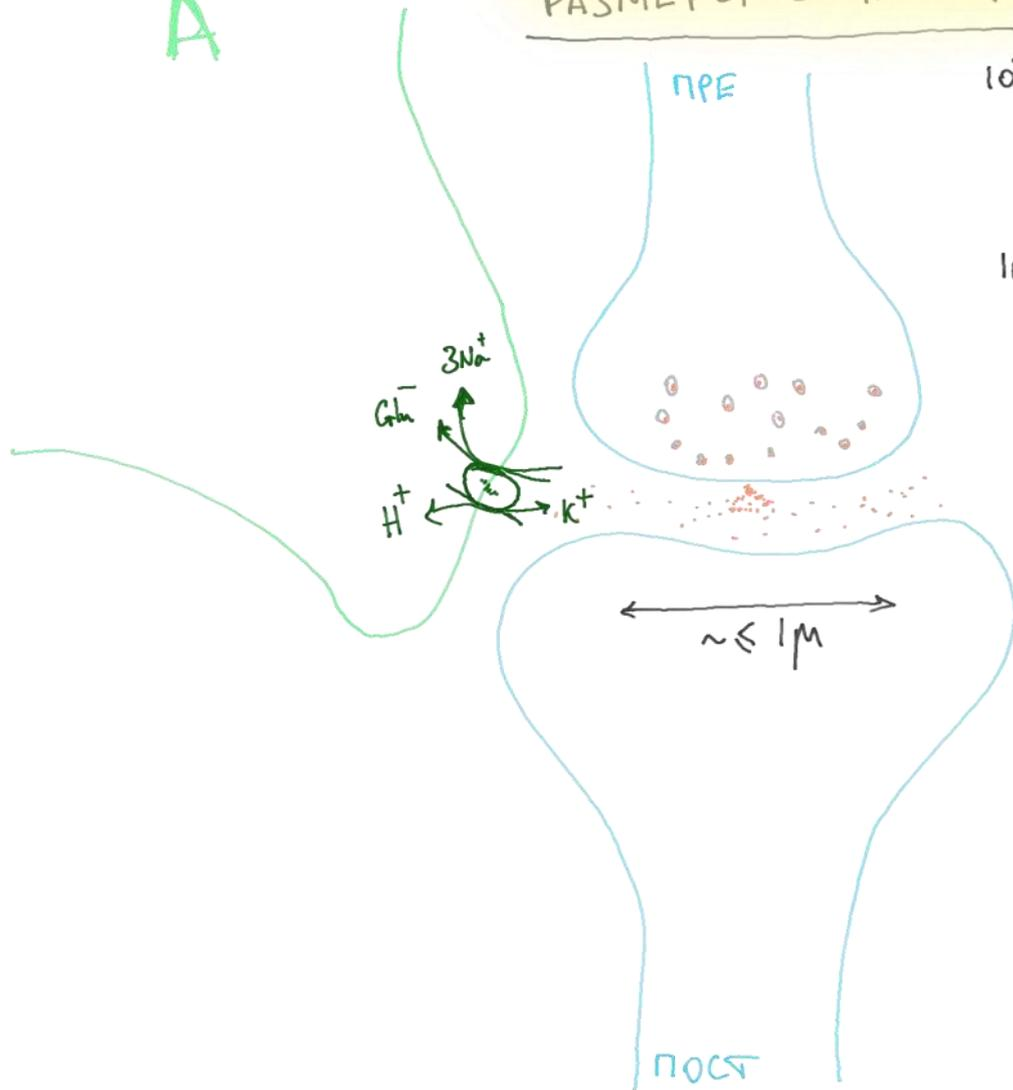
Harris, Jolivet, Attwell, 2012:
doi:dx.doi.org/10.1016/j.neuron.2012.08.019

Передача информации через синапс и метаболические ограничения



A

ГЕОМЕТРИЧЕСКИЕ РАЗМЕРЫ СИНАПСА



$$D^* \sim 0.5 \mu^2 / \text{мсек}$$

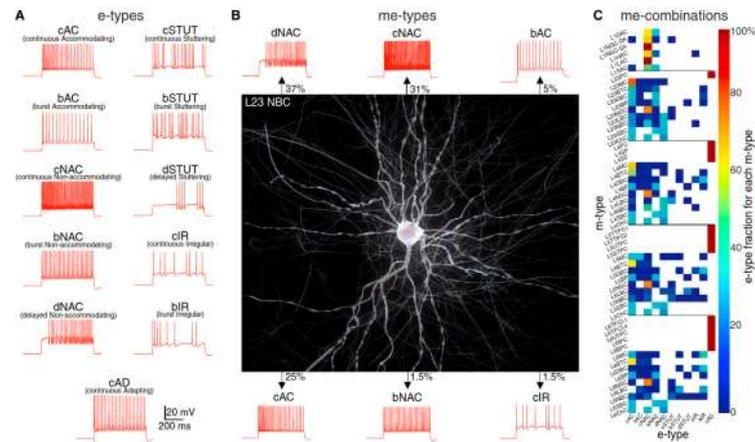
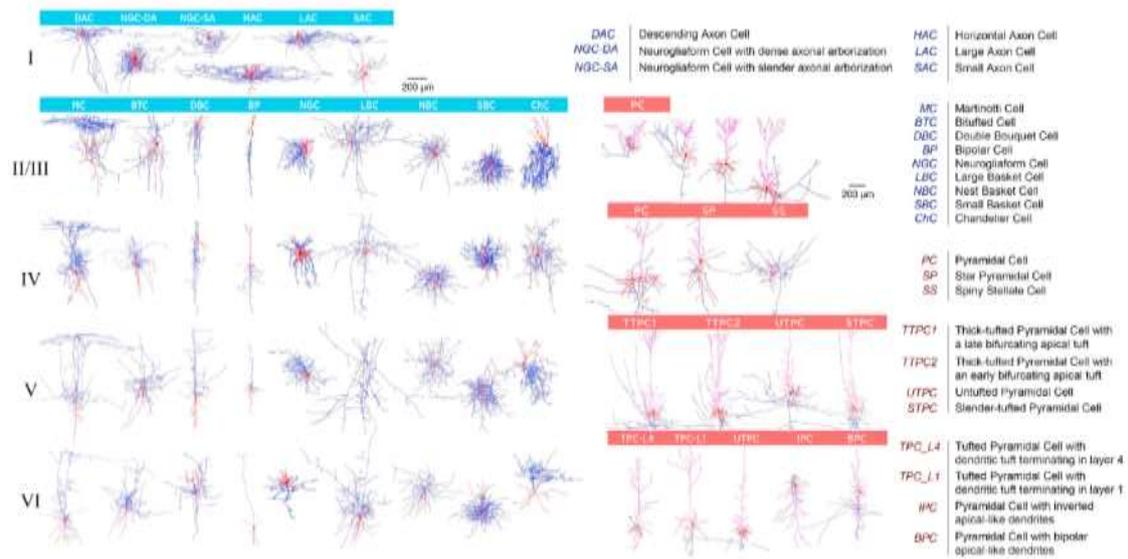
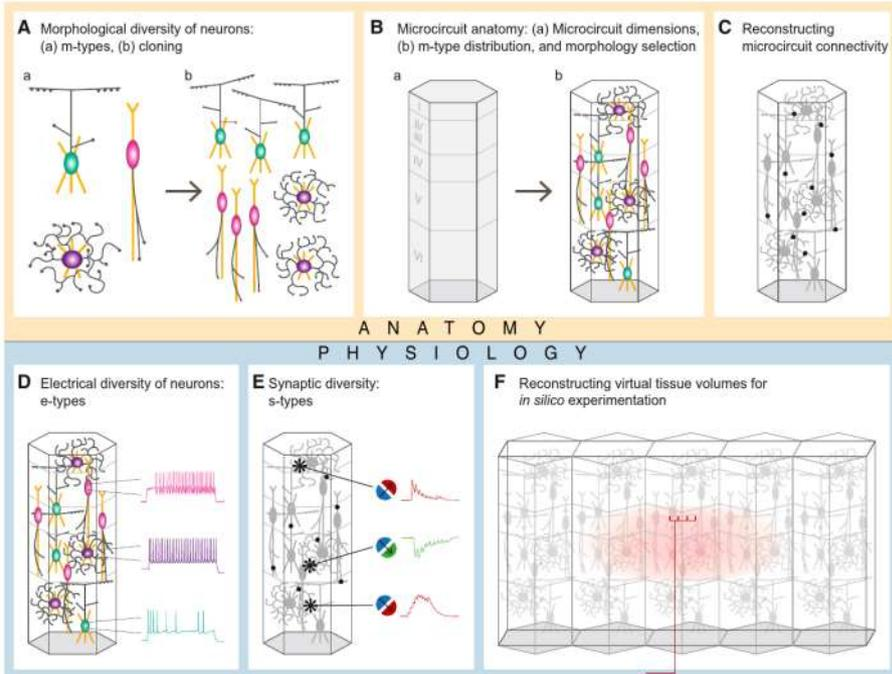
$$\langle \Delta x \rangle \sim \sqrt{D t}$$

Для работы с
характерным
временем $\tau = 1 \text{ мс}$,
размер синапса
р.с. $\sim 1 \mu$

Оптимизация затрат АТФ на уровне постсинаптической мембраны

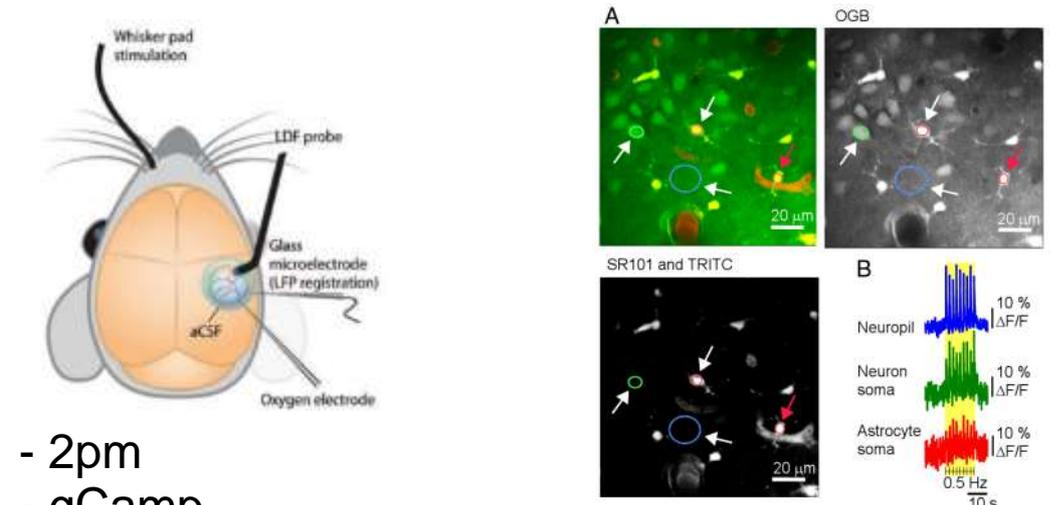
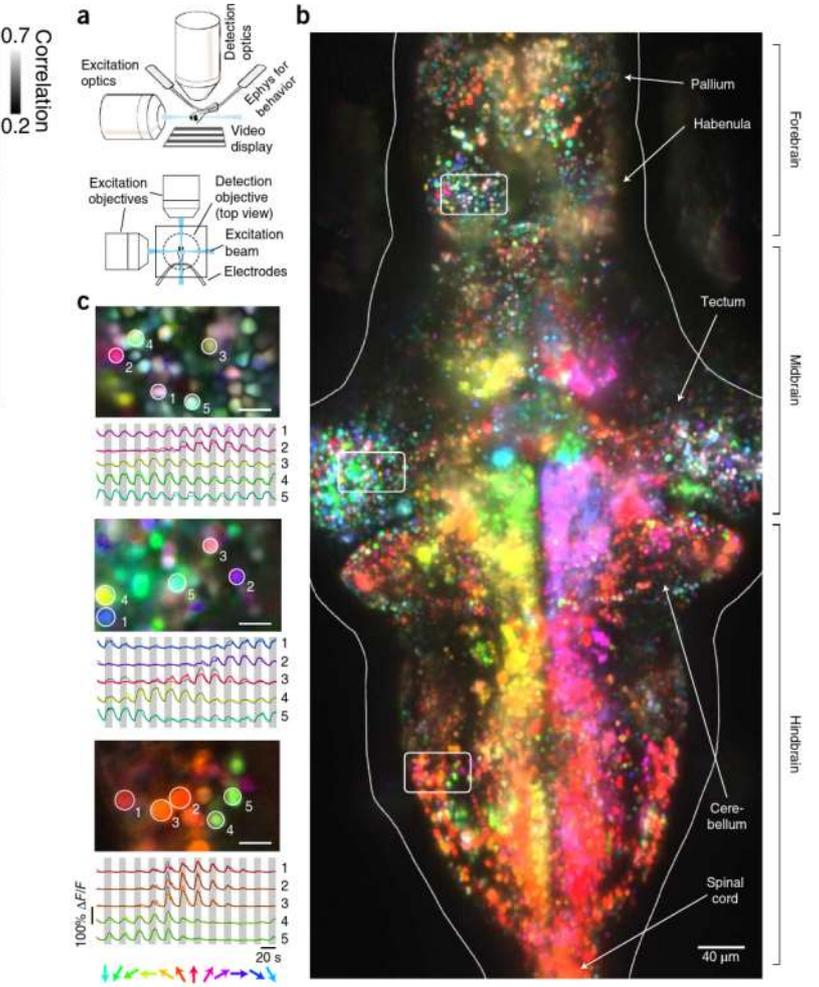
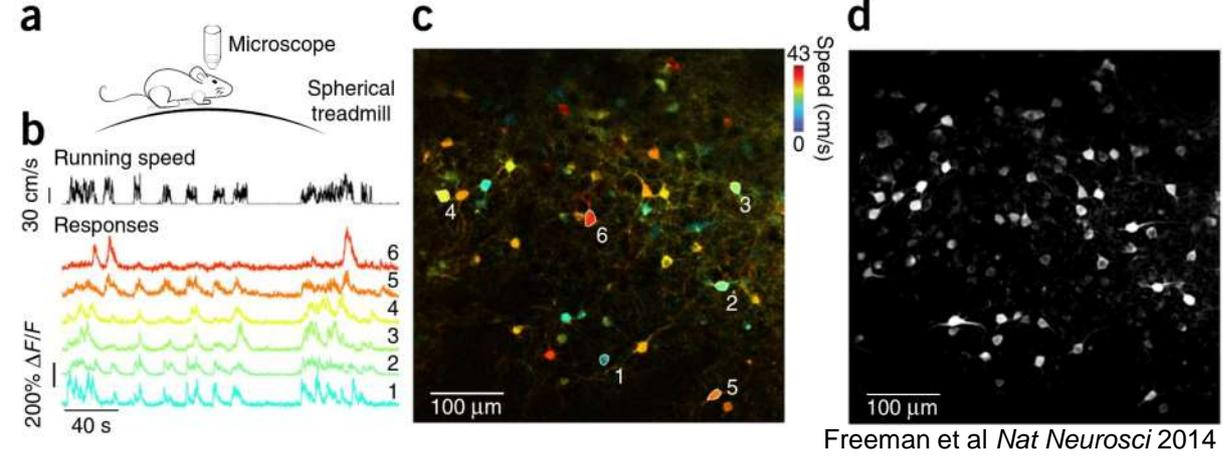
- Размер синаптического бутона ($\sim 1\mu$) продиктован **временной шкалой ($\sim 1\text{мс}$)**
- Количество рецепторов на постсинаптическую мембрану ограничено **плотностью и затратами энергии**
- Низкая афинность AMPA-рецепторов к глутамату определяется **необходимостью быстро диссоциировать при временной шкале 1мс**

Масштабные биофизические модели нервных клеток



Markram et al. *Cell* 2015

Как исследуют активность нейронов *in vivo*

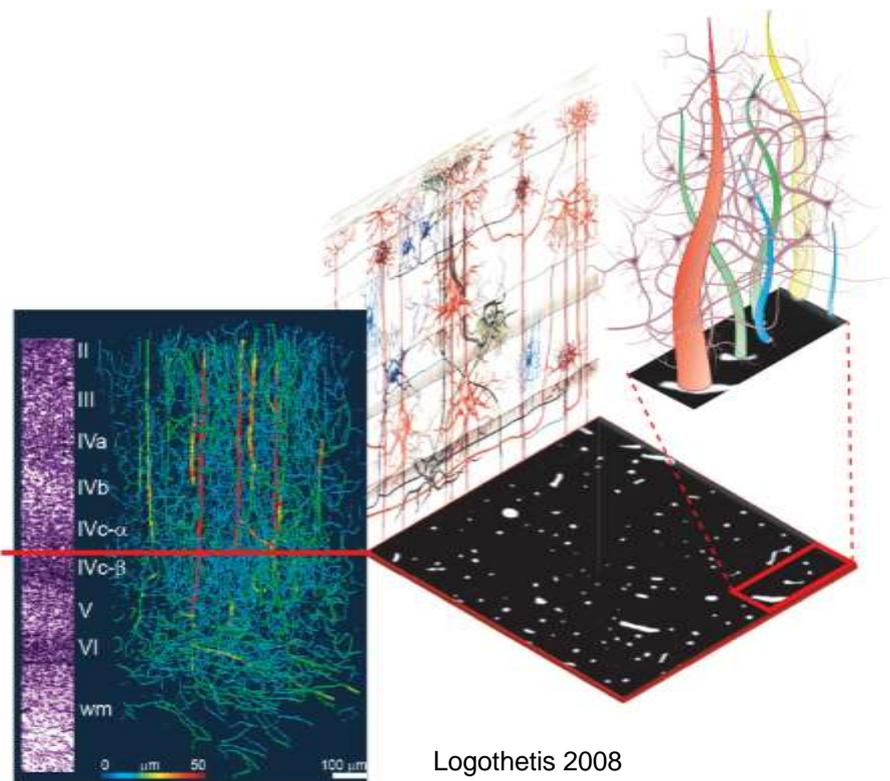


- 2pm
- gCamp

Lind, Brazhe, Jessen, Tan, Lauritzen *PNAS* 2013

Freeman et al *Nat Neurosci* 2014

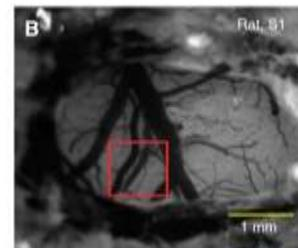
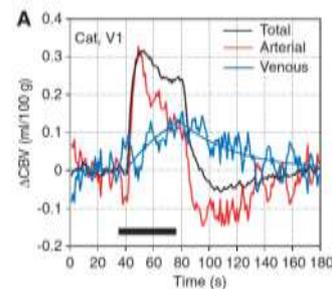
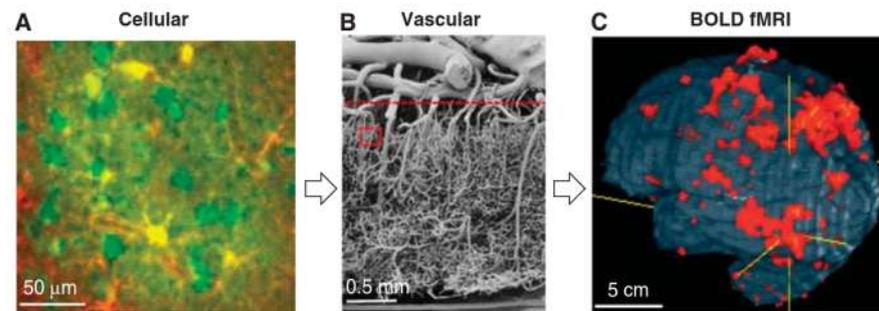
Что измеряется в fMRI?



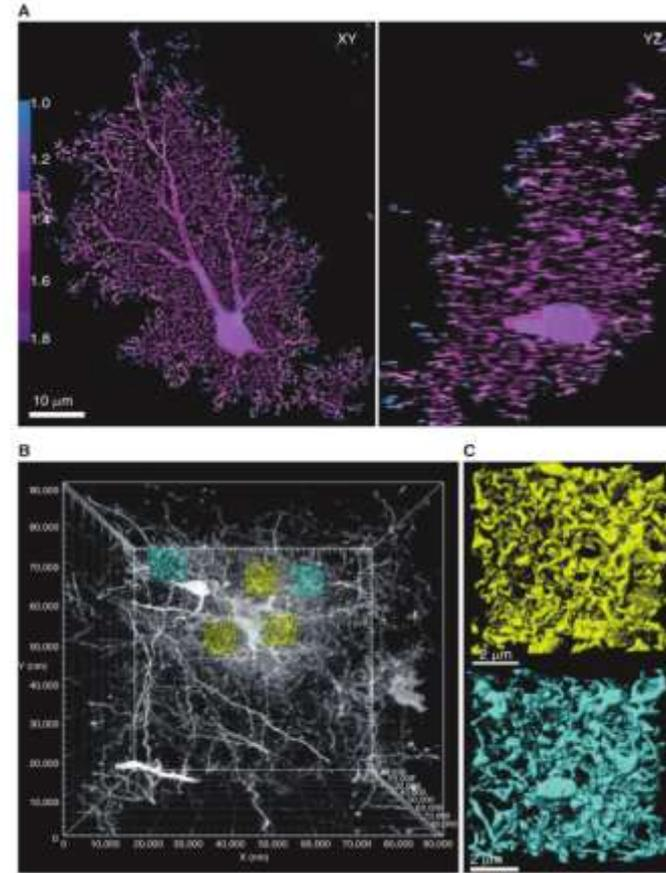
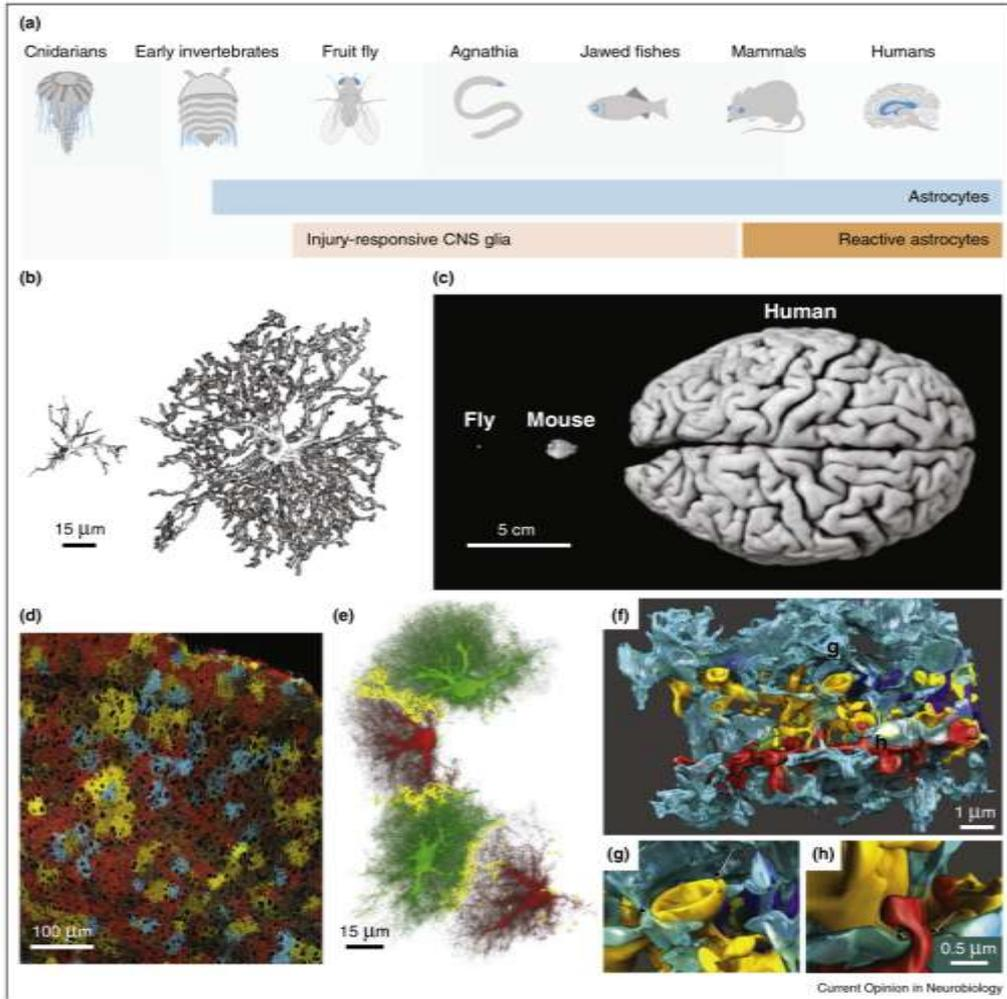
Logothetis 2008

Figure 3 | Neural and vascular contents of a voxel. The left panel demonstrates the relative density of vessels in the visual cortex of monkeys. The dense vascular mesh is displayed by perfusing the tissue with barium sulphate and imaging it with synchrotron-based X-ray microtomography (courtesy B. Weber, MPI for Biological Cybernetics). The vessel diameter is colour coded. Cortical surface without pial vessels is displayed at the top; white matter at the bottom. At the left of the panel is a Nissl slice from the same area, showing the neural density for layers II through to the white matter (wm). Although the density of the vessels appears to be high in this three-dimensional representation, it is actually less than the 3% (see section at the

right; white spots are cross-sections of vessels). The average distance between the small vessels (capillaries) is about 50 μm . This is approximately the distance that oxygen molecules travel by diffusion within the limited transit time of the blood. The dense population of neurons, synapses and glia occupy the intervascular space, as depicted in the drawing at the top right—a hypothetical distribution of vascular and neural elements in a small section (red rectangle). The drawing in the background shows some of the typical neuronal types (for example, red, large pyramidal cell; dark blue, inhibitory basket cells; light blue, chandelier inhibitory neurons; and grey, stellate cells) and their processes.



Астроциты



Khakh, MacCarthy.
Cold Spring Harb Perspect Biol 2015;7:a020404

Astrocytes Control Synapse Formation, Function, and Elimination



Won-Suk Chung¹, Nicola J. Allen², and Cagla Eroglu³

Copyright © 2015 Cold Spring Harbor Laboratory Press; all rights reserved
Advanced Online Article. Cite this article as *Cold Spring Harb Perspect Biol* doi: 10.1101/cshperspect.a020370

W.-S. Chung et al.

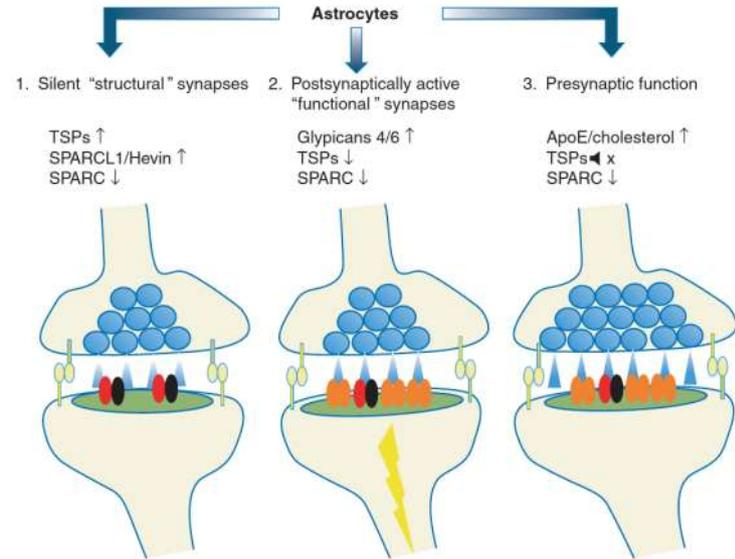
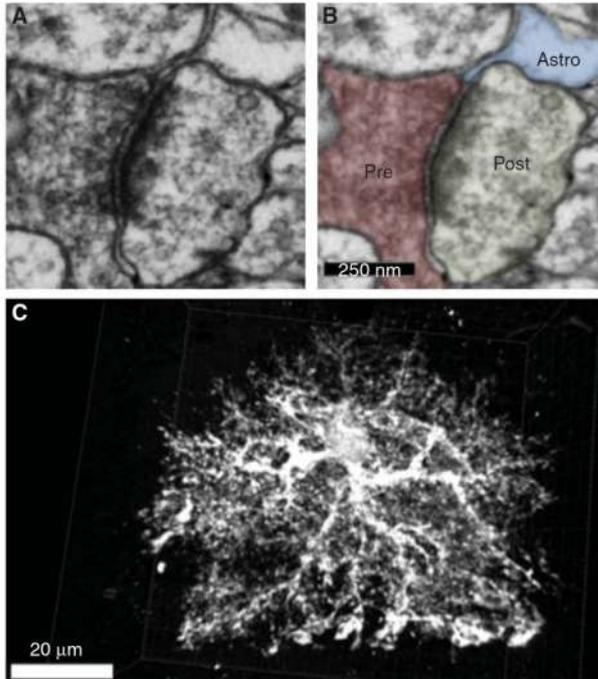


Figure 3. Astrocyte-secreted factors control different aspects of excitatory synaptic development. (1) Astrocytes increase the number of structural synapses. These synapses have normal morphology and contain *N*-methyl-D-aspartate (NMDA) receptors (red and black). However, they lack AMPA-type glutamate receptors (orange). (2) Astrocytes increase postsynaptic activity by inducing AMPA receptor localization to the postsynaptic density. (3) Astrocytes enhance presynaptic release by increasing release probabilities.

Astroglial cradle in the life of the synapse

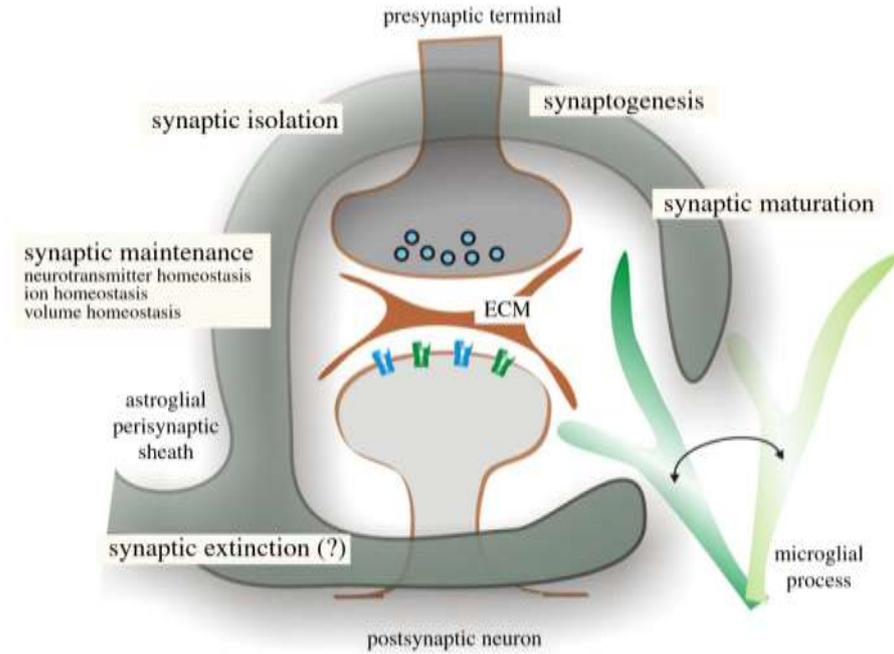
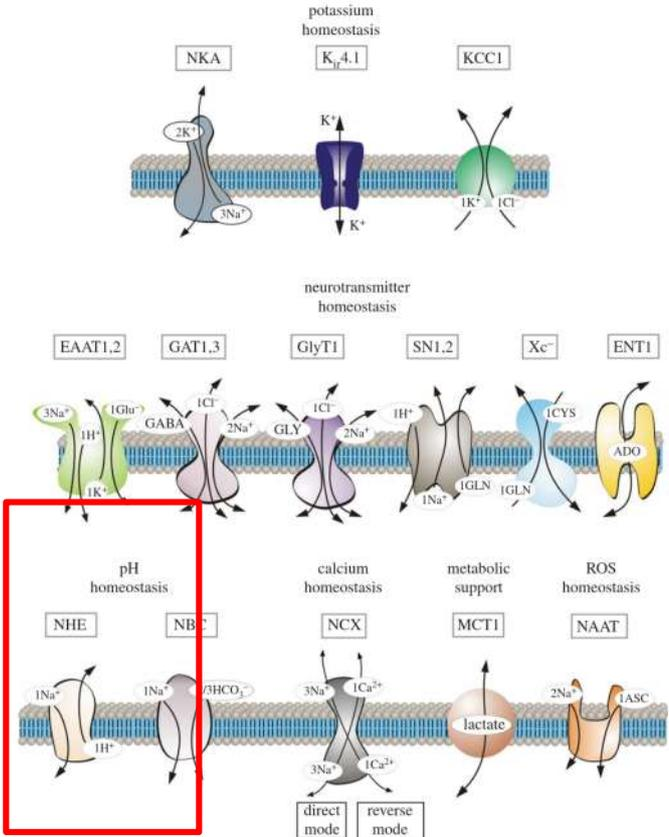
Alexei Verkhratsky^{1,2,3} and Maiken Nedergaard⁴

¹Faculty of Life Sciences, University of Manchester, Manchester, UK

²Achucarro Center for Neuroscience, IKERBASQUE, Basque Foundation for Science, 48011 Bilbao, Spain

³University of Nizhny Novgorod, Nizhny Novgorod 603022, Russia

⁴Division of Glia Disease and Therapeutics, Center for Translational Neuromedicine, University of Rochester Medical School, Rochester, NY 14580, USA



Astroglial perisynaptic sheath covers the majority of synapses in the central nervous system. This glial coverage evolved as a part of the synaptic structure in which elements directly responsible for neurotransmission (exocytotic machinery and appropriate receptors) concentrate in neuronal membranes, whereas multiple molecules imperative for homeostatic maintenance of the synapse (transporters for neurotransmitters, ions, amino acids, etc.) are shifted to glial membranes that have substantially larger surface area. The astrocytic perisynaptic processes act as an 'astroglial cradle' essential for synaptogenesis, maturation, isolation and maintenance of synapses, representing the fundamental mechanism contributing to synaptic connectivity, synaptic plasticity and information processing in the nervous system.

Астроциты: Ca^{2+} возбудимость

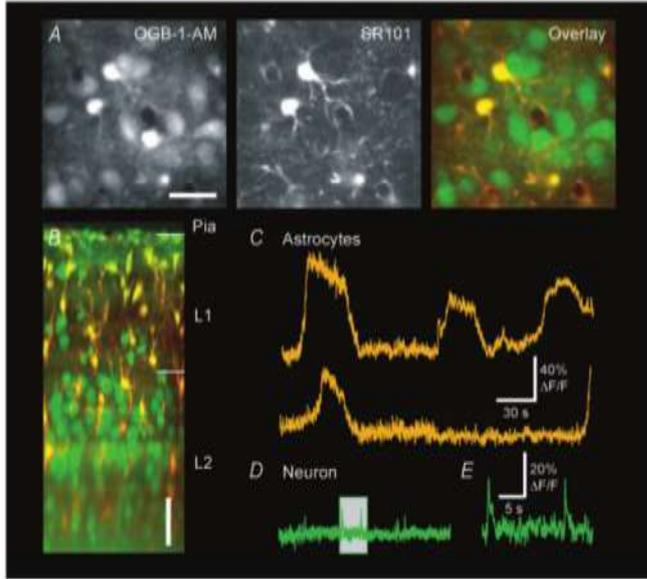


Figure 1. Calcium imaging of astrocytic and neuronal network excitation *in vivo*

A. Nimmerjahn, *J. Physiol.* (2009), **587**(8):1639-1647

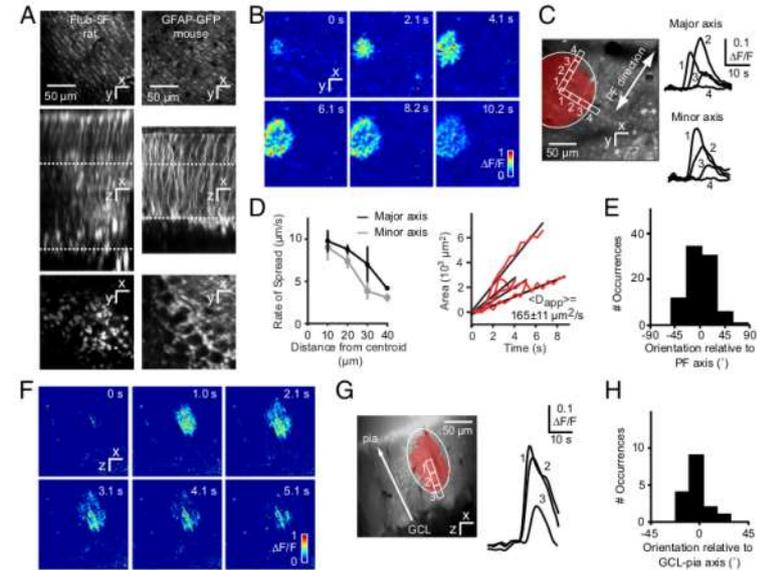


Fig. 1. Transglial calcium waves in the cerebellar cortex *in vivo*. (A) Staining patterns of the cerebellar cortex bolus-loaded with fluo-5F/AM (rat) or expressing GFP under the glial cell-specific GFAP promoter (mouse). (Top) Optical sections acquired in the molecular layer (ML, locations indicated by the upper dotted lines (Middle)] show a distinct striate pattern matching lateral protrusions from stem processes of Bergmann glia (BG). (Middle) Maximal side projection showing similarity between fluo-5F/AM labeling and GFAP-GFP expression. (Bottom) Optical sections taken from the Purkinje cell layer, with BG somata arranged around Purkinje cells. (B) Spontaneous radial wave measured in the ML. (C) Putative stem processes and side branches from BG show calcium increases with a time course typical of glial signals. (D) (Left) Wavefront slowing with distance from the initiation site. (Right) Linear rate of increase of wave area, with an average apparent diffusion constant $D_{app} = 165 \mu\text{m}^2/\text{s}$. Data are shown for 4 waves. (E) Distribution of wave orientation relative to the parallel fiber (PF) axis. (F) Radial wave in ML measured in an *xz* parasagittal plane orthogonal to the surface of the cerebellum. (G) Wave orientation along the axis of BG stem processes. (H) Distribution of wave orientation relative to the pia-Purkinje cell axis.

Hoogland et al, *PNAS* (2009), **106**(9) 3496-3501

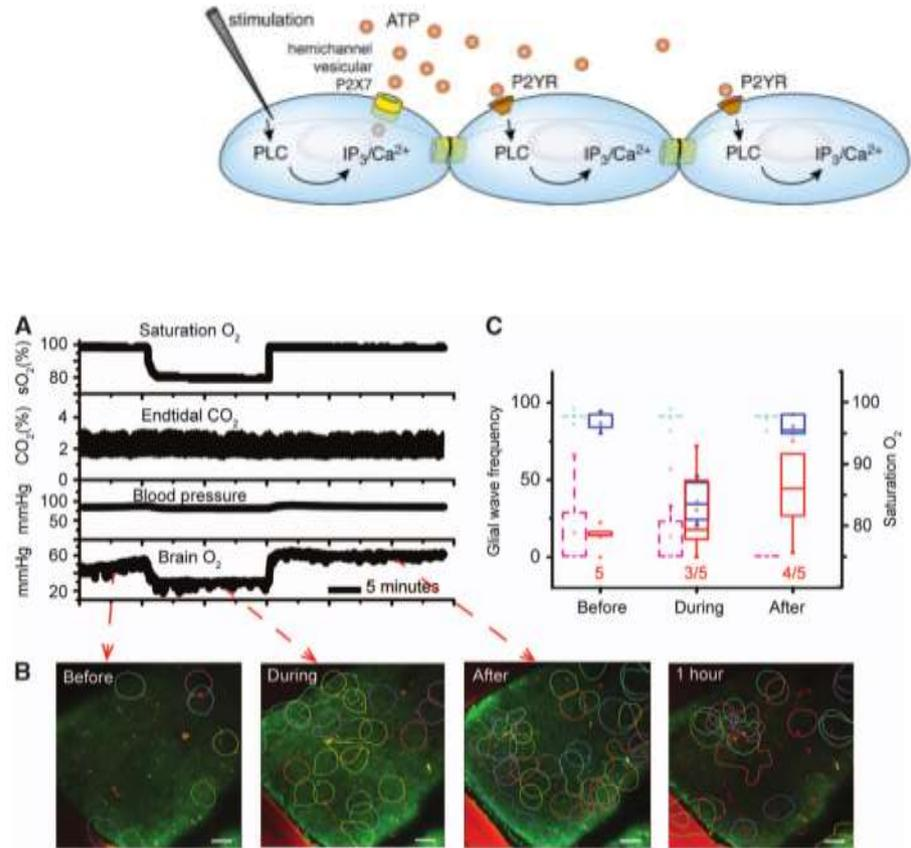
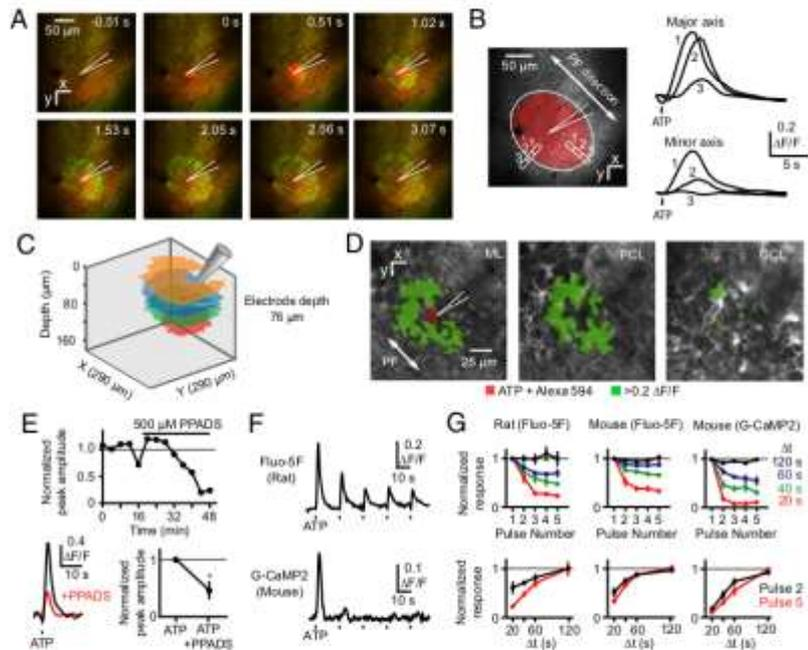
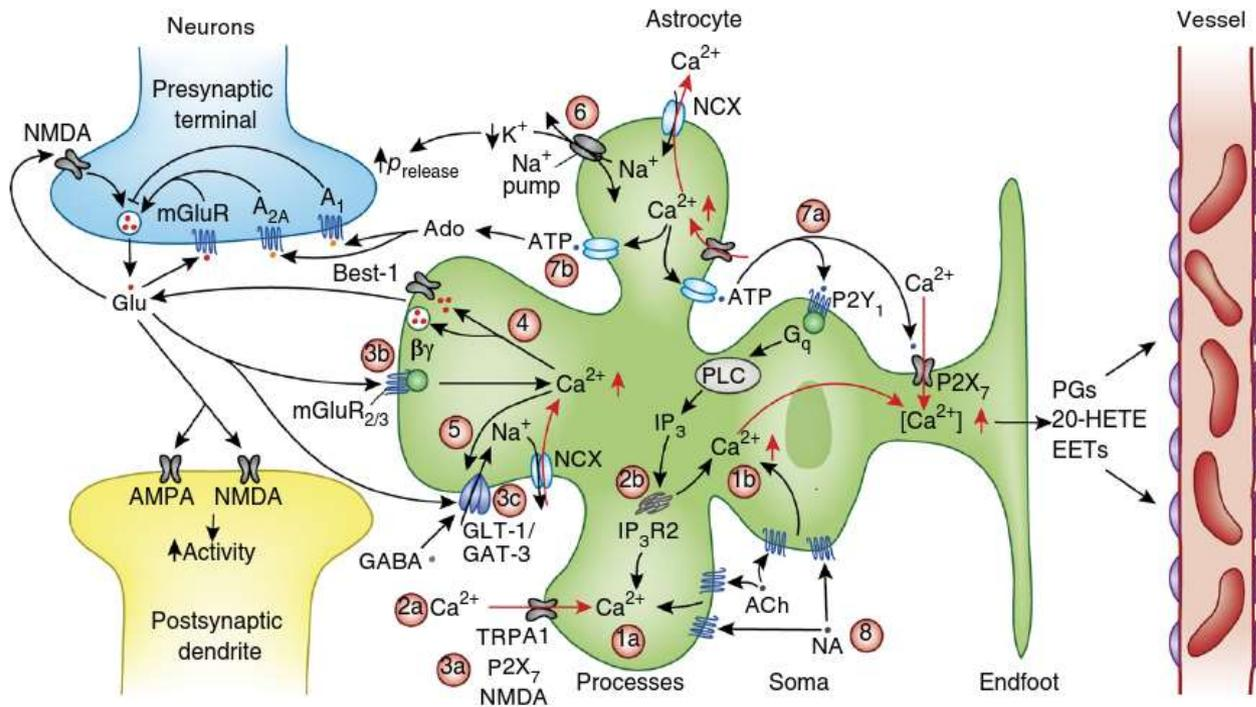


Fig. 4. ATP-triggered transglial calcium waves in vivo. (A) A transglial calcium wave evoked by ejection of ATP (pipette concentration: 1 mM, 10 ms, 0.07 bar) into the molecular layer. Green, Fluo-5F calcium signal; red, Alexa 594 and SR101. (B) Elliptical domain oriented along the PF axis in an ATP-triggered wave. (C) Waves triggered in rat cerebellar cortex at different imaging depths after ATP ejection at the same depth. (D) Activation of velate astrocytes in the granule cell layer after ATP ejection in lower third of the molecular layer, imaged by using G-CaMP2. (E) Reduction of ATP-triggered transglial signals by the P2 antagonist PPA2S. (F) Decrease in successive calcium responses after repeated application of ATP. (G) Dependence of response amplitude after 5 pulses of ATP injected at different time intervals.

Hoogland et al, *PNAS* (2009), **106**(9) 3496-3501

Mathiesen, Brazhe, Thomsen, Lauritzen, *JCBFM* 2012



Оптогенетика

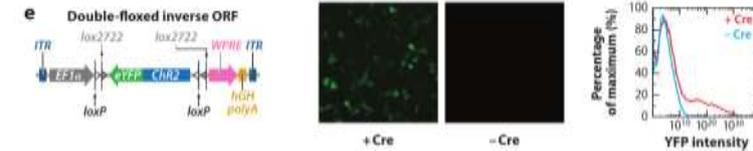
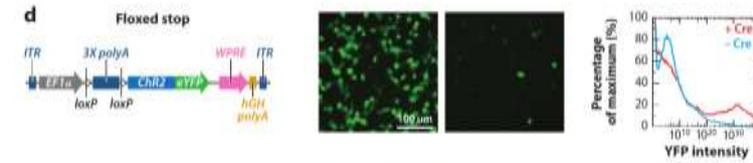
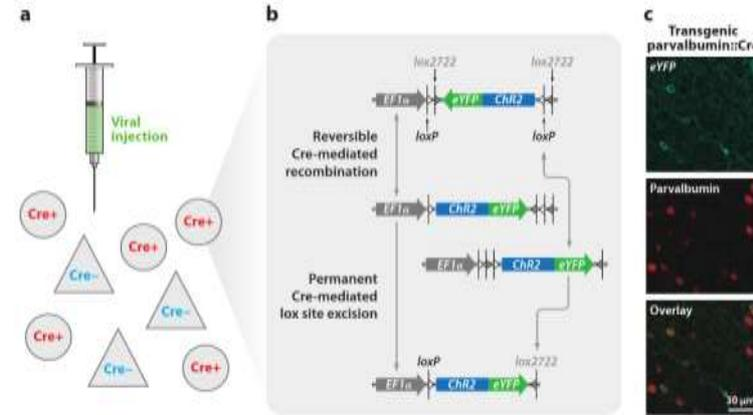
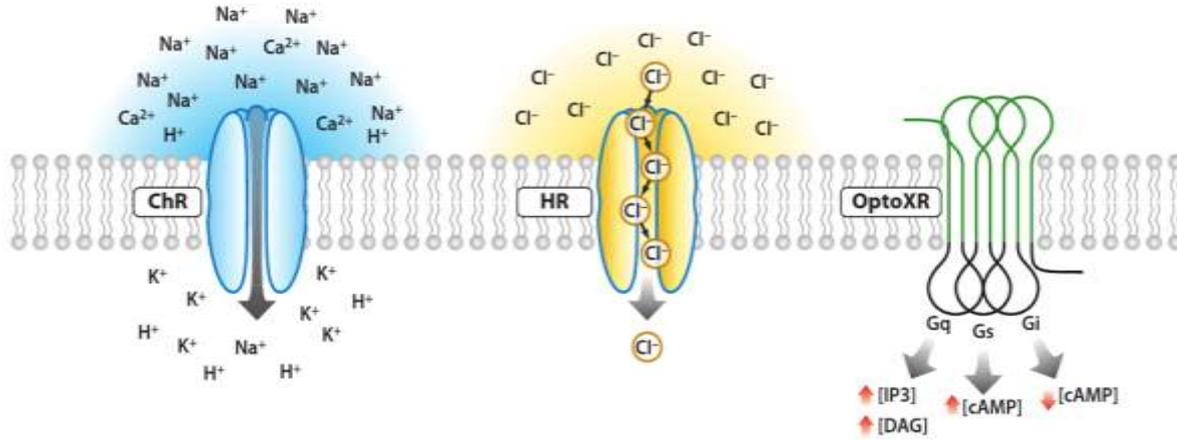


Figure 1

Optogenetic tool families. Channelrhodopsins conduct cations and depolarize neurons upon illumination (*left*). Halorhodopsins conduct chloride ions into the cytoplasm upon yellow light illumination (*center*). OptoXRs are rhodopsin-GPCR (G protein-coupled receptor) chimeras that respond to green (500 nm) light with activation of the biological functions dictated by the intracellular loops used in the hybrid (*right*).

Fenno et al 2011

Связь физико-химических свойств мембран с ПД

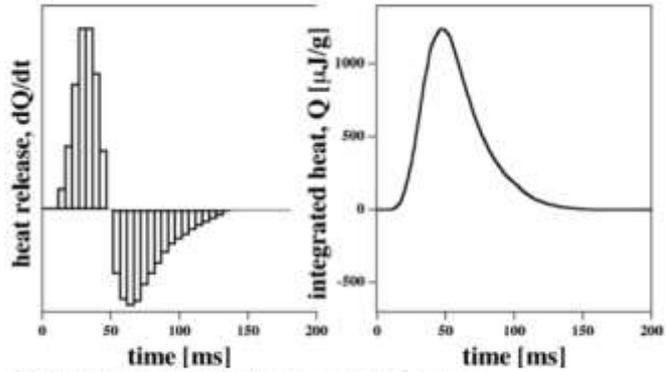


Fig. 18.5 Heat release in garfish olfactory nerve. Left: During the action potential one finds an initial phase of heat release that is followed by a phase of heat absorption. Right: Integration of the rate of heat release reveals that within error no net heat is released. Data adapted from Ritchie and Keynes (1985).

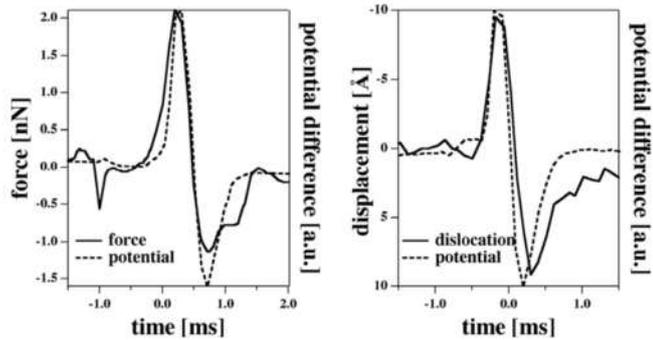
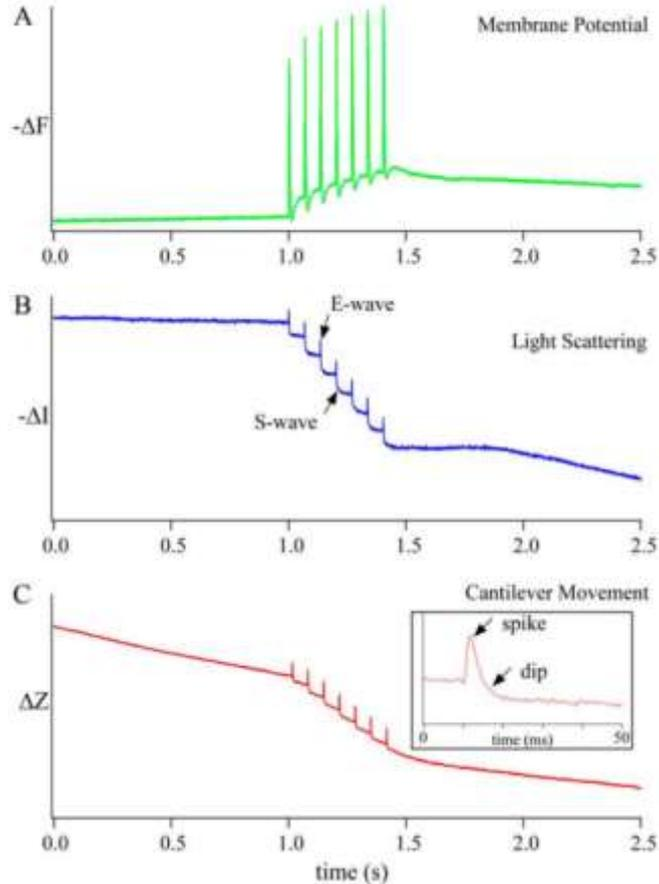
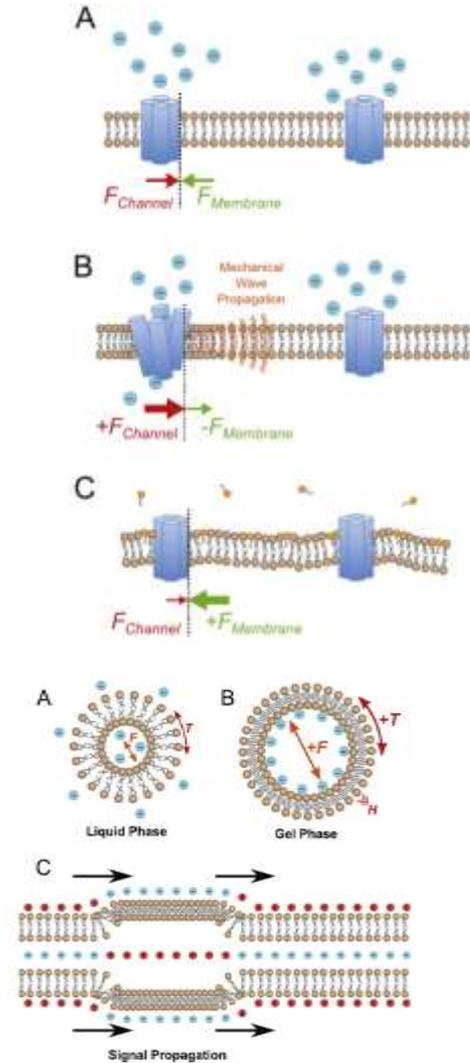


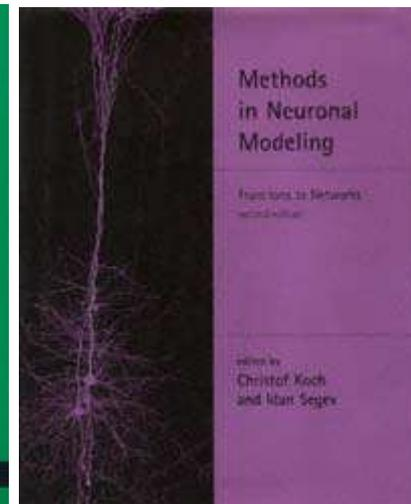
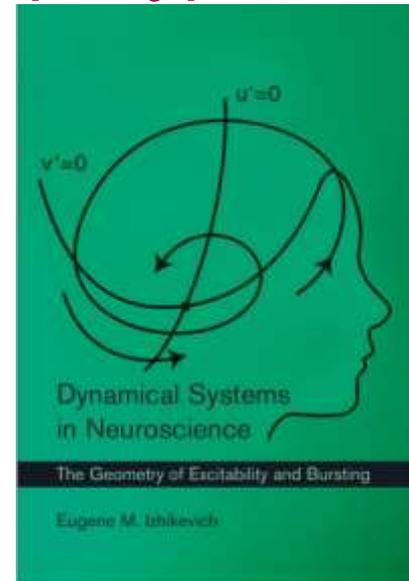
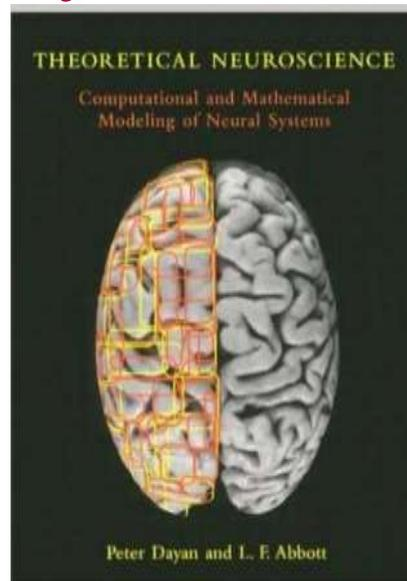
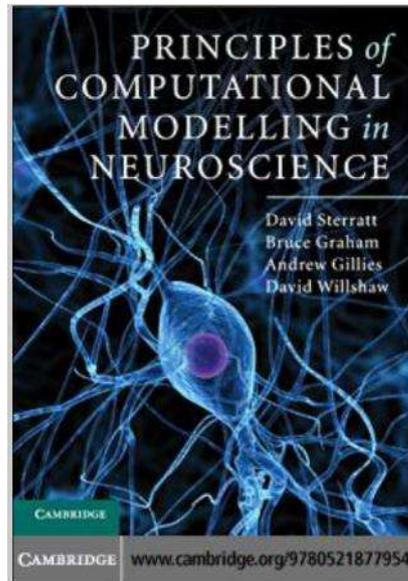
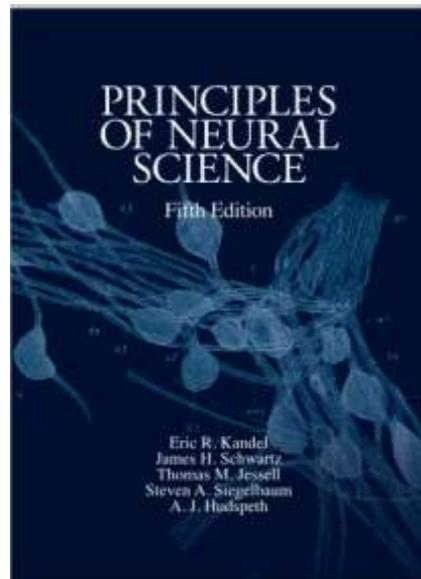
Fig. 18.7 Mechanical changes during the action potential. Left: Force on a piston during the action potential in a squid axon. The solid line represents the voltage changes and the dotted curve the force. Right: During the nerve pulse in a squid axon the thickness of the nerve changes proportional to the voltage. Data adapted from Iwasa and Tasaki (1980).



Kim et al *Biophys J* 2007



Рекомендуемая литература



(+ ссылки на слайдах и учебник Рубина)